Inaugural dissertation

for

obtaining the doctoral degree

of the

Combined Faculty of Mathematics, Engineering and Natural Sciences

of the

Ruprecht – Karls – University

Heidelberg

Presented by

Guillaume Wassmer, Master of Science (M.Sc.)

Born in: Strasbourg, France

Oral-examination: April 12th, 2023

Antigen-armed antibodies (AgAbs)
in the treatment of
Acute Myeloid Leukemia (AML)

Referees: Prof. Dr. Martin Müller

Prof. Dr. Dr. Henri-Jacques Delecluse

Index

SUMMARY

Acute myeloid leukemia (AML) accounts for 80% of acute leukemia cases in adults and results from the accumulation of immature malignant myeloid progenitor cells at the expense of healthy differentiated counterparts. These cells invade the bone marrow, the blood and can also infiltrate organs in the periphery. While recent progresses in AML management moderately improved the survival of patients below the age of 65, about 70% of older patients succumb to the disease within one year after diagnosis. Therefore, the search for more therapeutic options in AML is imperative.

In this doctoral work, a novel approach based on the AML-specific antibodies designed to deliver immunodominant Epstein-Barr virus (EBV) epitopes to AML tumour cells is assessed. These antigen-armed antibodies (AgAbs) target surface markers upregulated on AML cells, namely CD33, CD123, CLL-1 and FR-β. After receptor-mediated endocytosis, the viral epitopes included in the AgAbs are shuttled into the endosomal compartments of the target cells, where the epitopes can be processed for MHC class II-restricted presentation on the cell surface. In EBV-positive individuals (95% of the human population worldwide), circulating memory virus-specific cytotoxic $CD4^+$ T cells can recognize the MHCII-bound peptides and mediate cell lysis. This strategy aims at boosting the low basal immunogenicity of AML blasts in order to redirect a potent anti-viral immunity toward these cancer cells. *In vitro* experiments with multiple AML cell lines demonstrated the potency of AgAbs to target the aforementioned surface marker, culminating in the presentation of epitopes at the cell surface. This led to a strong EBV-specific $CD4^+$ T cell activation, characterized by IFNγ and granzyme B secretion. These activated T cells were also capable of directly eliminating AgAb-treated AML cell line cells. Furthermore, AgAb-mediated T cell activation was shown to eliminate bystander malignant cells, probably through IFNγ and TNF-α signaling. *Ex vivo* experiments with AgAbs showed a promising potential to stimulate EBV-specific memory $CD4^+$ T cells from AML patients. Upon AgAb treatment, these cells proliferated and killed a substantial proportion of patient blasts. Finally, a murine model of AML was developed. AgAbs fused to murine cytomegalovirus epitopes potently expanded murine $CD4^+$ T cells *in vivo*, culminating in a prolonged survival in AgAb-treated tumour-bearing mice.

Altogether, the promising results from this study demonstrate the potential of AgAbs to redirect endogenous $CD4^+$ cytotoxic T cells against AML cells loaded with EBV antigens, paving the way for future studies and clinical trials.

ZUSAMMENFASSUNG

Die akute myeloische Leukämie (AML) macht 80% der akuten Leukämiefälle bei Erwachsenen aus. Sie resultiert aus der Ansammlung von unreifen malignen myeloischen Vorläuferzellen zum Nachteil gesunder differenzierter Zellen. Diese Blasten dringen in das Knochenmark und Blut ein und können auch periphere Organe infiltrieren. Obwohl die neuesten Fortschritte im AML-Management das Überleben von Patienten unter 65 Jahren moderat verbesserten, sterben etwa 70% der älteren Patienten innerhalb eines Jahres nach der Diagnose an der Krankheit. Deshalb ist die Suche nach weiteren therapeutischen Optionen bei AML zwingend notwendig.

In dieser Doktorarbeit wird ein neuartiger Therapieansatz basierend auf AML-spezifischen Antikörpern untersucht, der immundominante Epstein-Barr-Virus (EBV)-Epitope an AML-Tumorzellen überträgt. Diese Antikörper *(„Antigen-armed antibodies“* - AgAbs) zielen auf die Oberflächenmarker CD33, CD123, CLL-1 und FR-β ab, die auf AML-Zellen hochreguliert sind. Nach einer rezeptorvermittelten Endozytose werden virale Epitope in die endosomalen Kompartimente der Zielzellen verlagert, wo sie für die MHC-Klasse II-gebundene Präsentation auf der Zelloberfläche verarbeitet werden können. Bei EBV-positiven Menschen (95% der Weltbevölkerung) können zirkulierende, virusspezifische zytotoxische $CD4^+$ T-Zellen die MHCII-gebundenen Peptide erkennen und eine Zelllyse bewirken. Die Strategie zielt darauf ab, die niedrige basale Immunogenität von AML-Blasten zu erhöhen, um eine starke antivirale Immunität gegen diese Krebszellen hervorzurufen.

In vitro-Experimente mit mehreren AML-Zelllinien zeigten die Wirksamkeit von AgAbs auf, die auf die oben genannten Oberflächenmarker abzielen, was in der Präsentation von Epitopen auf der Zelloberfläche gipfelte. Dies führte zu einer starken Aktivierung von EBV-spezifischen $CD4^+$ T-Zellen, gekennzeichnet durch IFN und Granzym B Sekretion. Diese aktivierten T-Zellen waren auch in der Lage, AgAb-vorbehandelte AML-Zelllinienzellen direkt zu eliminieren.

Darüber hinaus konnte gezeigt werden, dass die AgAb-vermittelte T-Zellaktivierung auch nicht zielgerichtete maligne Bystander-Zellen, vermutlich durch IFNγ und TNFα Freisetzung, eliminieren konnte. *Ex-vivo*-Experimente mit AgAbs zeigten ein vielversprechendes Potenzial zur Stimulierung von EBV-spezifische $CD4^+$ T-Gedächtniszellen von AML-Patienten. Nach der Behandlung vermehrten sich diese Zellen und töteten einen beträchtlichen Anteil der Patientenblasten ab. Schließlich wurde ein murines Modell für AML entwickelt. AgAbs, die an murine Cytomegalievirus-Epitope fusioniert sind, bewirkten eine starke Expansion muriner $CD4^+$ T-Zellen *in vivo*, was zu einem verlängerten Überleben in AgAb-behandelten tumortragenden Mäuse führte.

Insgesamt zeigen die vielversprechenden Ergebnisse dieser Studie das Potenzial von AgAbs, endogene $CD4^+$-zytotoxische T-Zellen, die mit EBV-Antigenen beladen sind, gegen AML-Zellen umzuleiten. Dies ebnet den Weg für zukünftige klinische Studien.

1. Introduction

1.1. Acute myeloid Leukemia (AML)

1.1.1. Pathology, diagnosis and epidemiology of AML

The normal haematopoiesis is a highly regulated process, layered around a hierarchy of progenitors, which leads to the production of functional blood cells from different lineages. Myeloid differentiation produces red blood cells, monocytes, granulocytes and platelets. The generation of these mature cells relies on the proliferation and the differentiation of hematopoietic stem cells and progenitors within supportive bone marrow niches.

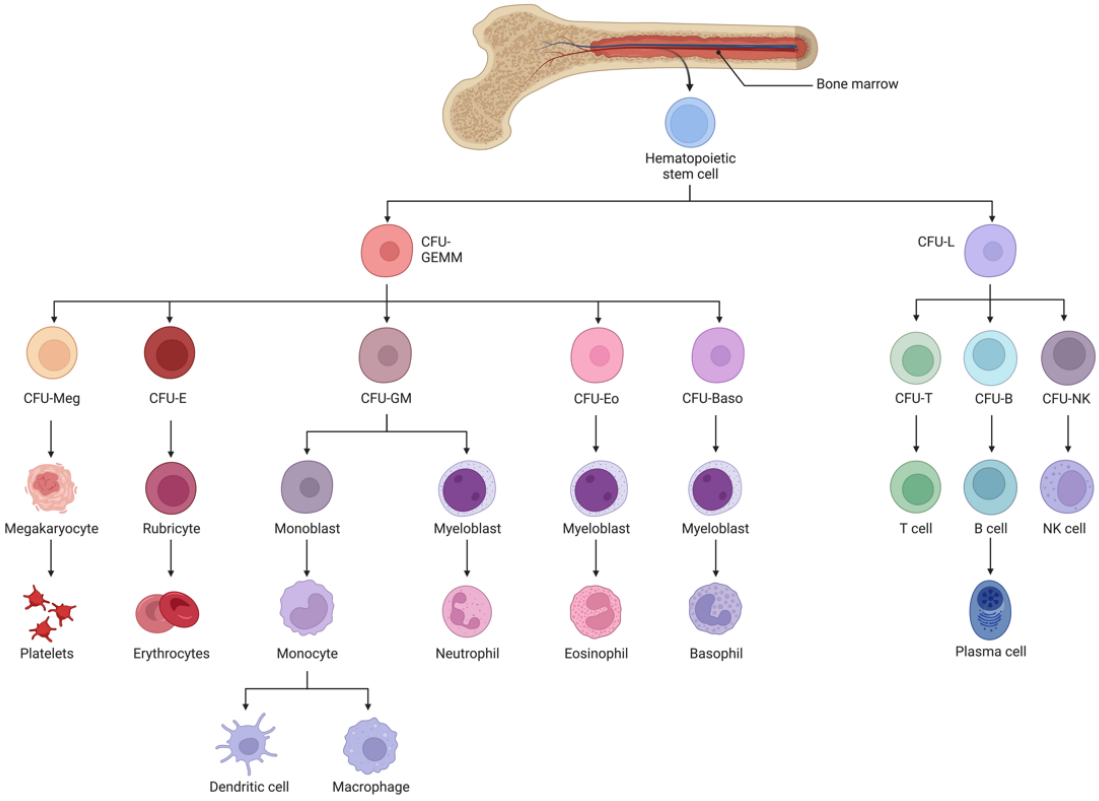

Figure 1: Normal haematopoiesis in the bone marrow
Baso=Basophils, Eo=Eosinophils, BFU=Burst-forming unit, CFU=Colony-forming unit, GEMM= Granulocyte, Erythrocyte, Monocyte, Megakaryocyte, L=Lymphocytes. *Created with BioRender.*

Acute myeloid leukemia (AML) is a disease associated with increased proliferation and stalled differentiation of these myeloid progenitors [1]. Some alterations in the maturation program can affect the differentiation of the progenitor cells, leading to an accumulation of blasts within the bone marrow [2]. These blasts can ultimately invade the blood and peripheral organs.

Until 2022 and a revised classification of haematological malignancies, AML used to be characterized by a blast count in the blood and in the bone marrow superior to 20%. The clinical relevance of this limit was contested, but this boundary distinguished AML from myelodysplastic syndrome (less than 20% of blasts) [3, 4]. In comparison, a healthy bone marrow contains less than 5% of blasts and the blood is free from these cells. With the exception of some specific types of AML (see 1.1.2), an acute myeloid leukemia can be diagnosed with blast percentages over 10% [5, 6].

Beyond a reduced production of mature myeloid cells due to the stalled maturation processes, the high number of blasts in AML patients alters the normal bone marrow microenvironment. This translates into a bone marrow failure, characterized by neutropenia, thrombocytopenia or anaemia [7].

Early symptoms arise in AML patients by fatigue, loss of weight, joint pains, bleedings and increased infections, mainly due to the decreased production of mature blood cells [8]. A blood test can then reveal a low number of differentiated cells and the presence of blasts. The final diagnostic is confirmed with a comprehensive analysis after a bone marrow aspirate (cytochemistry, cytogenetic, FISH, …) [9].

The mean of age at diagnosis for AML patients is 68 years. Moreover, 75% of the patients are older than 65. This tumour type has a higher prevalence in developed countries. Although the aetiology of most AML cases is not clearly established, prior exposition to some chemicals or radiations can increase the prevalence of this cancer [10]. For example, patients who previously received chemotherapy to treat another tumour have an increased risk to develop a secondary AML, and represent 10-15% of all AML cases [2]. Also, people with an occupational exposition to some chemicals (benzene, formaldehyde, …) or to radiations have an increased risk to develop AML [11].

Acute myeloid leukemia is the most common acute leukemia in adults, but represents less than 10% of leukemia in infants. Between 1990 and 2019, more than 16 million cases have been reported worldwide. Strikingly, the incidence is on the rise, especially in developing countries [12]. The median survival time of AML patients is 8.5 months and the overall five-year survival rate is 24%, which makes AML one of the cancers with the poorest survival [10]. In patients younger than 20, prognosis has improved over the last decades, with a five-year survival rate over 60% [13]. However, about 70% of older patients succumb to the disease within one year after diagnosis (five-year survival rate below 8% for patients older than 60 years old) [14].

1.1.2. Classifications and molecular abnormalities in AML

The myeloid differentiation is a complex process involving multiple steps of maturation. The progenitors from all these different maturation stages can be the cell of origin in AML, making the disease highly heterogeneous.

The first classification of AML cases was based on the affected lineage and the differentiation stage of the blasts. This classification was first published in 1976 and is called the "French-American-British" classification (FAB). It segregates AML in eight different categories, from M0 to M7 [15] (Table 1).

FAB	Name	Myelogram	Frequency
M0	Undifferentiated Acute myeloblastic leukemia	Myeloblasts and promyelocytes	5%
M1	Acute Myeloblastic Leukemia with minimal maturation	>90% nonerythroid cells : Myeloblasts, promyelocytes and myelocytes (<10% maturation)	15%
M2	Acute Myeloblastic Leukemia with maturation	>90% nonerythroid cells : Myeloblasts, promyelocytes and myelocytes (>10% maturation)	25%
M3	Acute Promyelocytic Leukemia (APL)	Abnormal promyelocytes with Auer rods	10%
M4/eos	Acute Myelomonocytic Leukemia (AMML)	Myeloblasts and monoblasts (M4eos: increased eosinophilic progenitors)	20% (M4eos: 5%)
M5	Acute Monocytic Leukemia M5a = AMoL M5b= AMoL with maturation	>80% of the blasts are from monocytic lineage (M5a: monoblasts / M5b: monoblasts and promonocytes)	10%
M6	Acute Erythroid Leukemia	>30-50% of the blasts are nucleated red blood cells progenitors	5%
M7	Acute Megakaryoblastic Leukemia	>50% of the blasts are from megaryocytic lineage	5%

Table 1: French-American-British (FAB) classification for AML (data from [16]**)**

Progresses in genetics and cytogenetics unravelled recurrent genetic abnormalities in AML patients. Most often, these alterations are translocations (which create onco-fusion proteins), tandem duplications, deletions or point mutations.

The most common translocations are AML-1-ETO (t(8;21), 10% of AML), PML-RARα (t(15,17), 10% of all AML but 95% of APL), CBFβ-MYH11 (inv(16), 8% of AML) and MLL-rearrangements (der(11q23)) [17]. Monosomies or trisomies are also often found in AML karyotypes [17]. However, approximately half of the patients have a normal karyotype.

Some recurrent mutations are found in patients with normal karyotypes, such as mutations in the RAS family (15% of AML), FLT3 (30% of AML), KIT, IDH, NPM1 or DNMT3a [17]. The overall number of genetic alterations in AML adult patients is very low, below 0.5 somatic mutation per megabase and is even lower in infants, making AML one of the cancers with the lowest mutational burden [18, 19]. On the average, 13 mutations in genes are found in an AML patient, of which an average of five are in genes that are recurrently mutated in AML [20].
The recurrent genetic alterations and their impact on the prognostic favoured the establishment of a new classification by the World Health Organization (WHO) in 1999 [21]. This classification was revised in 2016 and in 2022, and includes the most common genetic alterations found in AML patients (Table 2) [22].

Acute myeloid leukaemia with defining genetic abnormalities
Acute promyelocytic leukaemia with *PML*::*RARA* fusion
Acute myeloid leukaemia with *RUNX1*::*RUNX1T1* fusion
Acute myeloid leukaemia with *CBFB*::*MYH11* fusion
Acute myeloid leukaemia with *DEK*::*NUP214* fusion
Acute myeloid leukaemia with *RBM15*::*MRTFA* fusion
Acute myeloid leukaemia with *BCR*::*ABL1* fusion *
Acute myeloid leukaemia with *KMT2A* rearrangement
Acute myeloid leukaemia with *MECOM* rearrangement
Acute myeloid leukaemia with *NUP98* rearrangement
Acute myeloid leukaemia with *NPM1* mutation
Acute myeloid leukaemia with *CEBPA* mutation *
Acute myeloid leukaemia, myelodysplasia-related
Acute myeloid leukaemia with other defined genetic alterations
Acute myeloid leukaemia, defined by differentiation
Acute myeloid leukaemia with minimal differentiation
Acute myeloid leukaemia without maturation
Acute myeloid leukaemia with maturation
Acute basophilic leukaemia
Acute myelomonocytic leukaemia
Acute monocytic leukaemia
Acute erythroid leukaemia
Acute megakaryoblastic leukaemia

Table 2: 2022 World Health Organisation (WHO) for AML (data from [5]**)**
* = AML categories which still require 20% of blasts for diagnosis

Furthermore, the European LeukemiaNet (ELN) stratified the patients in three different risk-categories (ELN1: Favorable / ELN2: Intermediate / ELN3: Adverse) based on their cytogenetic abnormalities [6] (Table 3). This classification has gained a dramatic importance in the patient management, especially in the orientation of the therapeutic strategy.

Risk category	Genetic abnormality
Favorable	• t(8;21)(q22;q22.1)/*RUNX1*::*RUNX1T1* • inv(16)(p13.1q22) or t(16;16)(p13.1;q22)/ *CBFB*::*MYH11* • Mutated *NPM1*, without *FLT3*-ITD • bZIP in-frame mutated *CEBPA*
Intermediate	• Mutated *NPM1*, with *FLT3*-ITD • Wild-type *NPM1* with *FLT3*-ITD (without adverse-risk genetic lesions) • t(9;11)(p21.3;q23.3)/*MLLT3*::*KMT2A* • Cytogenetic and/or molecular abnormalities not classified as favorable or adverse
Adverse	• t(6;9)(p23.3;q34.1)/*DEK*::*NUP214* • t(v;11q23.3)/*KMT2A*-rearranged • t(9;22)(q34.1;q11.2)/*BCR*::*ABL1* • t(8;16)(p11.2;p13.3)/*KAT6A*::*CREBBP* • inv(3)(q21.3q26.2) or t(3;3)(q21.3;q26.2)/ *GATA2*, *MECOM(EVI1)* • t(3q26.2;v)/*MECOM*(*EVI1*)-rearranged • −5 or del(5q); −7; −17/abn(17p) • Complex karyotype, monosomal karyotype • Mutated *ASXL1, BCOR, EZH2, RUNX1, SF3B1, SRSF2, STAG2, U2AF1, and/or ZRSR2* • Mutated *TP53*

Table 3: 2022 ELN risk stratification of AML patients based on their cytogenetic abnormalities (data from [6])

1.1.3. Current AML patient management and development of small molecules

The standard of care for patients with AML is most often composed of intensive chemotherapy (Figure 2). The treatment is divided into two phases, namely induction and consolidation. People with a high count of blasts sometimes also need to undergo leukapheresis [23].

The induction phase is an intensive treatment with chemotherapeutic agents, in order to eliminate the vast majority of leukemic cells.

The condition of each patient should be carefully evaluated to ensure that the treatment will be tolerated without threatening its life. For patients that are fit enough to tolerate intensive chemotherapy, the classical induction therapy is the "7+3 regimen". This treatment consists in a continuous infusion of cytarabine for seven days along with point infusions of an anthracycline (daunorubicin, …) every day for the first three days of treatment [24]. This protocol has been approved in 1973, dramatically improving the survival rate of patients in comparison to previous treatments [25]. A new liposomal formulation, combining daunorubicin and cytarabine in a synergistic 1:5 ratio, has recently been approved (CPX-351), and is now used in therapy-related or secondary-to-MDS AML [26]. Depending on the cytogenetic abnormality, hypomethylating agents can also be included in the induction regimen (Azacytidine, Decitabine) [27]. Fludarabine or etoposides can also be suitable to some patients [28, 29].

Recently, targeted therapies have joined the therapeutic armada, and are used in patients with specific molecular alterations. These molecules can be used in combination with classical intensive chemotherapy or can be also used in monotherapy in weaker patients [27]. Such molecules can be, among others, Midostaurin or Gilteritinib (FLT3-mutated AML), Venetoclax (Bcl-2-mutated AML), Ivosidenib (IDH1-mutated AML), Enasidenib (IDH2-mutated AML) [27, 30–32].
For patients too weak to undergo intensive treatment, low intensity chemotherapy is proposed. This regimen combines lower doses of cytarabine (LDAC) or hypomethylating agents with other drugs such as Venetoclax or Melphalan [27, 33].
The induction phase is successful solely if clinical remission is achieved (less than 5% of blasts in a bone marrow biopsy) [34]. Although induction phase usually kills the vast majority of leukemic blasts, some resistant cells may remain. These cells can initiate a short-term relapse, which is the reason why a consolidation phase is needed.

In fitter patients, the consolidation phase is often composed of cycles of high-dose chemotherapy (cytarabine), with the possibility to combine it with targeted therapies [35, 36]. Frailer patients may receive lower doses of chemotherapy, possibly in combination with targeted therapies. For some patients (especially those at high risk of relapse), an allogenic/autologous stem cell transplantation can also be conducted as a maintenance therapy. The fitness for conditioning regimen, as well as the availability of a compatible donor (allogenic) or the possibility to collect leukemia-free stem cells from the patient (autologous) are fundamental prerequisites [37]. The availability of a suitable donor and high risks of complications in patient restrict the applicability of HSCT [36]. Recently, oral Azacytidine has been shown to be effective in maintenance therapy for a broad spectrum of AML patients ineligible for HSCT [38].

An exception to the aforementioned treatments are the patients with a FAB M3 AML (promyelocytic leukemia). This type of leukemia is often characterized by the PML-RARα fusion gene and responds generally well to differentiating agents. The lead drug is all-trans-retinoic acid (ATRA), commonly given in combination with arsenic trioxide or chemotherapy for high-risk patients (anthracycline or cytarabine) [39]. The consolidation treatment is generally composed of the same drugs, given at different doses or timing. For patients with a high-risk of relapse, long-term maintenance therapy can be recommended, involving ATRA along with chemotherapy.

For most types of AML, remission is achieved in two patients out of three (50% for patients older that 60). In APL, a higher remission-rate is observed, in 90% of the patients [40].

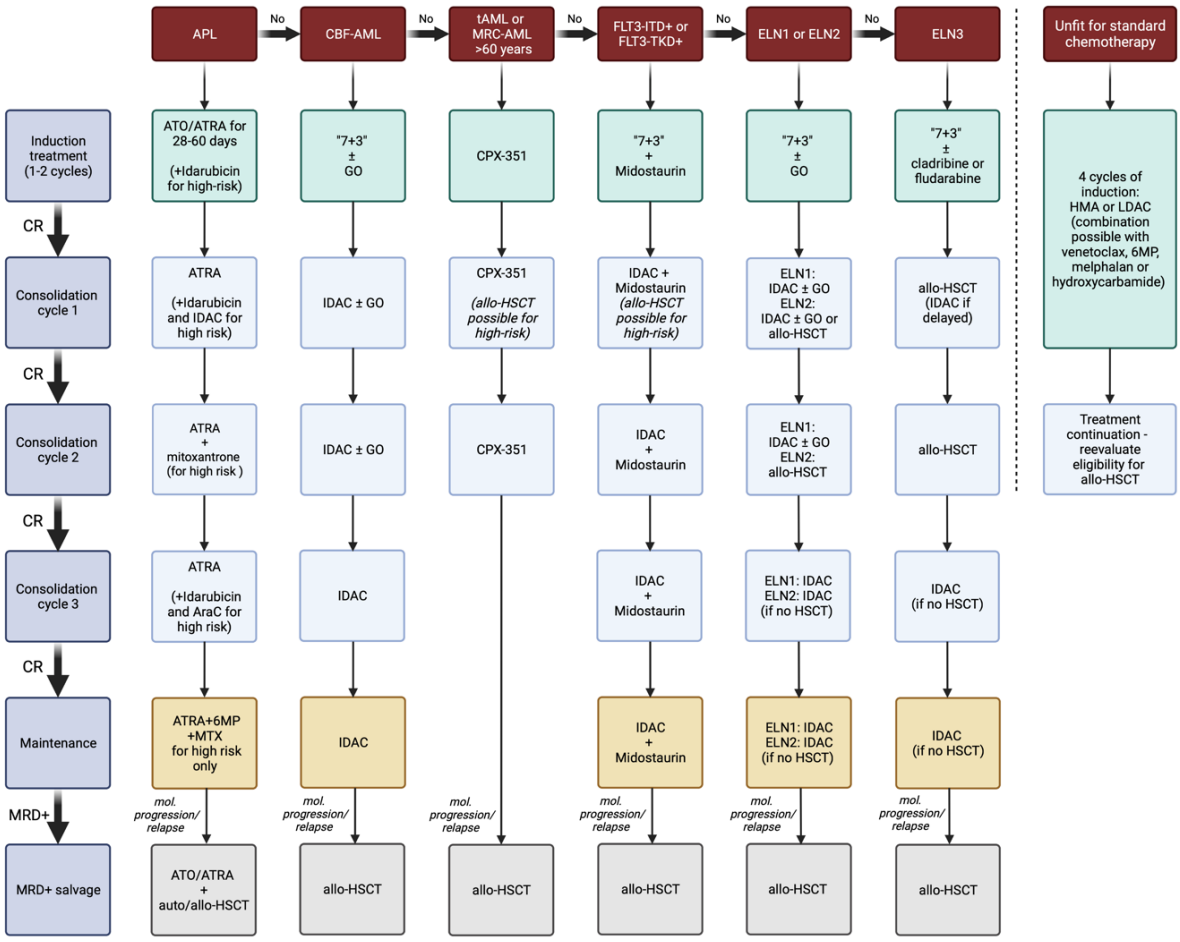

Figure 2: Frontline treatment in AML patients (based on data from [41]).
APL=Acute promyelocytic leukemia, AraC=Cytarabine, ATO= Arsenic trioxide, ATRA= All-trans retinoic acid, CBF=Core-binding factor, CR=Complete response, ELN= European LeukemiaNet, GO=Gemtuzumab Ozogamycin, HMA=hypomethylating agent, HSCT=hematopoietic stem cell transfer, IDAC= Idarubicin/cytarabine, LDAC=Low-dose cytarabine, MRC-AML= AML with myelodysplasia-related changes, MRD+= Positive for measurable residual disease, tAML= therapy-related AML, 6MP=6-mercaptopurine
Small molecules can also be given in addition to chemotherapies depending on specific cytogenetic abnormalities, and are not indicated on this figure. *Figure created with BioRender.*

These heavy treatments are not devoid of side effects, most patients experiencing severe burden which are often correlated to the efficacy of the therapy [42].

In spite of recent combinations with new chemotherapies and small inhibitors, the very low survival rate of AML patients highlights the need for innovative therapies.

The recent progresses in the field of cellular pathways and the understanding of their role in leukemogenesis promoted the development of targeted molecules. Inhibitors of pathways such as MAPK (MEK), mTOR or Jak/STAT are currently under clinical investigation [43–45].
Inhibitors of epigenetic mechanisms (HDAC), cell cycle control (MDM2, CDK, Aurora Kinase…), and also anti-apoptotic adaptations (PARP, proteasome, Mcl-1…) have been developed and are under evaluation [45–49].
Although these new targeted inhibitors shall be beneficial for patients with specific molecular alterations, resistances very often develop within a few months. These are mainly associated with compensatory mechanisms (alternative cellular pathways) or with a multi-drug resistance status (efflux pumps, autophagy, …) [50].

1.1.4. AML immunological status

An efficient tumour cell recognition by the immune system would lead to the elimination of these cells, leading to the control of the tumour. However, the invasion of the bone marrow, blood and peripheral tissues by malignant progenitors highlights the inability of the immune system of the patients to control the malignant cells.
It has been proposed that the defective recognition of leukemic cells by T cells can partly be associated to the low mutagenic burden of AML. While genomes of some tumours can accumulate hundreds of mutations that give rise to immunogenic neoantigens, the average number of mutations in an AML patient is one the lowest among cancers (with the exception of TP53-mutated AML) [18–20].

The tumour microenvironment is also responsible for this lack of tumour cell control (Figure 3). Myeloid-derived suppressor cells (MDSCs) are suspected to have a central immunosuppressive role in AML [51]. MDSCs are immature myeloid cells that can secrete immunosuppressive molecules, such as indoleamine 2-3 dioxygenase (IDO), arginase-1 (ARG1), inducible nitric oxidase (iNOS) and reactive-oxygen species (ROS) [51–53]. IDO degrades tryptophan, an essential amino-acid, into a toxic product, the L-kynurenine [54]. ARG1 and NOS both consume arginine from the tumour microenvironment. The depletion of crucial amino-acids together with ROS production impair the T cell activation and proliferation [54–56]. Arginine depletion also impairs the phenotype of macrophages, favouring a M2-polarization, with anti-inflammatory and tumour supportive properties (IL-10 secretion, …) [57, 58].

A fraction of MDSCs can originate from healthy cells. However, AML cells have been also shown to have MDSC-like properties, with a similar secretion profile [59]. AML blasts can also express CD39 and CD73. The former degrades ATP into AMP (CD39) and the latter metabolizes AMP into adenosine (CD73), a potent T cell inhibitor [60]. IDH1/2-mutated AML cells have also been shown to secrete 2-hydroxyglutarate (2-HG), which induces epigenetic changes and favours leukemia progression, but also Th17 helper T cell differentiation [61, 62]. A defective antigen presentation by dendritic cells has been described in AML patients, and tolerogenic DC seem to be actively induced by AML cells through secretion of exosomes [63, 64]. Antigen-presentation by AML cells themselves can also be decreased, or altered [64, 65].

Interestingly, the overall number of T cells in the bone marrow of AML patients have been found to be comparable in diseased and healthy patients [66]. Furthermore, the count of T cells in the peripheral blood of AML patients is even higher compared to that of healthy controls [65]. However, the frequency of regulatory T cells is much higher in the blood and in the bone marrow (tumour microenvironment) of AML patients, and this seems to increase with tumour development [67]. Tregs are directly induced by AML cells but also by MDSCs, M2-macrophages and defective DCs [67, 68]. Regulatory T cells also support a tolerogenic microenvironment via the secretion of anti-inflammatory cytokines (TGF-β, IL-10, …) and metabolites consumption. Additionnaly, they have a direct effect on effector T cells, via the expression of immune checkpoints [68, 69]. More detailed immunosuppressive mechanisms of Tregs are given in the section 1.3.1.

Besides Tregs dysregulation, helper T cell function is also impaired in AML. Several studies have shown a diminished expression of IFNγ by Th1 cells in both the bone marrow and the peripheral blood of AML patients compared to healthy individuals [70, 71]. Interestingly, studies tend to show that T cells from AML samples, although silenced, are not irremediably deprived of their functional cytokine capacity [72, 73].

The inhibitory microenvironment, a high Treg frequency and an impaired Th1 function result in a poor CTL function, and immune evasion of AML blasts [68].

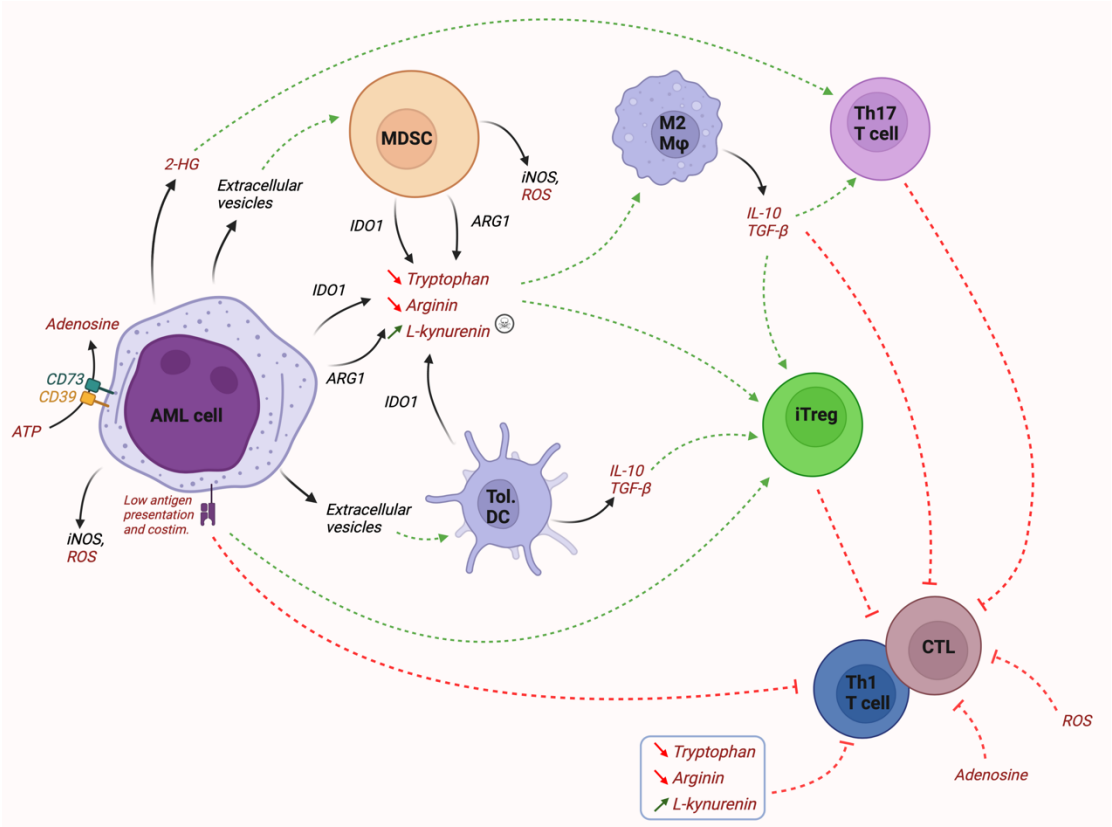

Figure 3: The immunosuppressive environment in AML leads to the immune evasion of cancer cells

CTL=Cytotoxic T lymphocyte, iTreg= induced regulatory T cell, MDSC=Myeloid-derived suppressor cell, Mφ=macrophage, ROS=Reactive oxygen species, Tol. DC=Tolerogenic dendritic cell.
Figure created with BioRender.

1.1.5. AML immune markers and immunotherapies

The limited progress in the overall survival for AML patients, as well as recent considerable advances in the field of immunotherapies in cancer (rituximab approved for lymphoma treatment in 1997), aroused the interest for this class of medication in AML.

Allo-HSCT is already considered as a type of immunotherapy, taking advantage of a "graft-versus-leukemia" effect mediated by engrafted NK and T cells [37]. However, approaches based on antibodies have gained interest over time.

The first approach of immunotherapies in AML is the direct targeting of leukemia cells.

The most explored marker in AML is CD33 (see part 1.4.3. for the characteristics of this marker). Gemtuzumab-Ozogamycin (Mylotarg®) is an anti-CD33 covalently bound to ozogamycin, a coumpound able to induce DNA strand breaks [74]. It has been approved in

2000 for the treatment of R/R AML, but was withdrawn from the market in 2010, due to severe toxicity and poor efficacy [74, 75]. Subsequent trials with lower doses of GO identified cohorts of patients that would benefit from the addition of this antibody, which lead to its re-approval in 2017 [76]. It is yet used in combination with chemotherapy in induction regimen, especially in patients that are ineligible for high-dose chemotherapy, and AML with core-binding factor mutations [77]. Numerous clinical trials are ongoing combining GO with other molecules [78].
Besides CD33 antibodies, CD123 (IL-3 receptor alpha) is also widely investigated. Several approaches are currently assessed based on CD123 antibodies [79].
Other markers have also gained interest, such as CD38 (cyclic ADP ribose hydrolase), FLT3, CD30, CD45 and many others [78–80].

Antibodies can be used to deliver a toxic payload to target cells. This compound is usually a cytotoxic drug (forming an antibody-drug conjugate – ADC), commonly too toxic to be given systematically [79, 80]. Other approaches with radioactive compounds are also explored (radio-immunotherapy), especially in conditioning regimen before allo-HSCT [79–81].
Conjugated antibodies have met a mitigated success to date, as illustrated by the initial withdrawal of GO. This is explained by their toxicity and by the restricted applications where they offer a therapeutic benefit [75, 82].

Numerous unconjugated antibodies are also developed. Some of these candidates exert their therapeutic effect by binding the AML cells and by recruiting immune cells through their constant region (Fc), triggering ADCC or ADCP (antibody-dependent cell cytotoxicity/phagocytosis), or by binding the complement (CDC) [78, 80].
Unconjugated antibodies can also act through antagonistic effects, by directly blocking binding sites for ligands (e.g anti-CXCR4, …) [83, 84]. The groundbreaking immune checkpoint inhibitors (The Nobel prize 2018 went to their discoverers, T. Honjo and J. Allison) also belong to this category of unconjugated antibodies. Although very efficient in some solid tumours, today's consensus tends to show that these molecules have a modest efficacy in monotherapy in AML [78, 85]. This is partly explained by the limited immunogenicity of AML cells [18, 19].

Various format of multivalent antibodies (BiTE, BiKE, …) are also currently developed. These molecules often combine a scFv targeting an AML marker (most often CD33, CD123), and another scFV binding CD3 (T cell engager) or CD16 (NK cell engager) [79, 80].

Finally, yet importantly, cellular therapies are also of a major interest in AML. CAR-T cells or CAR-NK cells are currently investigated [79, 86]. T or NK cells are genetically engineered to recognise AML cells (recognition of one or several markers that are expressed on AML cells) and infused in patients, possibly in combination with other agents. Cellular vaccines, based on DC presenting AML epitopes are also under clinical investigation [80, 87]. Although these approaches can be promising, these tailored therapies are very time and cost-demanding [88].

1.2. Epstein-Barr virus: key data, infection and T cell responses

1.2.1. Virus classification and EBV-associated diseases

The Epstein-Barr virus (EBV), also called human γ-herpesvirus 4 (HHV-4), is an orally-transmitted pathogen that infects more than 90% of the population worldwide [89]. This virus was initially discovered in cells from an African Burkitt's lymphoma. EBV has a classical herpesvirus structure, with an icosahedral nucleocapsid surrounded by a tegument and an outer viral membrane [90, 91]. Its genome is a linear, double-stranded, DNA fragment measuring 172kbp and has been reported to encode more than 85 genes [91].

Infection generally occurs during early childhood and is mostly asymptomatic. However, infection at a more advanced age, during adolescence or adulthood, may result four to seven weeks post-infection in infectious mononucleosis. This disease is characterized by fever, lymphadenopathy and pharyngitis [92].

Numerous cancers have been proved to be related to EBV. Tumours can emerge from B cells, such as Burkitt's lymphoma (BL), Hodgkin's lymphoma (HL), diffuse large B cell lymphoma (DLBCL) or lymphoproliferative disease (PTLD) [93, 94]. EBV can also be etiologically linked to T/NK cell cancers, like lymphomas and leukemia. Nasopharyngeal carcinoma (NPC) and gastric carcinoma, as well as leiomyosarcoma can emerge from EBV-infected epithelial cells or smooth muscle cells [93, 94]. These cancers account for more than 220.000 new cases a year, worldwide [95].

1.2.2. Chronology of EBV infection

The saliva is the primary vector of contamination for EBV. After entry in the host, viral replication starts in the oropharynx (Figure 4). It is still unknown, though, whether initial infection occurs in squamous epithelial cells in the tonsils, or in B cells in Waldeyer's ring [96, 97]. High levels of virions are then produced in the course of the lytic replication, supported by virus-shedding cells. In oropharyngeal tissues, growth-transformed B cells (latency III) support the spread of the infection. Some EBV-infected B cells enter the memory B cell pool after downregulation of the latency III program, down-regulating the expression of EBV antigens (latency 0). After immune control of the primary EBV infection, this pool of memory B cells establishes the reservoir of EBV, persisting in a lifelong latent infection. Infected cells can sporadically switch from latent to lytic replication within oropharyngeal tissues, leading to intermittent production of viral particles [96–98]

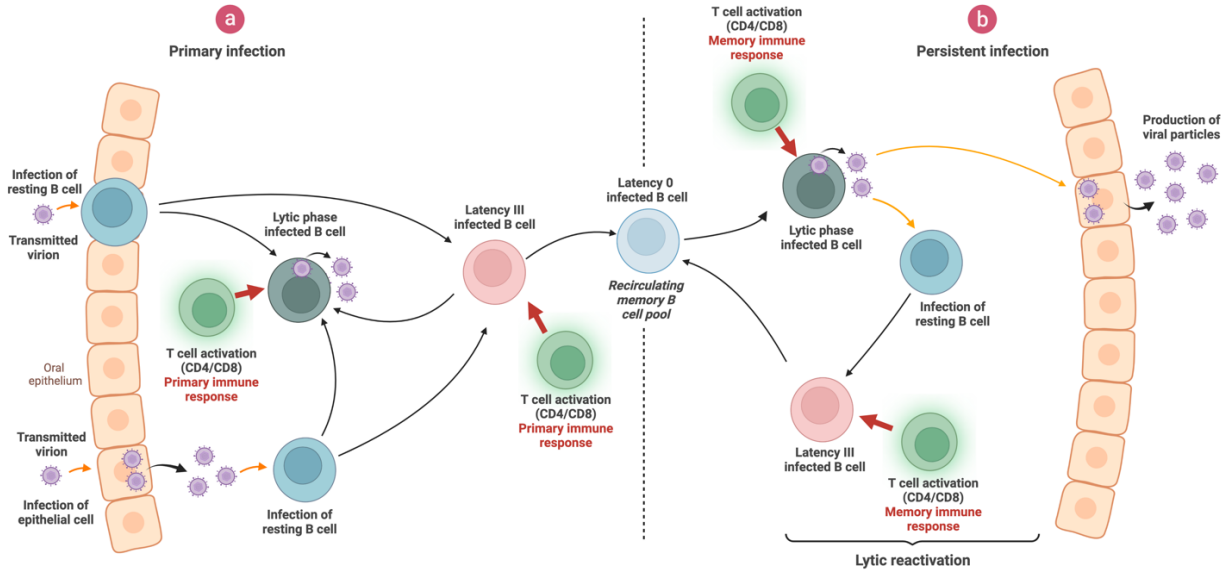

Figure 4: Primary and persistent infection by Epstein-Barr virus (data from [98]**)**
Figure created with BioRender.

1.2.3. Immune responses to EBV infection

Resolution of the initial replication of the virus, as well as the scarcity of long-term illnesses in healthy individuals underline a potent immune response toward EBV. Although unable to fully eliminate the virus, primary infection is associated with the activation of natural killer (NK) cells, together with the expansion of EBV-specific $CD4^+$ and $CD8^+$ T cells.

Natural killer cells have been shown to have a key role, both in the blood and in the tonsils in the course of EBV infection, through direct killing of EBV-infected cells and active secretion of pro-inflammatory cytokines [99, 100].
Other innate cell types play a role in the immune response. EBV-derived components can be recognised by toll-like receptors (TLRs) from monocytes (virions, TLR2) as well as myeloid (miRNA, TLR3) and plasmacytoid dendritic cells (unmethylated EBV genome, TLR9), paving the way for adaptive immune responses [101–103].

Primary infection also correlates with expanded $CD8^+$ and $CD4^+$ T cell pools, specific for EBV antigens (Figure 5). In patients with infectious mononucleosis (IM, symptomatic infection), specificity for lytic epitopes may account for up to 50% of the overall $CD8^+$ T cell pool [98].
The specificity for late proteins is decreased compared to immediate early antigens, consequently favouring immune evasion mechanisms in the course of the infection [104–106]. $CD8^+$ T cell responses to EBV latent epitopes account for up to 5% of the total $CD8^+$ T cell pool [107]. After resolution of the primary infection, pools of memory $CD8^+$ T cells specific for lytic and latent antigens persist in the host, and represent for up to 2% and 0,5% of the total $CD8^+$ T cell population, respectively [108, 109].
The magnitude of $CD4^+$ T cell response is weaker compared to the $CD8^+$ response. However, the EBV-specific $CD4^+$ T cells can constitute up to 1% of the total $CD4^+$ T cell pool [110, 111]. A pool of memory $CD4^+$ T cells also persists after resolution of the primary infection, and accounts for up to 0,1% of the overall $CD4^+$ T cell pool [110].
In EBV-seropositive patients, specificity for lytic antigens is equally distributed between immediate-early, early and late phases. However, the magnitude of $CD4^+$ responses toward latent antigens has been shown to exceed responses to lytic antigens [112, 113]. Three major latent antigens, namely EBNA-1, -2, and -3C, have been shown to elicit strong $CD4^+$ T responses [114]. Interestingly, it has also been reported that $CD4^+$ T cells specific for both lytic and latent antigens can be endowed with powerful cytotoxic properties [112, 115–118].

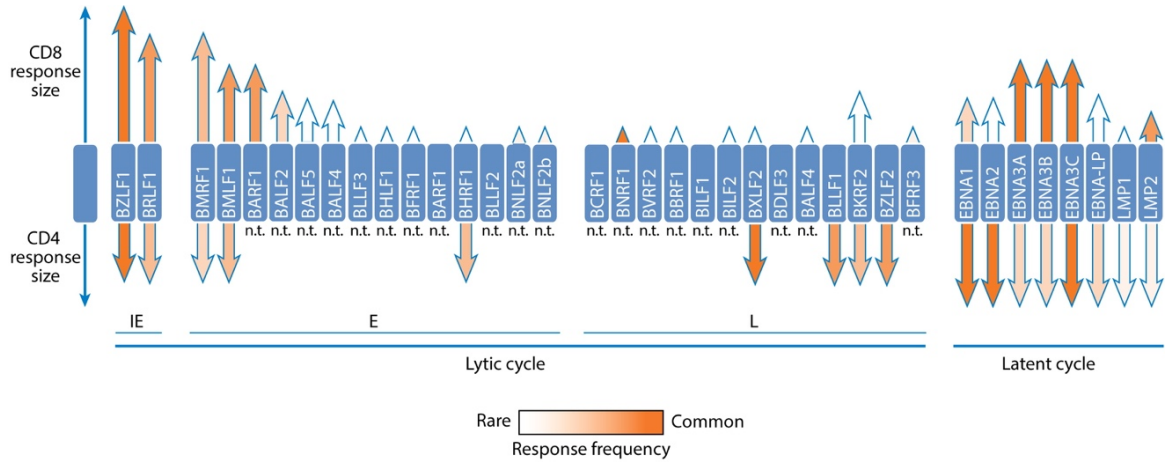

Figure 5: Response frequency of EBV-specific CD4$^+$ and CD8$^+$ T cells against lytic and latent cycle antigens in infected individuals (modified from [98]**).**
The height of each arrow corresponds to the response magnitude. The colour of each arrow (from light orange to dark orange) corresponds to the frequency of response across tested subjects. n.t. = not tested.

1.3. CD4$^+$ T cells: helper cells with a cytotoxic potential

1.3.1. T Helper phenotypes and implications in cancer

CD8$^+$ T cells are major actors of the adaptive immune response, acting through direct lysis of target cells after recognition of matched MHC-I/epitope. These cells are the preferred tool in cancer therapies since they directly recognise antigens presented at the surface of tumour cells. In contrast, CD4$^+$ T cells are mainly known as "helper T cells". They have been shown to be a cornerstone of adaptive immune response, through secretion of diverse cytokines influencing CD8$^+$ T cells and B cells, as well as cells from innate immunity.

After recognition of a matched MHC-II/epitope by their CD3/CD4 TCR complex, naïve CD4$^+$ T cells (also called Th0) can polarize into various helper phenotypes. These are characterized by their capacity to release different cytokines in their environment. At least 7 different types of CD4$^+$ T cell polarization have been described, namely Th1, Th2, Th9, Th17, Th22, Tfh (follicular helper T cells) and iTreg (regulatory T cells). The cytokine environment as well as the type of APC (pDC, cDC, …) are thought to be the main parameters that orchestrate the fate of CD4$^+$ T cells upon activation, triggering different cascades of master transcription factors. However, it has recently been shown that the strength of the TCR signal has also a role to play in the polarization [119].

Depending on the helper polarization, these cytokines can promote pro- or anti-inflammatory immune responses. As a consequence, polarized T cells can either play an antitumor role or conversely, support tumour development (Figure 6).

Three major polarizations have been found to have anti-tumour properties.

The Th1 polarization is the predominant anti-tumour helper phenotype. This pro-inflammatory phenotype also plays an important role in the defence against intra-cellular pathogens, including viruses [120]. Th1-helper T cells secrete IFNγ, IL-2 and TNF-α [121].

IFNγ is a pleiotropic cytokine that increases inflammation in the tumour microenvironment, through the recruitment of effector cells, such as tumoricidal M1-macrophages, NK cells and $CD8^+$ T cells [122–124]. This cytokine also boosts cytotoxic properties of these aforementioned cell types and favours cross-presentation by pDC (combined with CD40/CD40L interaction) [125]. Not only shaping the TME, IFNγ directly influences tumour cell immunogenicity by increasing the expression of MHC-I/-II [125]. IFNγ also has a direct tumoricidal effect on tumour cells [124], and raises their sensitivity to Fas/FasL and TRAIL death pathways [122–124].

IL-2 promotes the recruitment and the proliferation of NK cells and $CD8^+$ T cells [126, 127]. It also augments the expression of granzyme B by $CD8^+$ T cells [128].

TNF-α is a pro-apoptotic cytokine that can trigger cell death upon binding to its cognate receptors on tumour and endothelial cells [122, 129]. Besides its direct tumoricidal effect, it disrupts tumour vasculature [121].

Th9 helper T cells represent another potent antitumor polarization, with a similar functional profile. Interestingly, they have been found to be less sensitive to exhaustion in the TME [130]. These cells can secrete IL-9 and CCL20, which stimulate antigen uptake by DC and cross-presentation to $CD8^+$ T cells [130–132]. Moreover, secreted IL-3 reduces DC apoptosis and prolongs CTL activation, while secreted IL-21 increases the secretion of IFNγ by Th1 cells [132].

Although initially thought to have a role only in secondary lymphoid organs, follicular helper T cells seems to play a role in antitumor responses. They have been described among tertiary lymphoid structures in different tumour types and correlate with increased CTL function and survival [133–135].

It is important to note that some Th polarizations have contrasted effects on tumour control. Th17 and Th22 helper T cells are both endowed with the ability to secrete pro-inflammatory cytokines (CCL4, CCL17, CCL22, IL-21, IL-1β, TNF-α) but can also secrete IL-10 and TGF-β, two powerful anti-inflammatory cytokines [121, 136–138]. Furthermore, VEGF and IL-6 secretion mediated by Th17 cells promotes angiogenesis, recruitment of tumour-associated macrophages (TAMs) and myeloid-derived suppressor cells (MDSCs), resulting in an immunosuppressive TME [136].

Anti-inflammatory Th phenotypes are detrimental to an efficient anti-tumour response.
Th2 cells secrete IL-4, IL-5 and IL-13, which have been documented to contribute to cancer growth and metastasis [121, 139, 140]. Moreover, Th2 cells secrete IL-10, which suppresses antitumour Th1 cells, decreases MHC-II presentation and supports tumour cell survival via the activation of anti-apoptotic pathways [141, 142].
Low doses of pro-inflammatory cytokines, such as IL-2, together with the presence of anti-inflammatory cytokines, such as TGF-β, can favour the polarization of $CD4^+$ T cells into induced regulatory T cells (iTreg) [143]. These cells have a critical role in the maintenance of self-tolerance, and their malfunction can lead to auto-immune diseases [121, 143]. However, they play a detrimental role in cancer progression, suppressing antitumor responses and favouring cell dissemination [69]. Elevated levels of iTregs in the TME correlates with poor survival in patients with AML [68, 144]. First of all, they secrete potent immunosuppressive cytokines, such as IL-10, IL-35 and TGF-β [143, 145]. It has been shown that high doses of TGF-β can suppress the cytolytic activity in the TME [146]. iTregs decrease the availability of IL-2, trapping this cytokine with their high expression of membrane IL-2Rα (CD25) [143, 147]. Another aspect of iTreg suppression is the metabolic disruption of the TME, through the degradation of ATP into adenosine (CD39/CD73 pathway), another powerful anti-inflammatory mediator [143, 148]. Lastly, iTreg can influence antigen presentation through CTLA-4-mediated downregulation of CD80/86 (cell-cell contact mediated inhibition) [149].

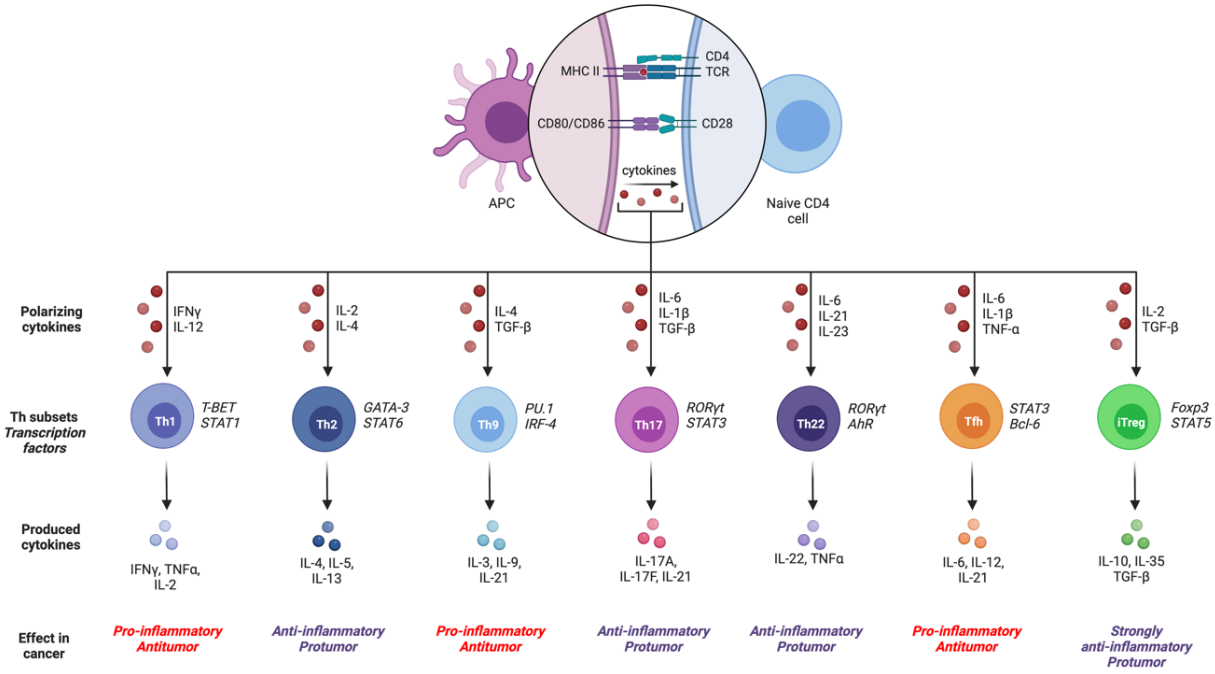

Figure 6: Polarizing cytokines, transcription factors and produced cytokines from the different helper CD4$^+$ T cell polarizations
Figure created with BioRender.

1.3.2. Cytolytic CD4$^+$ T cell: beyond the helper phenotype

In addition to their helper phenotypes, many reports have described cytolytic properties from CD4$^+$ T cell clones isolated from both human and mouse [150–153]. However, these cells being often cultured *in vitro* for long periods, their cytotoxic properties have been considered for long as artefactual.

More recently, CD4$^+$ CTL have been identified among human peripheral blood lymphocytes. This cell population was found to be expanded in pathological conditions, especially in chronic viral infections, such as human-immunodeficiency virus 1 (HIV-1), human cytomegalovirus (hCMV), Epstein-Barr virus (EBV) and hepatitis viruses [117, 118, 154–162]. CD4$^+$ CTL have also been observed in the acute phase of infection with other viruses (influenza, dengue, parvovirus B19, …), as well as after vaccination, showing that these cells are not restricted to chronic infections [163–170]. It is unclear, though, whether these cells have the same characteristics in acute and chronic infections.

In addition to human studies, CD4$^+$ CTL have been described in mouse infected with different viruses (MCMV, MHV68, ECTV, …) [171–174].

Beyond the secretion of cytokines, $CD4^+$ CTL have a crucial role in viral infections, especially in the fight again viruses that impair $CD8^+$ CTL function (EBV, CMV are prime examples of viruses that lead to downregulation of MHC-I) [175, 176].

Although these cells have mostly been studied in viral infection models, their role has now been established in other pathologies, including autoimmune diseases and cancer [177–180]. In several tumour models, $CD4^+$ CTL were found to be expanded in TILs, such as B-cell chronic lymphocytic leukemia (B-CLL) and melanoma [178–180].

In thymocytes, commitment to CD4 or CD8 lineage is controlled by master transcription factors. In MHC-II restricted $CD4^+$ T cells, *ThPOK* (T helper-inducing POZ Krueppel factor) has been shown to suppress cytolytic activity. In MHC-I restricted $CD8^+$ T cells, *RUNX3* (Runt-related transcription factor 3) has an antagonist effect and promotes CTL activity. It has been shown that $CD4^+$ CTL could derive from transcriptional reprogramming of mature Th cells, which silenced *ThPOK,* leading to the disinhibition of the cytolytic program in mature $CD4^+$ cells [181].

However, *in vitro* experiments revealed that introduction of Eomesodermin (also known as T-box brain protein 2) is sufficient to induce CTL activity in fully differentiated Th cells [182, 183]. In T cells, Eomesodermin expression is regulated by Runx3. Recent *in vivo* observations established that $CD4^+$ CTL activity is linked to the upregulation of a $CD8^+$ T cell gene signature, including *EOMES* and *RUNX3*, but not necessarily with the silencing of *ThPOK* [183, 184].

Numerous studies evidenced a cytotoxic potential from all Th polarizations [175, 185–188]. Th9 cells have recently gained interest regarding their cytotoxic potential [130, 189].

However, the vast majority of $CD4^+$ CTL seems to derive from Th1 $CD4^+$ T cells [118, 156, 175, 190]. T-bet together with Eomesodermin, promote the expression of cytotoxic compounds along with pro-inflammatory mediators, mostly IFN-γ [163, 164].

Both the cytokine environment and the antigen characteristics seem to impact the generation of $CD4^+$ CTL [176]. Although IFN-γ may not be fundamental in the acquisition of cytotoxic properties, IL-2 has a critical role [163, 185]. A high dose of antigen has been shown to induce a moderate cytotoxicity in absence of IL-2, albeit essentially mediated by Fas/FasL pathway [176, 186]. Independently from the antigen dose, transcriptional activation of perforin and granzyme B mostly relies on IL-2 [176]. Other cytokines can synergize with IL-2, or compensate lower IL-2 concentrations, such as type-I IFN, IL-6 or IL-15 [181, 191, 192].

Two major cytotoxic pathways have been evidenced in $CD4^+$ CTL, which are shared with other cytotoxic cells, $CD8^+$ CTL and NK cells (Figure 7). The first major cytotoxic effector mechanism is the Fas/FasL pathway [176]. FasL (CD178), expressed at the surface of the CTL, can bind its cognate receptor Fas (CD95) at the surface of the target cell. Trimerization of CD95 prompts the recruitment of FADD together with pro-caspase 8, forming a Death-Inducing Signalling Complex (DISC) [193–195]. Activation of caspase-8 allows for the cleavage of caspase-3, which once activated cleaves further cell substrates, triggering apoptosis [196].

The second cytotoxic mechanism is mediated by the exocytosis of cytoplasmic granules that are released in the immunological synapse [176, 197]. These granules contain perforin, a pore-forming protein that can insert in the membrane of the target cell, enabling the cell entry of other compounds from the granules, namely granzymes and granulysin [197–200]. Five types of granzymes, which are pro-apoptotic serine proteases, have been described in the granules. Granzymes A and B are the most studied and the most abundant [200–203]. While granzyme A has a wide diversity of substrates, granzyme B induces the apoptosis through the direct cleavage of caspase-3 [200, 204].

Additionally, granzyme B can act independently from caspases, impairing other targets such as anti-apoptotic proteins or enzymes involved in DNA-repair [205].

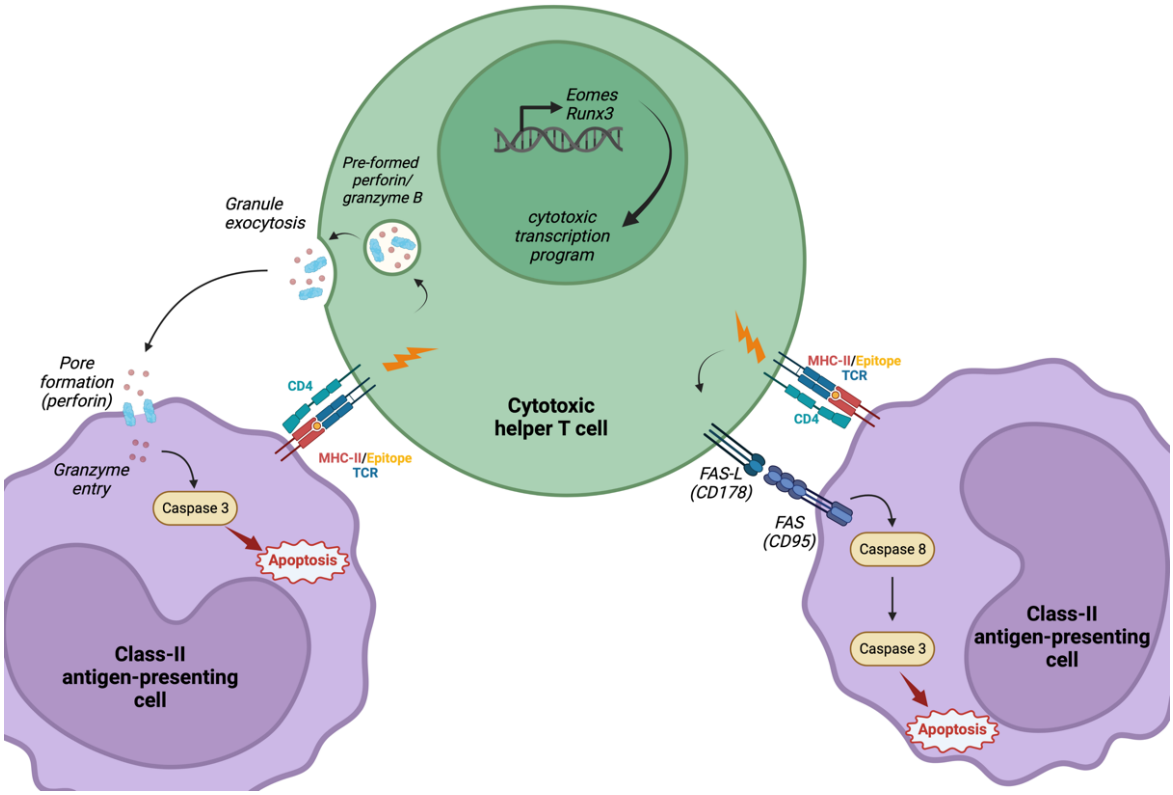

Figure 7: Cytotoxic pathways upon TCR engagement on a cytotoxic $CD4^+$ T cell.
Granzyme B/perforin and FAS-L pathways lead to the cleavage of effector caspases, culminating in the apoptosis of the antigen-presenting cell. *Figure created with BioRender.*

1.4. Principle of AgAbs therapy and application to AMLs

1.4.1. Concept and previous assessments of AgAbs

The concept of antigen-armed antibody, or AgAb, characterizes a chimeric fusion protein which comprises a monoclonal antibody fused to an antigenic region from an infectious agent (bacteria or virus). The antibody acts as a vector to specifically deliver the antigenic payload to a target cell that expresses the target marker and MHC-II. Upon binding of the AgAb to this marker, the whole complex can be internalized through receptor-mediated endocytosis. The endosome enclosing this complex then fuses with lysosomes, leading to the degradation of the AgAb by cathepsins. After fusion with a MHC-II loading compartment, the antigenic payload can be loaded on MHC-II molecules, depending on the compatibility with the haplotype of the cell (HLA-II in humans). MHC-II/antigen complex is finally relocalized to the plasma membrane, where it can be recognised by specific TCR from $CD4^+$ T cells. Activation of the specific $CD4^+$ T cell leads to the release of pro-inflammatory cytokines (IL-2, IFNγ, TNFα) and eventually to the lysis of the target cell [206, 207] (Figure 8).

These antibodies were firstly described in 1997 by Lunde and colleagues [206]. Designed to deliver T cell antigens to B cells, AgAbs were shown to increase the efficacy of antigen presentation by up to four orders of magnitude compared to the peptide [206–208]. This property raised the interest for AgAbs as a vehicle to deliver foreign peptides to APC in a vaccination setting [209].

In that respect, several studies mainly targeting dendritic cell makers (DEC-205, Langerin, Clec9a) demonstrated the potential of AgAbs in inducing a protective immune response against bacterial and viral antigens. These vaccines prompted potent $CD4^+$ T cell responses together with humoral responses specific for the delivered antigens in immunized mice [210–212]. AgAbs were also assessed in an anti-tumour vaccine strategy and were shown to elicit CTL responses specific for the tumour-associated antigen *in vivo* [213].

The ability of AgAbs to deliver epitopes in a specific fashion, together with an increased efficacy of T cell stimulation, widened their scope of application beyond vaccination.

Anti-DEC-205 AgAbs conjugated with EBV antigens successfully targeted EBV-transformed B cells, leading to the activation of EBV specific $CD4^+$ T cells [214].

In 2015, Yu and colleagues firstly reported the potential application of antigen-armed antibodies in the treatment of a haematological malignancy [215]. AgAbs against B cell markers CD19-CD22 and conjugated with EBV epitopes successfully targeted Burkitt's lymphoma

cells. Antigen presentation to EBV-specific CD4$^+$ T cells lead to their activation, culminating in the elimination of the lymphoma cells [215]. In 2019, Schneidt and colleagues successfully expanded EBV-specific CD4$^+$ T cells out of PBMC samples from B-cell chronic lymphocytic leukemia patients (B-CLL). AgAbs targeting B cell markers and conjugated with large fragments from Epstein-Barr virus Nuclear Antigen 3C (EBNA3C) were employed in this study. A large proportion of amplified CD4$^+$ T cells expressed granzyme B and successfully eliminated donor-matched CLL cells [216].

These recent studies indicate that AgAbs could be used to redirect cytotoxic activity from virus-specific CD4$^+$ T cells (especially EBV-specific T cells) toward tumour cells. This provides a tremendous advantage to AgAbs over many other T cell therapies that harness unspecific cytotoxicity (BiTE, CAR-T cells, …), increasing the severity of the side effects [217]. A strategy based on AgAbs may also be less onerous, easier and quicker to implement compared to cost and time consuming tailored therapy such as CAR-T cells.

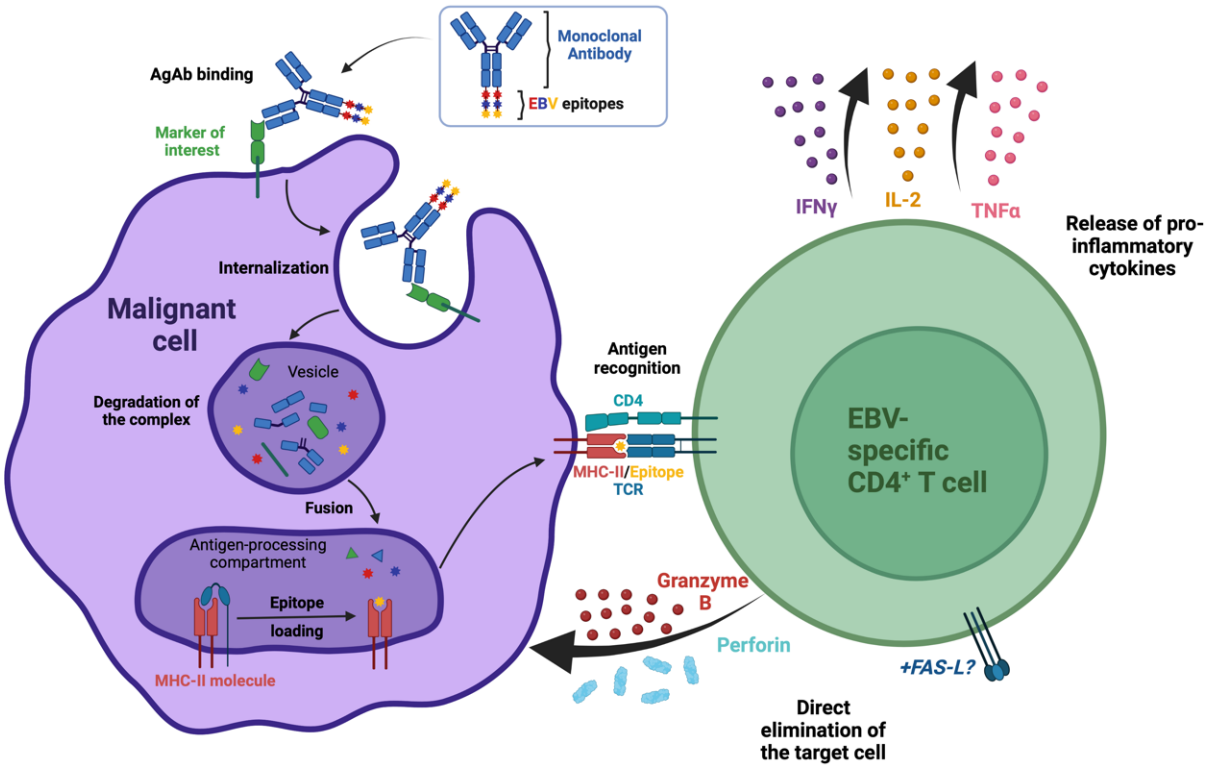

Figure 8: Principle of action of antigen-armed antibodies

AgAbs can internalize within the malignant cell upon binding of the target marker. After processing, class-II epitopes can be loaded onto MHC-II molecules. These complexes are then exposed at the cell surface, which can activate epitope-specific CD4$^+$ T cells. Activation of these cells is characterized by the release of pro-inflammatory cytokines (IFNγ, IL-2, TNFα) but also granzyme B and perforin. FAS-L=Fas-ligand, TCR=T cell receptor. *Figure created with BioRender.*

1.4.2. Application of the AgAbs strategy to AML

Application of AgAbs to cancer treatment has been restricted to date to B cell malignancies. However, several of the vaccination studies targeted dendritic cells with success, showing the feasibility to target cells from the myeloid lineage [210–212]. AML management has seen poor recent progress in its treatment armada, especially in immunotherapy, in spite of numerous clinical trials. Immune checkpoint blockades failed to demonstrate a significant efficacy, partly due to the low immunogenicity of AML cells [18, 19]. The use of AgAbs in this pathology would grant the delivery of a strong antigen to the tumour cells. This could ultimately boost the basal immunogenicity of tumour cells, favouring their recognition by the immune system, similarly to what has been described in BCL and B-CLL models.

Several studies reported defective T cell responses in AML patients [65, 218]. Low antigen stimulus, together with an immunosuppressive microenvironment impair the T cell response. However, it is now established that this suppressed phenotype is reversible [72, 73, 219]. Indeed, most of the compromised T cells from AML patients underwent activation and proliferation upon TCR stimulation in the presence of immune checkpoint inhibitor (either PD-1, Tim-3, or CTLA-4) [219]. Furthermore, the number of T cells in the blood and the bone marrow has been shown to be similar or higher in AML patients versus healthy individuals [65, 66]. This underlines the need of a strong antigen to activate specific T cells, and combination with an immune checkpoint therapy may be beneficial.

One cornerstone of AgAb therapy is the expression of MHC class II molecules. In previous assessments, expression of these molecules was not of concern since tumour B cells generally express high levels of MHC-II [220].
At diagnosis, expression of MHC-II molecules has been reported on more than 80% of AML samples. Of note, half of the samples with an undetected HLA-DR expression derived from patients with APL, which prognosis is the most favourable among all FABs, due to high response rate to ATRA treatments [40].
MHC-II expression has been shown to be dampened on some samples from patients after chemotherapy or allogenic hematopoietic stem cell transfer [221].
This sustains the applicability of AgAbs in AML patients, especially at diagnosis.

1.4.3. Markers to target AML blasts

The specificity of immunotherapies relies on the presence of markers on target cells, that are ideally absent from healthy tissues. Although such markers have not been described yet, several markers gained interest over the last decades due to their elevated expression on AML blasts.

CD33, also known as Siglec-3 or gp67, is a transmembrane sialic acid binding immunoglobulin-type lectin receptor expressed on hematopoietic cells. Upon binding of sialic acids, the phosphorylation of intracellular ITIM domains leads to the recruitment of SHP-1/-2 phosphatases, triggering pathways that inhibit the activation of myeloid cells [222]. Studies showed a decreased cell proliferation, together with a dampened secretion of cytokines (IL-1β, TNF-α, IL-8) upon binding of CD33 on myeloid cells [222]. CD33 expression is restricted to hematopoietic tissues. In healthy individuals, it is expressed on early multi-lineage progenitors (CFU-GEMM, CFU-GM, CFU-G and E-BFU), on monoblasts and myeloblasts, monocytes, and mast cells. It is also expressed on granulocyte precursors with a decreased expression on more mature stages [223, 224]. In contrast, CD33 is mostly absent from pluripotent hematopoietic stem cells, platelets, erythrocytes but also B, T and NK lymphocytes [223].
CD33 is expressed on 90% of AML samples, and its expression on bone marrow blasts is increased compared to healthy CD33-positive bone marrow cells (mean of 10.380 molecules per cell on bone marrow AML blasts versus 2997 molecules per cell on normal CD33-positive bone marrow cells) [225]. NPM1-mutated and FLT3-ITD AML have been shown to have high CD33 expression [226]. Furthermore, higher CD33 expression is associated to poorer overall survival and shorter event-free survival following CD33-unrelated treatment [227, 228].
In spite of promising pre-clinical and early clinical results, unconjugated monoclonal anti-CD33 antibodies failed to demonstrate a therapeutic benefit [229, 230]. Antibody-drug conjugates have also been developed, the Gemtuzumab-Ozogamycin reaching the market in 2000 after its FDA approval (before its withdrawal in 2010 and re-approval in 2017 – see part 1.1.5.) [74, 224].
CD33 has been widely investigated and is still the target of numerous constructs under clinical investigation. Various formats to target CD33 AML cells are evaluated, such as radioconjugates, bispecific antibodies (e.g. AMG330), tandem diabodies (AMV564) and CAR-T cells [81, 231–233].

CD123 is the alpha-chain of the interleukine-3 receptor. It heterodimerizes with CD131 (common to IL-5 receptor and GM-CSF receptor) to form the active IL-3 receptor [234]. IL-3 is mainly produced by T cells and its binding to CD123 decreases apoptosis while inducing proliferation and differentiation of myeloid progenitors [235]. CD123 is expressed on basophils, monocytes, dendritic cells and some endothelial cells [236–238]. Its expression has also been reported on a fraction of hematopoietic stem cells, mostly myeloid progenitors, but is mostly absent from pluripotent stem cells [239].

CD123 is expressed in several diseases, such as myelodysplastic syndromes, subsets of B-/T-ALL, in some lymphomas, and in blastic plasmacytoid dendritic cell neoplasms (BPDCN) [238]. More than 80% of AML samples are positive for CD123, the expression being detected both on blasts and on leukemic stem cells/leukemia initiating cells [234, 238]. Furthermore, the average expression of CD123 on AML cells is significantly higher compared to healthy blood and bone marrow cells [236].

CD123 expression is especially high in NPM1-mutated and FLT3-ITD AML [240]. Similar to CD33, high CD123 expression has been correlated to a poorer prognosis and to higher frequency of residual disease after induction chemotherapy [241, 242]. This observation can be associated to the anti-apoptotic effect of IL-3 signaling.

Interestingly, CD123 has been shown to be expressed on most CD33-negative samples, as a result, nearly all AML samples can be targeted with either anti-CD33 or anti-CD123 therapies [240].

One molecule targeting CD123 has already been approved in the treatment of BPDCN, named Tagraxofusp (approved in 2018 in the U.S and in 2021 in the E.U.) [243, 244]. This molecule is a cytotoxin consisting in recombinant IL-3 fused to a truncated diphtheria toxin. This compound is also tested in AML therapy, where encouraging effects have already been observed [244].

Like CD33, monoclonal antibodies targeting CD123 (Talacotuzumab, KHK2823) failed to demonstrate sufficient efficacy in AML treatment [244–246]. Various format of CD123-targeting molecules are under clinical trials: antibody-drug conjugates (IMGN632), bispecific antibodies (Flotetuzumab, XmAb14045, APVO436), and CAR-T cells (MB102), in single agents or in combination with other compounds [243, 244, 247–250].

Although therapies in current development have manageable toxicities, severe ones have dampened the development of several CD123-targeting drugs, especially capillary leak syndrome and other side effects linked to the binding of the molecules to endothelial cells (cardiac, gastro-intestinal and nervous disorders) [244, 245]. These latter may be reduced with

AgAbs since endothelial cells generally express low to no MHC-II (but inducible under stress conditions) [251, 252].

CLL-1 is a member of the C-type lectin superfamily. It is also known as CLEC12A (C-type lectin family member 12A), MICL or CD371. This molecule is a transmembrane glycoprotein that plays a crucial role in the control of myeloid cell activation during inflammation, by acting as a negative regulator of monocyte and granulocyte function [253, 254]. Its ligands are unknown though.

CLL-1 is restricted to hematopoietic cells. It is expressed on monocytes, granulocytes and on some committed myeloid progenitors, but is absent from hematopoietic stem cells [255, 256]. In contrast, CLL-1 has been shown to be expressed on 80% of AML samples, and its expression remains stable in the course of the disease [257–259]. Importantly, it is also significantly expressed on leukemic stem cells [260]. It has been suggested that CLL-1 can shape the tumour microenvironment, CLL-1^{high} patients having more infiltrating Tregs and higher expression of immune checkpoints [261].

Of note, CLL-1 has been shown to be one key target, in combination with CD33, in the treatment of paediatric AML [262].

Numerous approaches targeting CLL-1 on AML cells have been assessed in preclinical studies [254]. CLL-1 can efficiently internalize upon binding of a monoclonal antibody, which encouraged the development of ADCs. Interestingly, anti-CLL-1 ADCs were shown to be effective at depleting AML cells while having limited off-target toxicity in preclinical models [263–265]. Beyond monoclonal antibodies, bispecific antibodies have also been investigated, and one candidate even reached clinical assessment (MCLA-117) [254, 266]. CAR-T cells have also been developed, and several of these chimeric constructs are currently subjected to clinical assessment [257, 267, 268].

Folate receptor-beta (FR-β) is a GPI-anchored protein, with a high affinity for folic acid and for some its reduced derivatives (including 5-methyltetrahydrofolate). Upon binding of the ligand, the receptor internalizes and reduced pH in the endosome induces a conformational change that triggers the release of the cargo [269]. This protein was initially thought to be restricted to the placenta, but it was later detected on neutrophils and tissue-resident macrophages [270]. Interestingly it is absent from healthy $CD34^+$ hematopoietic stem cells [271]. In contrast, FR-β is expressed on more than 70% of AML samples, especially in promyelocytic leukemia, but also on CML cells [271]. Furthermore, it is expressed on M2 anti-

inflammatory macrophages, which support the tumour growth [270, 272, 273]. Furthermore, FR-β expression can be induced or upregulated on AML cells through ATRA-treatment [274]. The relatively narrow off-tumour expression pattern favoured the preclinical development of targeted therapies. FR-β has been investigated to deliver liposomal formulations of chemotherapies, such as doxorubicin [274–276]. More recently, several studies assessed monoclonal antibodies and anti-FR-β CAR-T cells in different models [273, 277–279]. Interestingly, some of these studies underlined the absence of cytotoxic activity toward healthy HSCs, confirming the absence of FR-β expression on these cells [278, 279].

The characteristics of these markers, including their internalization abilities, together with active investigations on tools targeting these molecules encouraged me to use them as targets for antigen-armed antibodies.

1.4.4. Conjugation of viral antigenic regions

Previous publications demonstrated that antigen-armed antibodies can vehicle epitopes from various pathogens into target cells. In the previous assessments from the laboratory, Epstein-Barr virus was the preferred source of epitopes. This is particularly linked to the very high seroprevalence of this life-long persistent virus among the human population. As a result, most of the individuals have a pre-existing immunity for EBV epitopes. Furthermore, this virus has been shown to elicit potent cytotoxic $CD4^+$ T cell response, especially for latent-cycle antigens (including EBNA1, EBNA2 and EBNA3C proteins) [98]. In principle, delivering EBV epitopes with AgAbs could recall a memory cytotoxic response in almost all individuals. In AML patients, EBV epitopes could serve as strong antigens to build a powerful immune response, relying on a pre-existing pool of cytotoxic $CD4^+$ T cells.
However, these delivered epitopes could only be presented on AML cells and activate $CD4^+$ T cells if the latter epitope and the AML cell haplotype display a compatible match.
For *in vitro* assessments, where the MHC-II haplotypes of target cells is known, single epitopes can be employed as antigenic load. This is made possible by the previous knowledge on EBV epitopes and correspondence between human haplotypes and the ability to present specific EBV peptides to $CD4^+$ T cells.

However, *ex vivo* assessments will more resemble to the situation with actual patients receiving the potential treatment: the MHC haplotype is rarely known in advance. Furthermore, single-epitope AgAbs would require a tailored approach for clinical treatment that would be both time- and cost-consuming. In previous assessments from the laboratory, it has been shown that AgAbs can deliver long antigenic domains to B cell lymphoma and chronic lymphocytic leukemia cells [215, 216]. Aside from being a universal source of epitopes adapted to a broad spectrum of patients, large antigenic domains would increase the number of recognised epitopes in a single individual.

Epstein-Barr nuclear antigen 3C (EBNA3C) was the preferred source of epitopes for AgAbs in the previous BCL and B-CLL studies. Similar fragments could be used in the AML study, in regard to the magnitude of the $CD4^+$ T cell response triggered by this protein in the course of the EBV infection [98, 280]. In addition, fragments from EBNA1 and EBNA2, two other immunogenic proteins with high $CD4^+$ T cell reactivity could be used to further enrich the repertoire of epitopes [98, 280]. Unlike EBNA3C, most of the described epitopes in EBNA1 and EBNA2 are gathered in a specific subpart of these proteins [110, 162, 280–282]. As a result, shorter fragments with higher antigen densities could be conjugated to antibodies.

In vivo assessments will also require the pre-existence of memory $CD4^+$ T cells in the mice. However, EBV is a human pathogen that does not infect mice. To circumvent this limitation, a model involving another herpesvirus can be used instead. Murine cytomegalovirus (mCMV) is a beta-herpesvirus with a similar infection cycle to the one of EBV. In addition, many class-II epitopes have been described in the two most common murine genetic backgrounds (namely BALB/c and C57BL/6) [283–285]. Interestingly, some epitopes have also been shown to induce a cytotoxic $CD4^+$ T cell reaction, which is consistent with observations in anti-EBV immunity [172].

1.5. Objectives of the present work

Antibodies loaded with EBV epitopes have been shown to be promising tools in the fight against different B cell malignancies, namely B cell lymphoma and chronic lymphocytic leukemia [215, 216]. Additionally, some studies already demonstrated the feasibility to target cells from the myeloid lineage, such as dendritic cells, with antibodies fused to an antigenic payload [210–212]. Altogether, these encouraging results provide the rational for testing antigen-armed antibodies in a myeloid pathology. The characteristics of acute myeloid leukemia cells as well as the poor prognosis of AML patients support the assessment of AgAbs in this cancer.

This doctoral work aims at demonstrating the validity of the AgAb-approach in the treatment of acute myeloid leukemia.

In that prospect, this study has four major objectives:

- Generation of a panel of antigen-armed antibodies suitablefor AML cells targeting.
- Assessment of the validity of the AgAb-approach using a panel of human AML cell lines *in vitro*.
- Evaluation of the therapeutic potential of antigen-armed antibodies with AML patient samples *ex vivo*.
- Development of an appropriate murine model of AML and assessment of the AgAb-strategy in this *in vivo* model.

2. Results

This chapter summarizes the principal experimental procedures and the results gathered during this doctoral work. The project was articulated around three main axes, each one being another model where antigen-armed antibodies have been extensively studied. I started with *in vitro* experiments, exploring the potential of AgAbs with human leukemia cell lines, then human leukemia patient samples have been used in *ex vivo* experiments, and finally, a mouse leukemia model was developed for *in vivo* assessments.

2.1. Development of an AgAbs-based strategy in acute myeloid leukemia and validation *in vitro*

2.1.1. Exploration of targetable markers at the surface of AML cells

Many molecular markers have been described as promising targets at the surface of AML cells. Among these molecules, CD33, CD123, CLL-1 (CLEC12A) and FR-β are well-characterized. These four molecules are at least over-expressed on AML blasts compared to healthy cells. Furthermore, some constructs which target these molecules (monoclonal antibodies, CAR-T cells, …) have already reached the stage of clinical trials. To deliver the antigen to MHC-II loading compartments within target cells, antigen-armed antibodies need to be directed against a marker endowed with internalization properties. Interestingly, these four markers seem to internalize upon targeting [77, 265, 286, 287].

In order to confirm the repartition of these markers on AML cells, I constituted a panel of 12 AML cell lines from different FAB classes. These cell lines were stained for CD33, CD123, CLL-1 and FR-β, but also for HLA-DR, a molecule crucial for antigen presentation (Figure 9). I found that all the stained cell lines expressed CD33, which is consistent with the clinical observations (more than 90% of the samples positive for CD33) [223]. CD123 and CLL-1 were also widely expressed (11 and 10 positive cell lines, respectively). FR-β was expressed on 5 cell lines but its expression could also be induced on further cell lines in response to all-trans retinoic acid (ATRA). Moreover, studies suggest that this marker is found on a higher proportion of patients (more than 70% [271]), which confirms its potential as a target for AgAbs. Finally and importantly, 9 cell lines (75%) were found to express HLA-DR at baseline,

and the three other lines could express it in response to IFNγ treatment (10ng/mL for 48 hours). Although expected, this portion is slightly lower than what is usually observed in AML patients (85% of AML patients positive for MHC-II at diagnosis) [288].

(A)

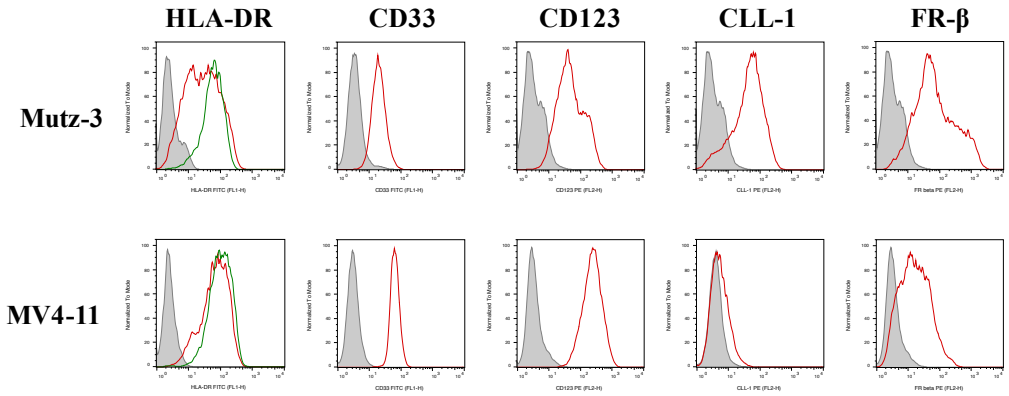

(B)

Cell line	FAB class	HLA-DR	CD33	CD123	CLL-1 (CD371)	FR-β
KG-1	M0	+	+	+	+	low
HL-60	M2	+	+	-	+	-
Kasumi-1	M2	+	+	+	-	-
GDM-1	M4	+	+	+	-	-
Mutz-3	M4	+	+	+	+	+
OCI-AML2 or 3	M4	Low (but Ind.)	+	+	+	low
MOLM-14	M5a	+	+	+	+	-
NOMO-1	M5a	+	+	+	+	low
MonoMac6	M5b	+	+	+	+	-
THP-1	M5b	Low (but Ind.)	+	+	+	+
MV4-11	M5	+	+	+	low	+

Figure 9: Expression profile of the investigated markers on AML cell lines
AML cells from 12 different cell lines were stained with markers specific for HLA-DR, CD33, CD123, CLL-1 or FR-β. Binding of the aforementioned antibodies was detected in flow cytometry. **(A)** Staining figures obtained for Mutz-3 and MV4-11 cell lines. The shaded curves represent isotype control binding (murine IgG1). The red curves represent the binding of the indicated antibodies (the green curves in HLA-DR staining represent the HLA-DR signal upon pre-treatment with 5ng/mL IFN-γ for 48 hours). **(B)** Summary of the stainings performed with the 12 cell lines. + indicates a positive expression / - indicates a negative expression. HLA-DR induction was tested with 5ng/mL IFN-γ for 48 hours.

In order to support the use of these markers for AgAb-therapy, I also confirmed the absence of expression on effector cells that act in tumour rejection, especially T and NK cells, but also on B cells. To this end, I stained the PBMCs from 6 healthy donors with antibodies specific for the markers of interest, in combination with antibodies specific for CD3, CD56 or CD19 (T cell, NK cell and B cell marker, respectively). In so doing, no significant event expressing both a T/B/NK cell marker and one AML marker could be detected in flow cytometry (no significant increase compared to the isotype controls, see figure 10 for assessment on T cells). Furthermore,

no significant event expressing both an AML marker and MHC-II could be detected in the lymphocyte population. This observation is consistent with the current knowledge about these markers.

Altogether, these first observations support the applicability of AgAbs to AML cells and their absence on normal immune cells. This encouraged me to construct antibodies specific for these four markers.

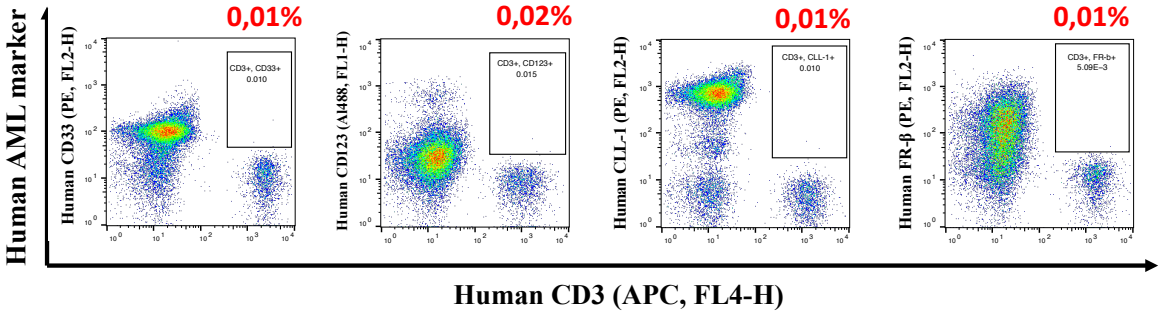

Figure 10: Expression of AML markers on T cells from healthy donor PBMCs

Healthy donor PBMCs were purified and stained with antibodies specific for one of the AML markers (CD33, CD123, CLL-1, FR-β), or the matching isotype control (mIgG1), and an antibody specific for CD3 (the same experiment was repeated with CD19 and CD56 – not shown). Fluorescence was then analysed in flow cytometry. No significant event expressing both CD3 and an AML marker could be detected (Isotype control: 0,02% in the same gate – *data not shown*).

2.1.2. Generation of AML cell lines that match EBV-specific CD4$^+$ T cell clones

For subsequent functional studies, I conducted a predictive analysis to match the HLA-DR$^+$ AML cell lines with EBV-specific CD4$^+$ T cell clones available in the laboratory. The haplotypes from all the AML cell lines were found on the TRON cell line portal or on the Expasy-Cellosaurus database [289, 290]. Several matches were predicted, including NOMO-1 with BZLF1 3H11, Mutz-3 and KG-1 with EBNA3C 3H10 and EBNA1 3G2, and MV4-11 with gp350 1D6. These predictions were confirmed in T-cell assays, where the predicted cell lines were pulsed with the matching peptides before co-incubation with the specific CD4$^+$ T cell clones. As positive controls, LCL cells generated from the same donors as each T cell clone were identically pulsed with the matching peptides. The co-culture supernatants were then screened for IFNγ, evidencing the T cell activation and thus, the functional presentation of the peptide by the AML cell line (Figure 11). KG-1, MonoMac6 and Mutz-3 cell lines effectively presented EBNA1 3G2 and EBNA3C 3H10 epitopes, and so did MV4-11 with gp350 1D6 and NOMO-1 with BZLF1 3H11.

For subsequent experiments, I decided to focus on EBNA3C 3H10 and gp350 1D6 epitopes, due to the efficient expansion of the specific $CD4^+$ T cell clones upon routine stimulation.

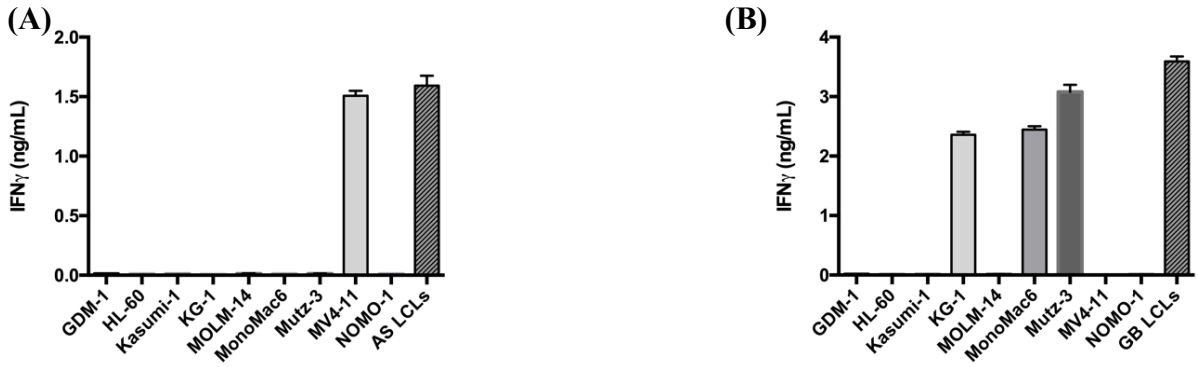

Figure 11: T cell assays with HLA-DR^+ AML cell lines, with gp350 1D6 (A) or EBNA3C 3H10 peptide (B)

Target AML cells (or control LCLs) were pulsed overnight with 100ng 1D6 **(A)** or 3H10 **(B)** peptide. The following day, the cells were washed and co-incubated with 1D6-specific **(A)** or 3H10-specific **(B)** $CD4^+$ T cells. After 18 hours, the supernatants were collected and checked for IFNγ in ELISA. All assays were performed in triplicates with means and standard deviations displayed in the graphs.

2.1.3. Generation of native anti-human antibodies and short AgAbs

Native antibodies were constructed by conjugating variables parts (V_H and V_L) to constant regions (C_H from a murine IgG2a and C_L from a murine kappa light chain) using a PCR-based approach. As illustrated in the methods section and in figure 12, V_H regions were PCR-amplified and extended in their 3'-end with the 5'-end of the C_H region. Conversely, the C_H region was PCR-amplified and extended in its 5'-end with the 3'-end of each V_H region. The variable and constant regions were then fused through overlap PCR. The same principle was adopted for the cloning of the four light chains. During the overlap PCR step, short epitope sequences (EBNA3C 3H10 or gp350 1D6) were added at the 3'-end of all the heavy chains to create short AgAbs coding sequences (epitope sequence included in the reverse primer used for the overlap). All heavy and light chains were finally inserted in pRK5 vectors and transformed into DH5α *E.coli* bacteria. The list of all the produced clones (light chains, heavy chains in their native form or conjugated to either EBNA3C 3H10 or gp350 1D6) is given in the table 11 from the material section.

The antibodies were produced in HEK293T cells. For that purpose, light and heavy chains (either native or conjugated to an epitope) were mixed respecting a 3:1 mass ratio and complexed with branched polyethylenimine (PEI, 1:1 mass ratio PEI:DNA).

The complexes were then dropped onto pre-plated HEK293T cells. The media were changed for serum-free condition (FreeStyle 293 medium) 6 hours post-transfection. The supernatants containing the antibodies were harvested after 5 to 7 days and concentrated.

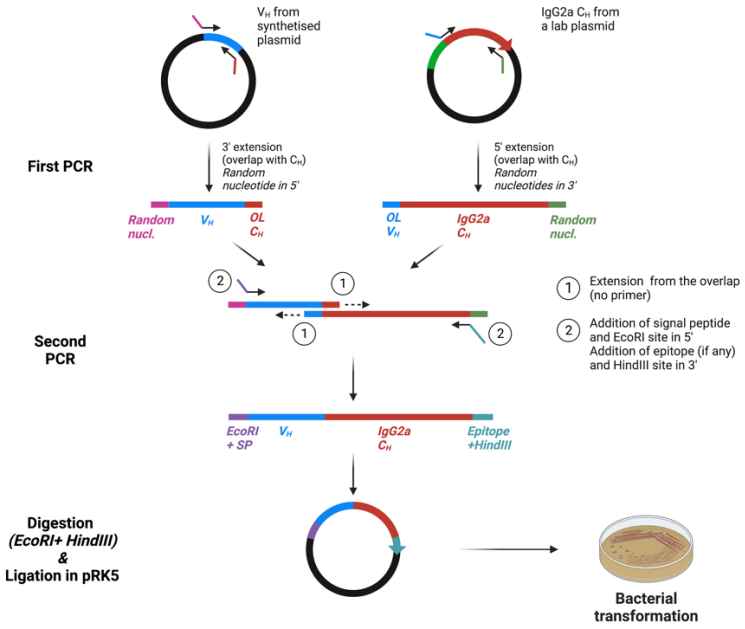

Figure 12: Overview of the cloning strategy for the generation of native or antigen-armed heavy chains
Variable and constant parts were first PCR-amplified with primers allowing the creation of an overlap. The second PCR primarily bound variable and constant regions through their overlap (extension steps), then, primers were added to amplify the whole heavy chain (reverse primer including the epitope in the case of an AgAb). The heavy chains were finally digested with EcoRI/HindIII and inserted in pRK5 vector before bacterial transformation. *Figure created with BioRender.*

Anti-CD21 mIgG2a was also produced with the corresponding plasmids that were available in the laboratory (B233 for heavy chain and B200 for the light chain). Once produced, this antibody was used in a binding assay with AML cell lines, in order to verify the absence of off-target signal with an antibody targeting a marker not expressed on these cell lines. The binding assay yielded a strong signal with all the tested AML cell lines, although negative for CD21 (increase in the mean of fluorescence by 10-fold versus secondary antibody only – Figure 13). This observation was explained by the binding of the Fc-region from the murine IgG2a to human high affinity gamma receptor I (hFcγRI), which is highly expressed on myeloid cells [291]. The double substitution leucine into alanine at positions 234 and 235 ($L_{234}A$, $L_{235}A$ – called "LALA") in the Fc region of the mIgG2a has previously been described to reduce FcγR binding [292]. This double mutation was introduced in the Fc region of murine IgG2a heavy chain through site-directed mutagenesis. Fc-mutated anti-CD21 could no longer bind hFcγRI,

as evidenced by the absence of signal in a binding assay (Figure 13). However, the mutations neither affected the production yield, nor the specific binding of anti-CLL-1 to KG-1 cells. This supported the interest of using Fc-mutated (LALA) murine IgG2a for further experiments. Antibodies targeting CD33, CD123, CLL-1 and FR-β, in their native form or conjugated to EBNA3C 3H10 or gp350 1D6 were cloned using this mutated heavy chain constant region.

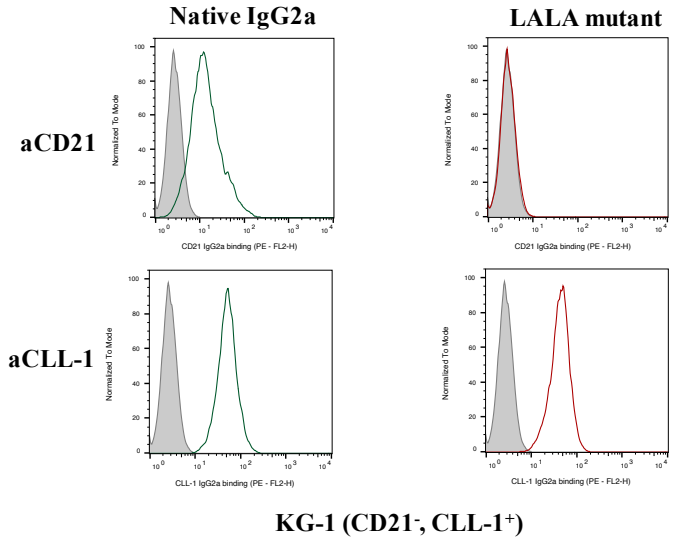

Figure 13: Binding assay of anti-CD21 and anti-CLL-1 IgG2a with or without LALA Fc-mutations

KG-1 cells ($CD21^-$, $CLL\text{-}1^+$) cells were incubated with anti-CD21 or anti-CLL-1 native mIgG2a with (green curves) or with $L_{234}A/L_{235}A$ mutations (red curves). Binding of the respective antibodies was detected using a secondary anti-mouse IgG (H+L) antibody and the fluorescence was measured in flow cytometry. The shaded curves represent the signal obtained with the secondary antibody only.

All these antibodies were produced in HEK293T as described above. Their correct assembly and size were checked in western-blot, in non-reducing conditions, using a 7.5% acrylamide gel (Figure 14). The titers were always checked in a IgG2a-specific enzyme-linked immunosorbent assay (ELISA), and were commonly ranging from 2 to 10µg/mL depending on the target.

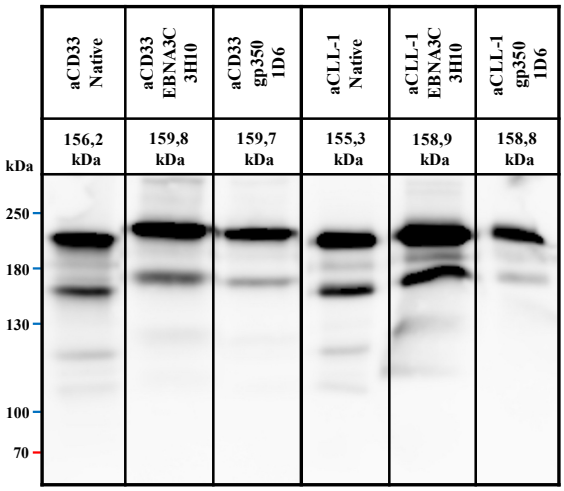

Figure 14: Expression profile of anti-human CD33 and CLL-1 antibodies, either native or conjugated to EBNA3C 3H10 or gp350 1D6 epitopes

5µL of transfection supernatants were mixed with protein loading buffer (non-reducing conditions) and loaded onto a 7.5% acrylamide gel. Antibodies were detected on the membrane with an anti-mouse IgG (H+L) HRP antibody. The membrane was exposed with substrate for 5 minutes in a chemiluminescence imager.

2.1.4. Anti-human AgAbs can deliver their viral payload to human AML cells

Once produced and characterized (Western-Blot and ELISA), native antibodies and short AgAbs were ready for further assessments.

First of all, I verified that both native antibodies and the AgAb counterparts could bind their targets on AML cell lines (Figure 15). For that purpose, binding assays were conducted, where Mutz-3 cells were incubated with all 4 native antibodies (CD33, CD123, CLL-1, FR-β) and their EBNA3C 3H10-conjugated counterparts. An anti-CD21 with the LALA mutations was used as an isotype control. The binding of these antibodies was detected with an anti-mouse IgG secondary antibody. No significant difference could be detected between native antibodies and their AgAb counterparts. The same experiment was conducted with gp350 1D6 antibodies and the MV4-11 cell line.

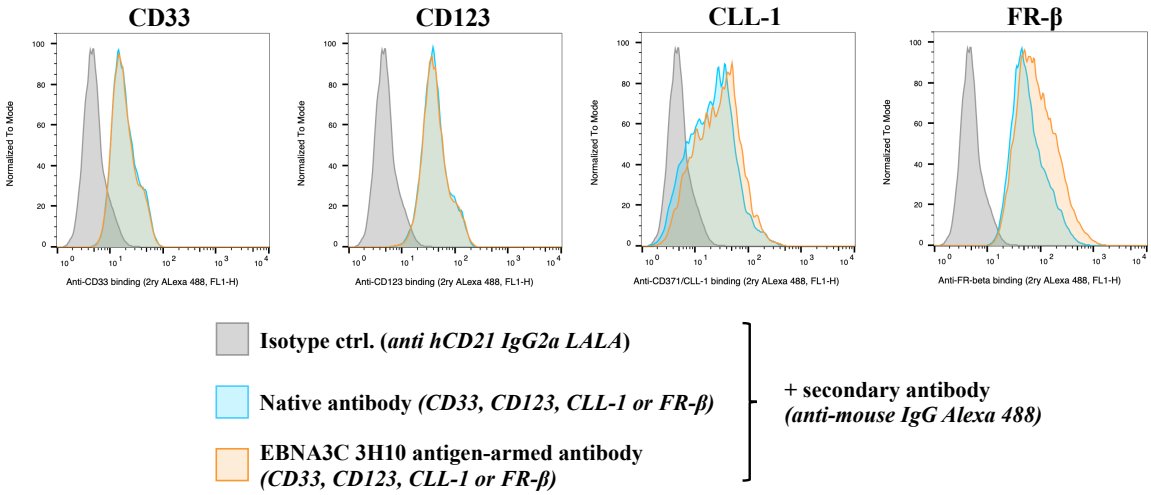

Figure 15: Assessment of the binding capacities of the cloned antibodies, in their native form or conjugated to EBNA3C 3H10 epitope

Mutz-3 cells were incubated with anti-CD33, CD123, CLL-1 or FR-β mIgG2a (LALA), unconjugated (Native, blue curves) or conjugated with EBNA3C 3H10 (orange curves). Binding of the respective antibodies was detected using a secondary anti-mouse IgG (H+L) antibody and the fluorescence was measured in flow cytometry. The shaded curves represent the signal obtained with the anti-CD21 (LALA) which was used as an isotype control.

Next, I assessed the ability of the AgAbs to be processed and to deliver their viral payload to the target cells. For that purpose, Mutz-3 cells were incubated overnight with different doses of 3H10 AgAbs or peptide (ranging from 0.1ng to 100ng per 5.10^4 target cells in 150µL), or native antibodies (100ng per 5.10^4 target cells in 150µL – highest dose only). The following day, Mutz-3 cells were washed to get rid of unbound peptides/antibodies and co-incubated with

EBNA3C 3H10-specific $CD4^+$ T cells (effector to target (E:T) ratio equal to 2:1). After 18 hours, the co-culture supernatants were screened for IFNγ in order to confirm the activation of the $CD4^+$ T cells. The results from three independent replicates were pooled together and are shown in figure 16A. All four AgAbs triggered a significant release of IFNγ at all tested doses, while native antibodies did not yield any significant signal. Interestingly, peptide treatment with doses lower than 10ng failed to activate T cells, although a significant release of IFNγ was still triggered by comparable doses of AgAbs, and this even at the lowest concentration. CD33 AgAbs appeared to be slightly more effective at activating T cells than AgAbs targeting the three other targets, although this observation could be related to the specific internalization properties of this particular CD33-specific antibody.

A similar experiment was conducted with the KG-1 cell line, which also matches EBNA3C 3H10, but displays a reduced HLA-DR expression compared to Mutz-3 cell line. Substantial IFNγ release could be detected upon AgAb treatment, although significantly lower than that observed with the $HLA\text{-}DR^{high}$ Mutz-3 cell line (Figure 16B).

The ability of AgAbs to target AML cells and to activate T cells was further assessed with another T cell clone. The MV4-11 cell line was used as a target after exposure to gp350 1D6 $CD4^+$ T cells (Figure 16C). Along with the previous experiments, anti-CD33, CD123 and FR-β 1D6-AgAbs could significantly activate gp350 1D6 T cells at all assessed doses, whereas the 1D6 peptide did not trigger significant activation at doses below 10ng. Interestingly, anti-CLL-1 AgAbs activated T cells at the highest dose, although CLL-1 expression can barely be detected at the surface of MV4-11 cells. This observation illustrates the ability of AgAbs to target cell clones with a decreased marker expression at the cell surface.

In conclusion, antigen-armed antibodies specific for markers expressed at the surface of AML cells can be efficiently processed and activate epitope-specific $CD4^+$ T cells, even when target markers or MHC-II are expressed at low levels.

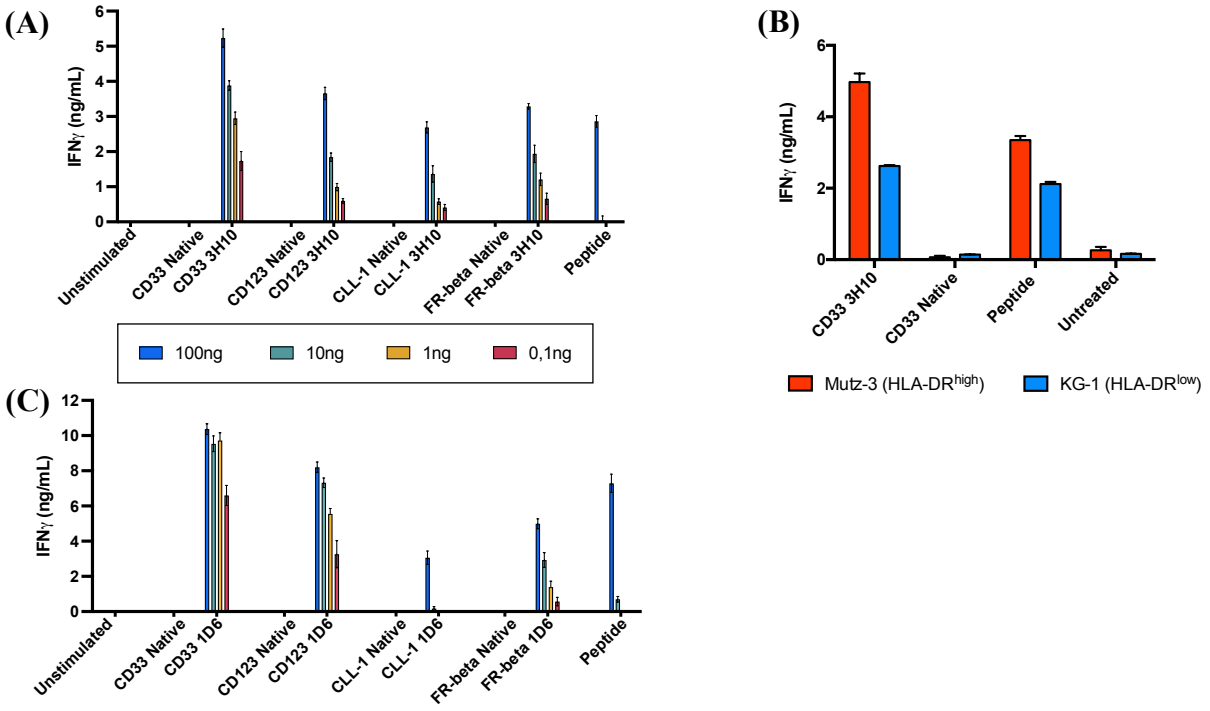

Figure 16: Antigen-armed antibodies can vehicle antigen to AML cells resulting in the activation of EBV-specific CD4$^+$ T cells

Target AML cells (Mutz-3 in **A**, KG-1 in **B**, MV4-11 in **C**) were pulsed overnight with 0,1-100ng EBNA 3H10 (**A** and **B**) or gp350 1D6 AgAbs (**C**), their native counterparts, or the epitope peptide only (amounts per 5.10^5cells). The following day, the cells were washed and co-incubated with 3H10-specific (**A** and **B**) or 1D6-specific (**C**) CD4$^+$ T cells at a E:T=2:1. After 18 hours, the supernatants were collected and checked for IFNγ in ELISA. All assays were performed in triplicates with means and standard deviations displayed in the graphs.

2.1.5. Short AgAbs can redirect anti-EBV cytotoxicity toward AML cells

It is well established that CD4$^+$ T cells specific for EBV epitopes can be endowed with cytotoxic properties, most often characterized by the secretion of granzyme B, a serine protease that can cleave cellular proteins and trigger cell death.

In order to verify that the activation of CD4$^+$ T cells in response to AgAb exposure was accompanied by the release of granzyme B, the supernatants from T cell assays described in the previous section were also screened for the presence of this enzyme. The titers from three independent experiments were pooled and are shown in figure 17. Of note, discrepancies in the T cell reactivity from one replicate to another led to enlarged standard deviations.

Interestingly, granzyme B titers recapitulated the observations drawn for IFNγ release. In both Mutz-3/EBNA3C 3H10 and MV4-11/gp350 1D6 T cell assays, AgAb treatment yielded significant granzyme B release in the supernatants, evidencing a cytotoxic activation of both T cell clones in response to AgAbs (Figure 17). In line with the IFNγ-release, AgAbs triggered

granzyme-B release even at the lowest dose (except for CLL-1 1D6 and MV4-11), while granzyme B could be not detected for peptide doses below 10ng.

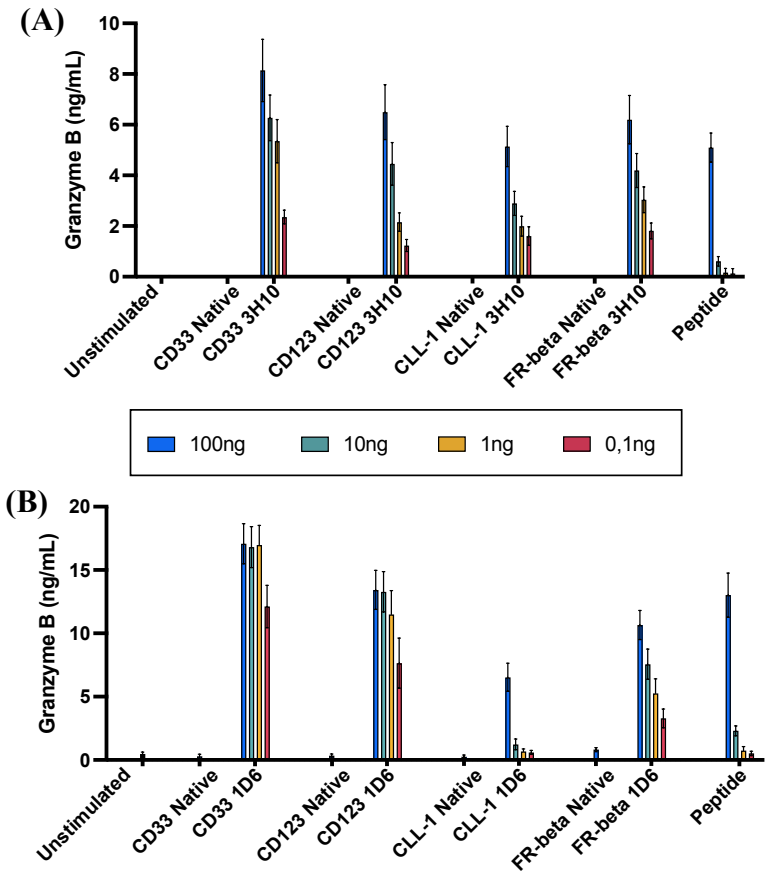

Figure 17: AgAbs can trigger granzyme B release upon activation of EBV-specific CD4$^+$ T cells

Target AML cells (Mutz-3 in **A**, MV4-11 in **B**) were pulsed overnight with 0,1-100ng EBNA3C 3H10 (**A**) or gp350 1D6 AgAbs (**B**), their native counterparts, or the epitope peptide only (amounts per 5.10^5 cells). The following day, the cells were washed and co-incubated with 3H10-specific (**A**) or 1D6-specific (**C**) CD4$^+$ T cells at a E:T=2:1. After 18 hours, the supernatants were collected and checked for granzyme B in ELISA. All assays were performed in triplicates with means and standard deviations displayed in the graphs.

Although secreted granzyme B gave a first evidence that AgAbs can redirect EBV-specific CD4$^+$ T cell cytotoxicity toward AML cells, a direct measurement of the AML cell viability after treatment was performed. To that aim, Mutz-3 AML cells were pulsed with 3H10 AgAbs or peptide, or native antibodies (100ng – highest dose from the TCA – per 5.10^4 target cells in 150µL). The following day, the cells were washed and stained with calcein-AM, a cell-permeant dye which is turned into a membrane-impermeant fluorescent dye by esterases in the cytosol of live cells. Finally, calcein-stained Mutz-3 cells were mixed with EBNA3C 3H10-specific CD4$^+$ T cells at different E:T ratios (ranging from 1:1 to 15:1), and co-incubated for 4 hours. The supernatants were then collected, and the fluorescence was measured to detect the release of calcein by cells that became permeable (cells that underwent apoptosis), allowing a direct quantification of Mutz-3 cell death. The results from three independent experiments were pooled and are shown in figure 18A. First of all, I confirmed that EBNA3C 3H10 T cells could kill Mutz-3 cells displaying the matched epitope (AgAb or peptide stimulation). Treatment with native antibodies did not lead to a significant T cell killing. Moreover, treatment with all four

AgAbs elicited a cytotoxicity at least as high as the one triggered by the peptide (over 30% of target cell eliminated). Furthermore, treatment with CD33 and CD123 led to an enhanced killing efficacy, which is in line with the previously observed higher IFNγ and granzyme B titers in response to these AgAbs. As expected, higher killing efficacies were observed at higher E:T ratios. Similar trends were obtained upon repetition of this experiment with MV4-11 cell line and gp350 1D6 $CD4^+$ T cells (this T cell clone seemed to be less cytotoxic than E3C 3H10 though – *data not shown*). In this setting, even CLL-1 1D6 successfully redirected T cell cytotoxicity toward MV4-11 cells, although to a lesser extent in comparison with other AgAbs. In order to evaluate the potency of AgAbs at more "physiological" E:T ratios, I decided to repeat the killing assay by adopting a different approach. Since calcein is toxic to the cells, overnight assessments were impossible to achieve. To circumvent this limitation, AgAb/peptide-pulsed Mutz-3 cells were stained with CFSE (lower toxicity) and mixed with an equal number of EBNA3C 3H10 $CD4^+$ T cells (E:T=1:1). The following day, the cells were recovered and stained with LIVE/DEAD™ Fixable Far-Red Stain (Invitrogen™). The T-cell cytotoxicity was evaluated in flow cytometry by the direct quantification of the LIVE/DEAD-positive fraction among CFSE-positive population. Strikingly, between 40% and 80% of target cells were specifically eliminated in response to AgAbs or peptide, CD33 3H10 remaining the most effective stimuli (Figure 18B and C).

In accordance to the results from the calcein-release assay, no significant cytotoxicity was detected upon treatment with the native antibody. Moreover, incubation of pulsed Mutz-3 cells with unmatched gp350 1D6 T cells did not lead to any T cell killing. Of note, extending the co-incubation did not significantly increase the killing efficacy, partly due to increasing background death of target cells from control conditions over-time (toxicity of CFSE, medium not favourable for T cell survival leading to the death of the effector cells, …). This prevented a long-term analysis of the killing efficacy from activated T cells. Increasing the E:T ratio could have increased the killing though, but an excessively high E:T ratio would have decreased the significance of the results due to an unphysical rate of T cells per target cell. Importantly, the survivor AML cells were still positive for the target markers.

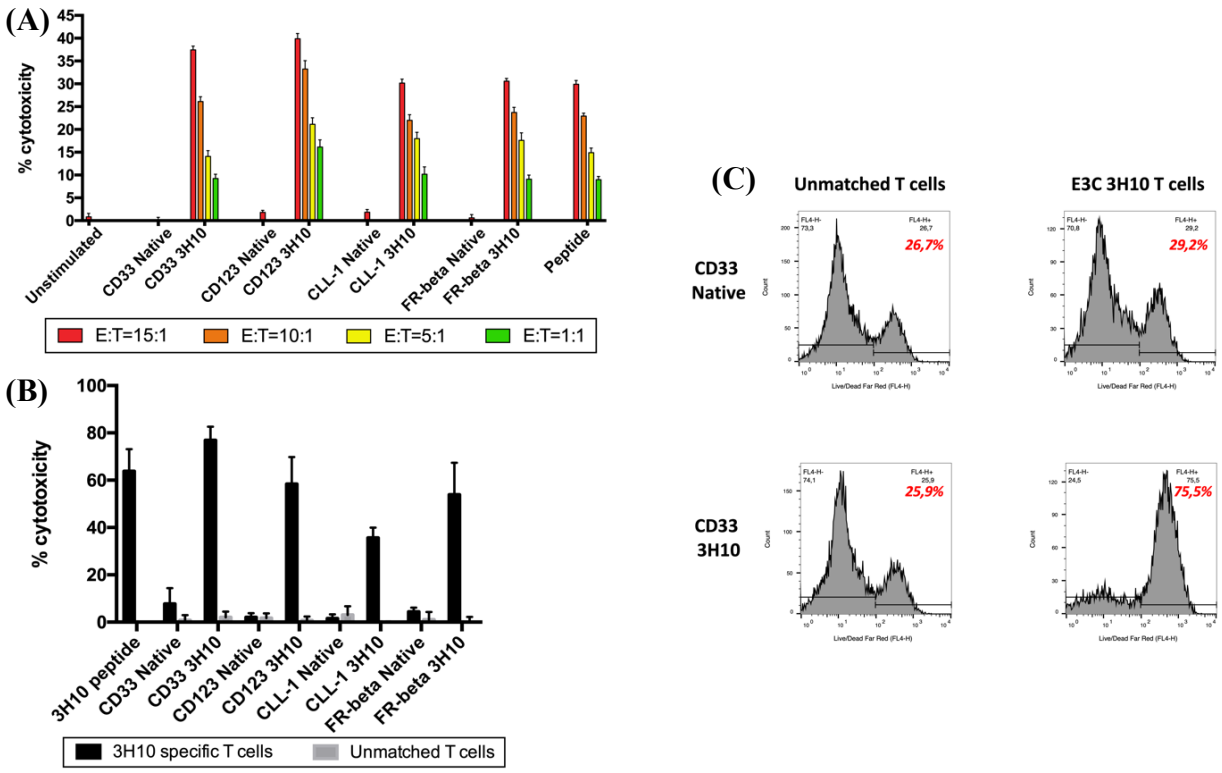

Figure 18: Antigen-armed antibodies can redirect CD4$^+$ T cell cytotoxicity toward target AML cells

(A) Short-term killing assay: Mutz-3 cells were pulsed overnight with 100ng 3H10-AgAbs or native counterparts, or 3H10 peptide. The following day, the cells were washed and stained with Calcein-AM before co-incubation with E3C 3H10-specific CD4$^+$ T cells at varying E:T ratios (from 1:1 to 15:1). After 3 hours, the supernatants were collected and calcein fluorescence was measured (λ_{ex}=485nm, λ_{em}=535nm). Cytotoxicity was calculated as the percentage of maximum killing (see methods section for formula). **(B-C)** Overnight- killing-assay: Mutz-3 cells were pulsed overnight with 100ng 3H10-AgAbs or native counterparts, or 3H10 peptide. The following day, the cells were washed and stained with CFSE before co-incubation with E3C 3H10-specific CD4$^+$ or unmatched T cells at an E:T ratio = 1:1. After 18 hours, the cells were collected and stained with LIVE/DEAD™ Fixable Far-Red Stain. The cytotoxicity was measured in flow cytometry as the percentage of L/D$^+$ cells among CFSE$^+$ cells (see methods section for formula). **(B)** presents the summary of the ON killing assay assessments; **(C)** presents an example of flow cytometry figure for CD33 native versus CD33 3H10 conditions (L/D stainings shown for a gating on CFSE$^+$ cells).

All assays were performed in triplicates with means and standard deviations displayed in the graphs.

2.1.6. Immune checkpoints are upregulated on T cells and target cells upon AgAb treatment

2.1.6.1. AgAbs treatment favours the upregulation of immune checkpoints on T cells and target cells

Immune checkpoints are membrane proteins expressed on effector or target cells which modulate the immune reaction upon binding of their ligands. Typically, these immune checkpoints are expressed on effector cells in response to their activation, or when cells are exposed to pro-inflammatory cytokines. I selected nine well-documented immune checkpoints commonly expressed on T cells – six inhibitory and three stimulatory immune checkpoints – and measured their expression on T cells upon AgAb-mediated activation.

PD-1 (CD279) interacts with PD-L1 (CD274). Lag-3 (CD233) binds MHC-II. TIGIT interacts with CD155. Tim-3 has multiple ligands including Ceacam-1 and Galectin-9. VISTA, which can be expressed on both T cells and APCs, binds PSGL-1. All these molecules are often expressed on exhausted or suppressed T cells, and their interaction with their ligands generally leads to the repression of the TCR signalling, due to the recruitment of phosphatases [293].

CTLA-4 (CD152) binds CD80/86 on APCs and out-competes CD28, which blocks co-stimulatory signal and leads to the inhibition of T cell cytotoxicity [293].

Stimulatory checkpoints include OX-40/CD134 (binds OX-40L/TNFSF4), 4-1BB/CD137 (binds 4-1BB-L/TNFSF9) and GITR/TNFRSF18/CD357 (binds GITRL/TNFSF18). These molecules are often upregulated on activated T cells (peaked expression generally 24 to 72 hours after T cell activation). The interaction of these molecules with their cognate ligand triggers cell pathways that lead to an increased T cell proliferation and survival, together with an augmented secretion of pro-inflammatory cytokines [293, 294].

Additionally, I determined the expression of PD-L1, an inhibitory immune checkpoint on both T cells and target cells.

Mutz-3 cells were pulsed with 100ng anti-CD33 3H10, since this AgAb triggered robust killing in functional assays. The native CD33 antibody served as a negative control. The cells were subsequently co-incubated with EBNA3C 3H10 T cells. In order to increase the number of survivor target cells for ensuing stainings, the E:T ratio was lowered to 1:3 (instead of 1:1 in killing assays). After 24 or 48 hours, the cells were harvested and stained for the immune checkpoints included in the panel, before analysis in flow cytometry. The signal was measured only on the relevant cell population (either target or effector cells – even for PD-L1, for which two separate assessments were conducted). CD69 was used as a surrogate marker for T cell

activation. For each molecule, the mean of fluorescence in the CD33 3H10 condition was normalized to the mean of fluorescence from the CD33 native condition (Figure 19). After one day of co-incubation, a three-fold increase in the MFI could be detected for CD69 on T cells, evidencing their activation in response to CD33 3H10 pre-treatment. All markers but TIGIT had an increased expression on T cells incubated with Mutz-3 cells pre-treated with AgAbs, in comparison to their native counterpart. PD-1, PD-L1 and CTLA-4 were the inhibitory checkpoints with the highest upregulation (up to four-fold versus native condition). Of note, CTLA-4, Lag-3 and Tim-3 only had a slightly higher normalized MFI at 48 hours after the beginning of the co-incubation. Interestingly, upregulations of OX-40 and 4-1BB stimulatory checkpoints on T cells were of a much higher magnitude (up to 10-fold). Finally, PD-L1 expression was also increased on survivor Mutz-3 cells pre-treated with CD33 3H10 compared to CD33 native.

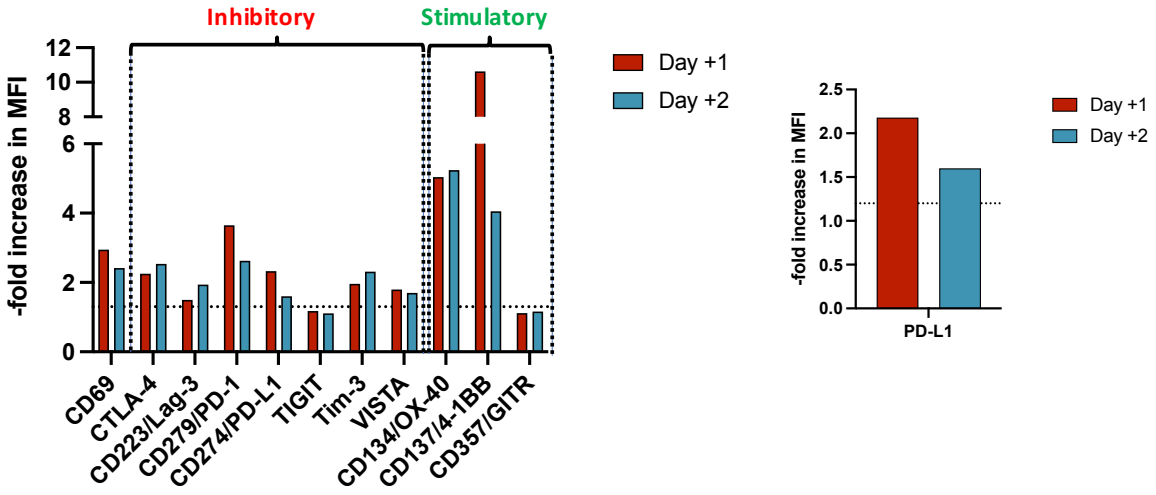

Figure 19: AgAb-treatment increase the expression of immune checkpoints on both T cells and survivor target cells

Mutz-3 cells were pulsed overnight with 100ng CD33 3H10 or CD33 native antibodies. The cells were then washed and co-incubated with E3C 3H10-specific $CD4^+$ T cells at E:T=1:1.

The following day (day +1) or two days later (day +2), the cells were collected and stained for CD123 (identification of AML cells) or CD3 (identification of T cells), in combination with one of the analysed stimulatory or inhibitory immune checkpoints. The figure shows the ratio of MFI between CD33 3H10 and CD33 native conditions for each analysed marker.

Since the T cells are derived from stimulation cultures and were thus activated ten days before the experiment, background levels of immune checkpoints were already high on T cells at baseline. Indeed, the MFI for most immune checkpoints was already increased when Mutz-3

were previously pulsed with native antibody, in comparison with the MFI obtained upon stainings with respective isotype controls.
I repeated the very same experiments with the MV4-11 AML cell line, together with gp350 1D6 T cells and CD33 1D6 AgAbs. All inhibitory checkpoints but TIGIT were upregulated, with the strongest increase observed for the PD-1/PD-L1 axis.
Altogether, these results encouraged me to assess combinations of AgAbs with immune checkpoint modulators, especially anti-PD-1/PD-L1 in further assays.

2.1.6.2. Addition of immune checkpoint inhibitors slightly increases the efficacy of AgAbs

The PD-1/PD-L1 axis seemed to be one of the most promising targetable pathways in regard to its consistent over-expression in the previous experiments. However, anti-PD-1/PD-L1 therapy failed to demonstrate a significant efficacy in patients with AML to date, which can partly be explained by the low immunogenicity of AML cells [17, 85]. Considering that AgAbs enhance the immunogenicity of AML cells by delivering viral epitopes, this strengthened the rationale for combining AgAbs with these immune checkpoint inhibitors.
To test the ability of AgAbs to synergize with immune checkpoint modulators, I repeated the T cell and killing assays with AgAbs or native antibodies (highest concentration only, 100ng per 5.10^4 target cells in 150µL) as a single agent, or in combination with either anti-PD-1, anti-PD-L1 or the combination of both (5µg/mL). The latter ICB were added upon co-incubation between Mutz-3 target cells and EBNA3C 3H10-specific $CD4^+$ T cells. In T cell assays, addition of anti-PD-1 or anti-PD-L1 slightly increased the titers of both IFNγ and granzyme B secreted in response to AgAbs (Figure 20A). No significant difference was found between PD-1 and PD-L1 blockade though. The combination of both immune checkpoint inhibitors generally further increased the cytokine titers, although the effect remained subtle. Interestingly, the addition of immune checkpoints did not increase the background cytokine titers detected upon stimulation with native antibodies, or in unstimulated conditions.
In killing assays, the addition of anti-PD-1/PD-L1 only minimally increased the killing efficacy of EBNA3C 3H10 $CD4^+$ T cells in response to AgAbs (Figure 20B). However, their addition did not increase the killing efficacies in response to native antibodies, consistently with the observations from the T cell assays.

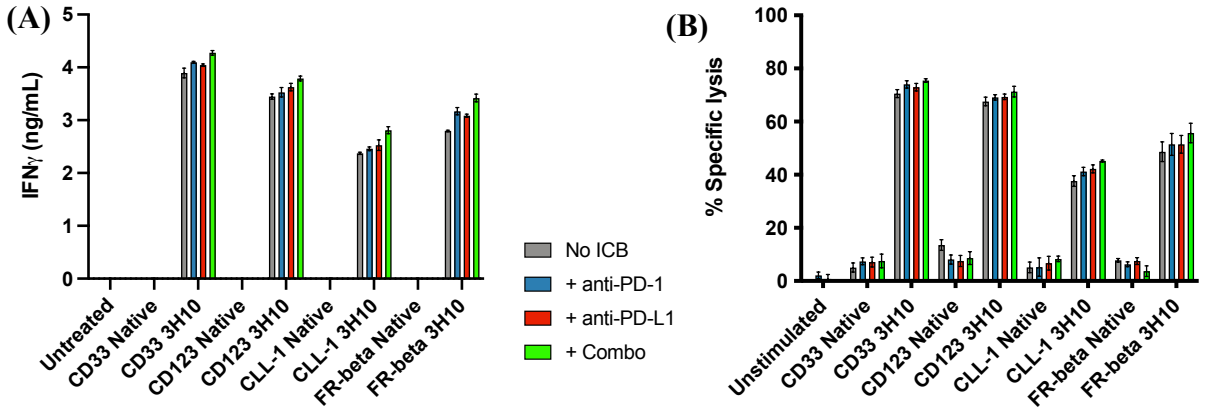

Figure 20: Immune checkpoint inhibitors slightly but not significantly enhance the activation of CD4$^+$ T cells in response to AgAbs

Mutz-3 cells were pulsed overnight with 100ng 3H10-AgAbs or native counterparts, or 3H10 peptide. The following day, the cells were washed and stained with CFSE before co-incubation with E3C 3H10-specific CD4$^+$ or unmatched T cells at an E:T ratio = 1:1. After 18 hours, the supernatants were collected and IFNγ titers were checked in ELISA **(A)**.The cells were also collected and stained with LIVE/DEAD™ Fixable Far-Red Stain **(B)**. The cytotoxicity was measured in flow cytometry as the percentage of LIVE/DEAD$^+$ cells among CFSE$^+$ cells (similar method as figure 18B - see methods section for formula). For all four AgAbs, the addition of ICB did not significantly improved the killing efficacies ($p \geq 0,1$ – two-tailed Mann-Whitney tests).
All assays were performed in triplicates with means and standard deviations displayed in the graphs.

In conclusion, the combination of AgAbs with anti-PD-1/PD-L1 antibodies further increased T cell activation in comparison to the AgAbs as single agents. In these experiments, this effect remains modest, but might be stronger in clinical settings.

2.1.7. T cell activation in response to AgAbs can eliminate AML bystander cells

Acute myeloid leukemia, as other cancer types, is a highly dynamic oligoclonal disease [295]. Some rare clones can acquire genome modifications (genetic or epigenetic) leading to the modulation of the expression of some genes [18, 295]. This cancer heterogeneity is a serious limitation to therapies aiming at the complete elimination of the tumour cells, including immunotherapies [296]. In the setting of AgAb-therapy, clones expressing reduced levels of a target marker may internalize lower amounts of AgAbs and be less effective at presenting epitopes to the T cells. Decreased MHC-II expression could have the same implications.

Interestingly, it has recently been described that Th1 cytokines (IFNγ, TNFα) can induce the senescence and ultimately the cell death of AML blasts [297].

This observation raised my interest, as the AgAb-mediated activation of $CD4^+$ T cell could theoretically have the same effect on bystander AML clones unable to efficiently present the epitopes to the T cells.

In order to mimic a situation where some AML cells would not be efficiently targeted by AgAbs, and to assess the effects of AgAb-mediated T cell activation on these bystander cells, I designed a bystander assay. For that purpose, Mutz-3 cells were pulsed with 100ng 3H10 peptide, CD33 3H10, or CD33 native counterpart. These cells were then co-incubated with CFSE-stained, unpulsed and HLA-unmatched, MonoMac6, NOMO-1, KG-1 or MV4-11 cells (bystander cells). Finally, EBNA3C 3H10-specific $CD4^+$ T cells were added into the wells. In each well, 5.10^4 Mutz-3 cells (APCs) were mixed with an equal number of unmatched $CSFE^+$-bystander cells and T cells. For each bystander cell line, control conditions with cytokines (5ng/mL IFNγ, 1ng/mL TNFα), with T cells but without APCs, or with conditioned medium from activated T cells were also assessed. After 2 days of co-incubation, the cells were harvested and stained with LIVE/DEAD™ Fixable Far Red Dead Cell Stain and PE-Annexin-V. The viability of $CFSE^+$ bystander cells was subsequently determined by flow cytometry (Figure 21). Interestingly, Th1 cytokines only (neither T cell nor APCs) already affected the viability of the bystander cells, with the combination of both cytokines yielding the strongest cytotoxic effects (ranging between 7,3% and 49,4% depending on the bystander cell line – relative to untreated control condition).

The addition of Mutz-3 cells treated with CD33 native antibody did not significantly altered the viability of bystander cell lines. However, the addition of Mutz-3 cells pulsed with the 3H10 peptide or CD33 3H10 and 3H10-specific T cells severely increased the fraction of dead bystander cells (ranging between 29,8% and 60,8% specific cytotoxicity depending on the bystander cell line – relative to untreated control condition).

Similar results were obtained upon co-incubation of the bystander cell lines (but MV4-11 replaced with Mutz-3) with pulsed MV4-11 AML cells (either CD33 1D6 or peptide) and gp350 1D6-specific $CD4^+$ T cells.

Furthermore, I tested the effects of IFNγ and TNFα on the viability of healthy PBMCs. No significant increase in the percentage of dead cells could be detected, even in the presence of both cytokines. The direct co-incubation with pulsed APCs and matched T cells was not

assessed with PBMCs due to the presence of NK cells in this population (NK cells would have been activated by HLA-unmatched APCs and T cells, similarly to a graft-versus-host effect).

In conclusion, eradication of bystander AML cells seems to benefit from the activation of cytokine release by $CD4^+$ T cells in response to the presentation of epitopes from antigen-armed antibodies.

At least IFNγ and TNFα mediated this effect, and could trigger significant cytotoxicity even when the bystander AML cells were not directly targeted by AgAbs.

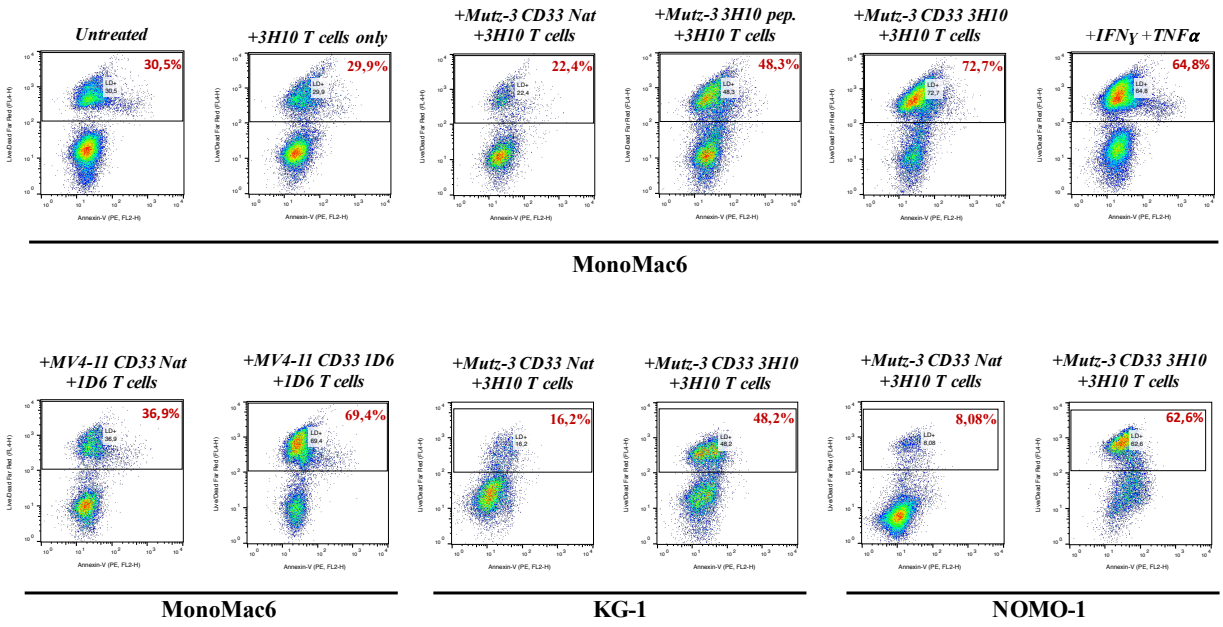

Figure 21: T cell activation mediated by AgAb-treatment can also eliminate untreated bystander AML cells

Mutz-3 cells were pulsed overnight with 100ng CD33 3H10, native counterpart, or 3H10 peptide. Likewise, MV4-11 cells were pulsed overnight with 100ng CD33 1D6 or native counterpart. The following day, the cells were washed and co-incubated with unpulsed, CFSE pre-stained, bystander AML cells (either MonoMac6, KG-1 or NOMO-1 cells) and either E3C 3H10- or gp350 1D6-specific $CD4^+$ (total effector:target:bystander=1:1:1). For MonoMac6, the effect of Th1 cytokines (IFNγ and TNFα) is also shown. After 2 days, the cells were collected and stained with LIVE/DEAD™ Fixable Far-Red Stain. The cytotoxicity was measured in flow cytometry as the percentage of L/D^+ cells among $CFSE^+$ cells (bystander cells – percentage in red on each FC figure).

Although these results are only preliminary, they already constitute a proof of concept that the AgAb-therapy may also be able to eliminate rare clones that are unable to efficiently present EBV epitopes (diminished marker expression or MHC-II presentation).

2.2. AgAbs can redirect EBV-specific immune responses from AML patients toward malignant cells

2.2.1. Construction and production of AgAbs with large antigenic domains

The use of AgAbs with short peptides is restricted to experiments where the haplotype of antigen-presenting cells and T cells is established. In this section, I conducted experiments with samples from patients whose haplotypes were not known. Therefore, the adopted strategy was to construct antibodies fused to large antigenic fragments, in order to maximise the global number of carried epitopes. This increased the chances of delivering epitopes matching the haplotype of the target tumour cells.

In regard to the previous work that was conducted in the laboratory with B-CLL samples, I decided to use the EBV latent protein EBNA3C as a source of epitopes [216]. This protein is known to be recognised by the vast majority of EBV-seropositive individuals through $CD4^+$ T cell responses, and CD19 AgAbs conjugated to EBNA3C fragments successfully expanded cytotoxic $CD4^+$ T cells from B-CLL patients *ex vivo* [98, 114, 216].

Furthermore, EBNA1 and EBNA2 are two EBV latent proteins with similar properties in terms of CD4 T cell response magnitude [98, 114]. A region from EBNA1, rich in CD4 epitopes, has previously been described in the laboratory and was included in the panel of antigenic domains for this study [281]. Lastly, a polypeptide including two promiscuous epitopes from EBNA2 has been described and also served for the construction of "larger" AgAbs [110, 162].

Large AgAbs were cloned for all four targets, CD33, CD123, CLL-1 and FR-β. For each molecule, five different AgAbs (e.g. five different antigenic domains) were constructed: three carrying one segment from EBNA3C (a.a. 1-341, or 322-679, or 653-992), one with the antigenic domain from EBNA1 (a.a. 400-622) and one with the promiscuous epitopes from EBNA2 (a.a. 278-293). EBNA3C and EBNA1 AgAbs were cloned through overlap-PCR (fusion of the native HC sequence with the respective antigenic domain in PCR, after creation of an overlap). The EBNA2 polypeptide was added to native heavy chains in PCR, employing a specific reverse primer including the nucleotide sequence (similarly to EBNA3C 3H10 and gp350 1D6 "short" AgAbs from the *in vitro* section).

All these AgAbs were produced in HEK293T cells, following the very same procedure as for native antibodies. The correct assembly and secretion of these antibodies was checked in western-blot (Figure 22).

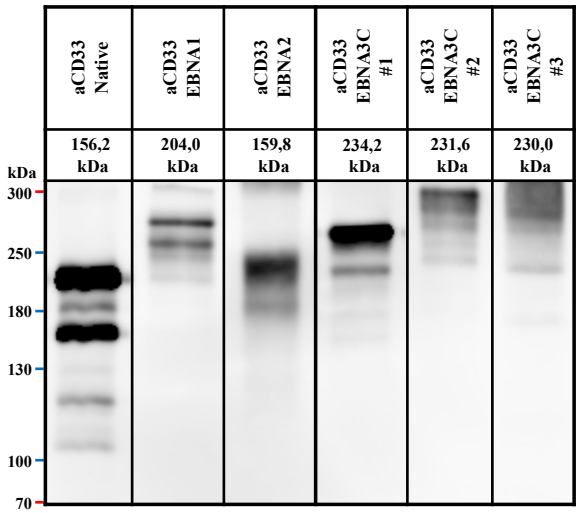

Figure 22: Expression profiles of antigen-armed antibodies conveying large EBV antigenic domains

5µL of transfection supernatants were mixed with protein loading buffer (non-reducing conditions) and loaded onto a 7.5% acrylamide gel. Antibodies were detected on the membrane with an anti-mouse IgG (H+L) HRP antibody. The membrane was exposed for 5 minutes with substrate in a chemiluminescence imager.

Of note, the addition of large antigenic domains dramatically altered the yields of these AgAbs. With the exception of EBNA3C#1 AgAbs, the yields were reduced between 5 and 50-fold compared to respective native antibodies.

2.2.2. Preliminary assessments of large AgAbs

2.2.2.1 Large AgAbs successfully vehicle epitopes into target cells

The addition of antigenic payload represented a substantial modification of the size of the heavy chain. Although the correct assembly of each AgAb has been confirmed in western-blot, it was unknown whether the addition of the antigenic domains could modify the three-dimensional structure and the properties of the antibodies. In order to verify the binding capacities of each AgAb, a binding assay was performed. Mutz-3 cells were incubated with native CD33, CD123, CLL-1 and FR-β, or their AgAbs counterparts (either EBNA1, EBNA2 or EBNA3C). Anti-mouse IgG (H+L) conjugated to Alexa 488 was then added to detect the binding of the antibodies and the signal was analysed in flow cytometry. For each molecular target, the addition of antigenic regions did not alter the binding capacities of each antibody in comparison to the native counterpart (Figure 23A).

We then verified the internalisation and processing efficacy of the large AgAbs. These properties were assessed in a T cell assay/killing assay. The EBNA3C 3H10 epitope (a.a. 627-640) is localised within the second fragment of EBNA3C (a.a. 322-679). This allowed a direct comparison between a short, well-characterised AgAb and the longest AgAb included in the panel for *ex vivo* studies. Mutz-3 cells were pulsed over-night with 100 or 10ng short AgAb

(3H10 only), long AgAb (EBNA3C #2), or peptide. The cells were then washed and co-incubated with EBNA3C 3H10-specific CD4$^+$ T cells (the target cells were stained with CFSE for the killing assay). IFNγ and granzyme B titers from the T cell assays were verified in ELISA and the elimination of Mutz-3 cells was assessed in flow cytometry (Figure 23B and C). Strikingly, there was no significant difference in the cytokine titers or in the killing efficacies between short and long AgAb for each single marker, and this was true both at 100 and 10ng.

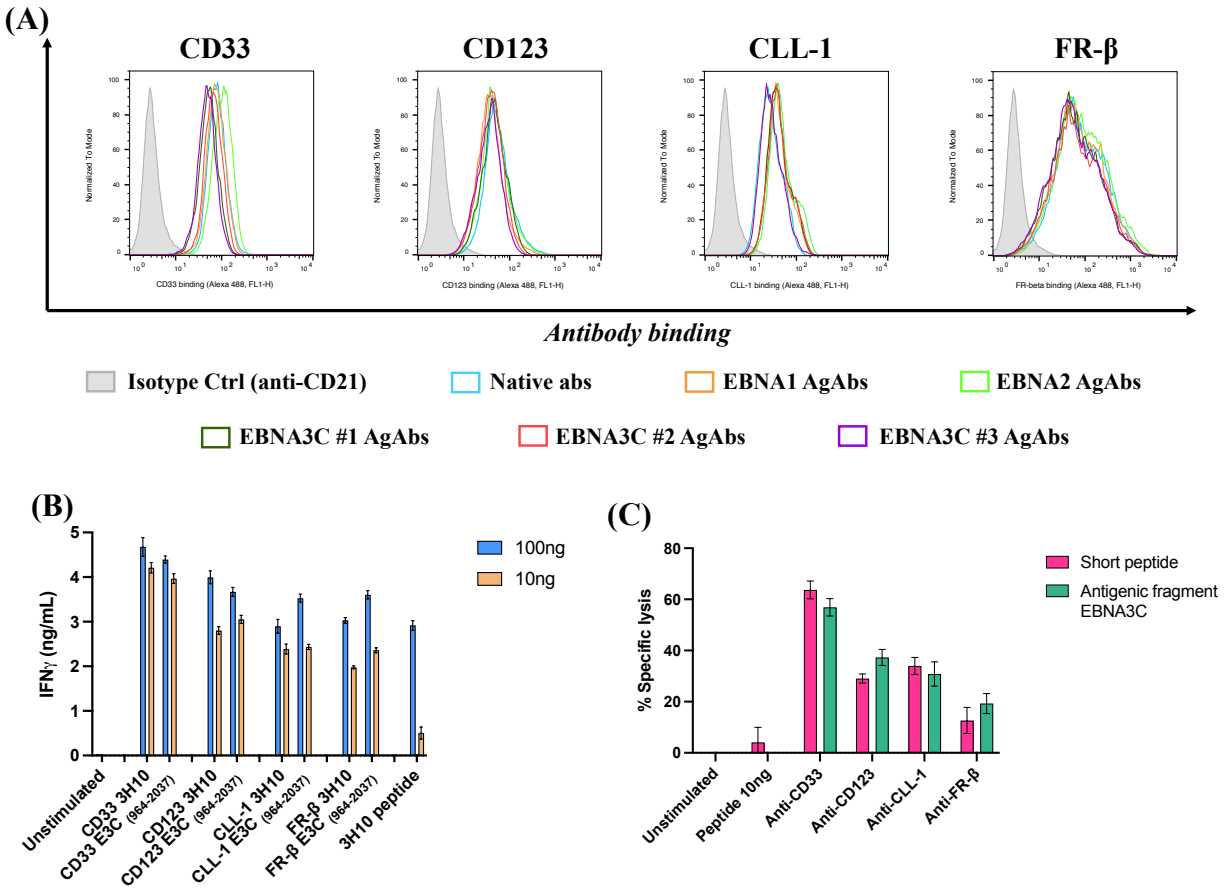

Figure 23: Large antigen-armed antibodies can bind their targets and vehicle epitopes to target AML cells *in vitro*

(A) Mutz-3 cells were incubated with anti-CD33, CD123, CLL-1 or FR-β mIgG2a (LALA), unconjugated or conjugated to large antigenic domains. The shaded curves represent the signal obtained with the anti-CD21 (LALA) which was used as an isotype control. Binding of the respective antibodies was detected using a secondary anti-mouse IgG (H+L) antibody and the fluorescence was measured in flow cytometry.

(B) and **(C)** Mutz-3 cells were pulsed overnight with 100ng or 10ng 3H10-AgAbs or EBNA3C #2 long AgAb, or 3H10 peptide (10ng only for **(C)**). The following day, the cells were washed and stained with CFSE before co-incubation with E3C 3H10-specific CD4$^+$ T cells at an E:T ratio = 1:1. After 18 hours, the supernatants were collected and IFNγ titers were checked in ELISA **(B)**. The cells were also collected and stained with LIVE/DEAD™ Fixable Far-Red Stain **(C)**. The cytotoxicity was measured in flow cytometry as the percentage of L/D$^+$ cells among CFSE$^+$ cells (see methods section for formula).
All assays were performed in triplicates with means and standard deviations displayed in the graphs.

These results confirmed that the larger antigenic regions did not alter binding or internalisation capacities of the antibodies, and that epitopes are correctly and efficiently processed and presented at the cell surface.

2.2.2.2. Large AgAbs can be processed and expand CD4$^+$ T cells from healthy donors

The capacity of large AgAbs to be correctly processed and to activate EBV-specific CD4$^+$ T cells was already assessed *in vitro*, with cell lines and T cell clones. In order to get a first insight into the ability of AgAbs to induce the *ex vivo* proliferation of primary T cells, I conducted a proliferation assay with primary PBMCs from six healthy donors.

Freshly isolated primary PBMCs (containing myeloid and lymphoid populations) were incubated with a cocktail of either CD33, CD123, CLL-1 or FR-β long AgAbs. In the perspective of future assessments with primary AML samples, two media were assessed to verify the effects on T cell proliferation. The cells were either incubated in a medium favouring the T cell proliferation (named "T cell medium" – AIM-V™ Medium supplemented with 10% (v/v) human serum and other supplements, see Methods) or with a medium supporting the survival of AML cells (named "AML Medium" – IMDM supplemented with 15% (v/v) BIT and other supplements, see Methods). The latter medium contains several cytokines, including IL-3, SCF and G-CSF, but also small molecules (UM729, SR1), whose effects on T cell proliferation are uncertain. For each $1{,}5.10^5$ PBMCs in 200µL, 10ng of AgAb cocktail (5 AgAbs – 2ng/AgAb) or native antibodies were dispensed every 4 days.

The cells were collected at day 9 and day 16 to assess the T cell proliferation (Figure 24A). The proportion of activated CD4$^+$ T cells was found to be increasing overtime in response to all four AgAbs, in all tested donors. The percentage of activated CD4$^+$ T cells (defined as CD69^{high}) at baseline was ranging between 0.5% and 3%. After 16 days, the percentage of activated CD4$^+$ T cells was not significantly altered in response to native antibodies, when the cells were cultured in AML medium. However, T cell activation was observed upon treatment with native antibodies in T cell medium (percentage of CD69^{high} ranging between 5 and 7,5%). In this medium, the percentage of CD69^{high} cells in response to the four tested AgAb-cocktails was further increased (up to 30%). Likewise, a dramatic increase in the CD69 expression could be observed on CD4$^+$ T cells in response to the four AgAb-cocktails in AML medium. No significant difference could be seen in the overall percentage of CD3$^+$/CD4$^+$ cells in response

to AgAbs, in spite of a significant activation. This may be linked to a modification of the TCR clonality among T cells, consistently with an increased CD69^{high} percentage among CD4.

These former observations underlined the interest of using AML medium for further analyses, and confirmed that the cytokines which aim at supporting AML cell survival in *ex vivo* culture do not alter the T cell activation.

Lastly, the effects of AgAb-treatment on the viability of healthy PBMCs was assessed. On day 16, the PBMCs were stained with a Live/Dead marker. First of all, in flow cytometry, no significant difference in forward and side scatter could be seen between cells treated with AgAbs and the native controls (myeloid cells representing between 30 and 40% of live events in flow cytometry for all the donors, with no difference between conditions for a given donor). In each population, the percentage of Live/Dead events only minimally varied between native- and AgAb-treated conditions.

Furthermore, staining the cells with the Live/Dead marker and lineage-specific antibodies did not yield any significant difference between AgAbs and native conditions (Figure 24B).

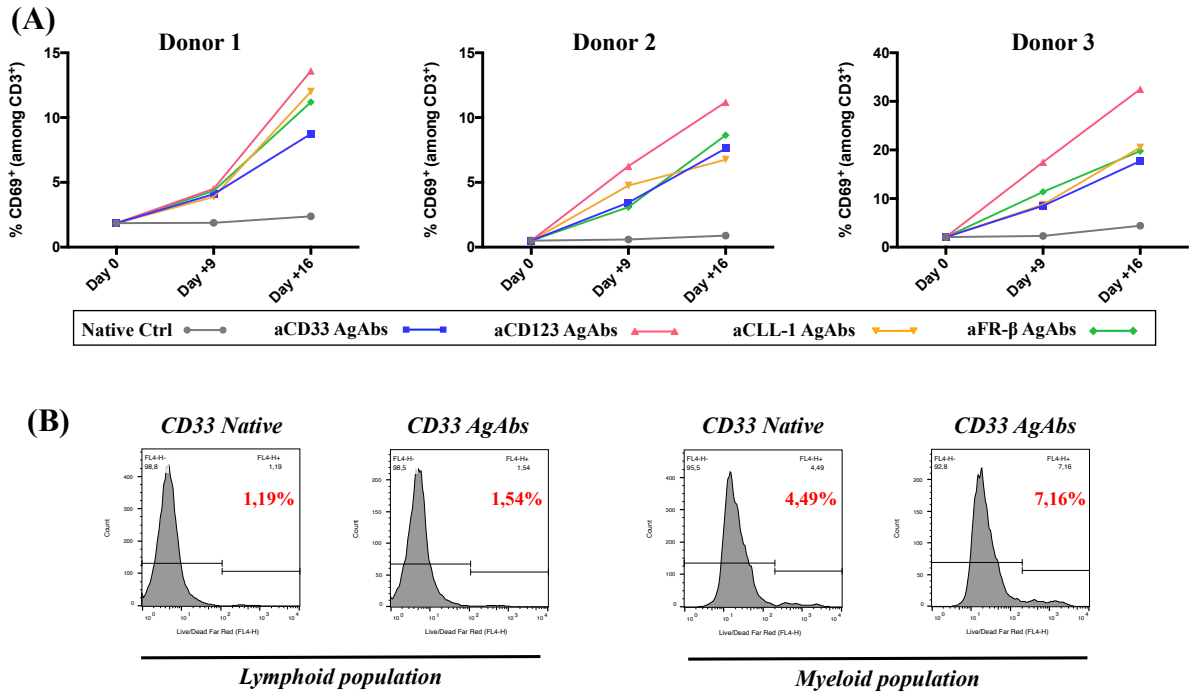

Figure 24: Large antigen armed antibodies can activate CD4$^+$ T cells from healthy donors
Freshly isolated PBMCs from healthy donors were isolated and pulsed either with native antibodies or AgAb-cocktails every fourth day. **(A)** The percentage of CD69$^+$ cells among CD4$^+$ events was evaluated in flow cytometry on day 9 and 16. The figure shows the evolution of CD69$^+$ fraction overtime for three donors. **(B)** Viability of myeloid and lymphoid cells in response to CD33 native or CD33 AgAb-cocktail was also evaluated. Treated cells were stained with a Live/Dead dye and viability of lymphoid and myeloid subsets (FSC/SSC gating strategy) was evaluated in flow cytometry.

2.2.3. Large AgAbs can effectively stimulate T cells from AML donors

2.2.3.1. Characteristics of patients

The large AgAbs were then assessed with blasts from AML patients. Five patients were included in this study. All the samples were kindly provided by Dr. med. Caroline Pabst from the *Universitätsklinikum Heidelberg*. These included purified bone marrow aspirates (n=3) and peripheral blood mononuclear cells (PBMC, n=2) from patients diagnosed with acute myeloid leukemia. The characteristics of the patients are summarised in the figure 25A. Neither the FAB classes nor the age of the patients was communicated. However, the percentage of blasts as well as the cytogenetic abnormalities are listed in the table from figure 25A.

For each sample, the cells were carefully thawed according to the protocol provided by the clinicians. AML cells were first stained for various surface markers. Expression of the molecules of interest (CD33, CD123, CLL-1, FR-β and HLA-DR), as well as the percentage of $CD3^+/CD4^+$ T cells, were of prime interest and were verified in flow cytometry (Figure 25B and C). Importantly, MHC-II (evaluated through HLA-DR expression) was highly expressed on blasts from three samples (patients 3-5), and was expressed at much discrete levels (but detectable) on blasts from two other samples (patients 1 and 2). CD33, CD123 and CLL-1 were detected on blasts from all five patients (although CD123 was expressed at much lower levels on blasts from patient 1). Finally, FR-β was expressed at different intensities between donors. The percentage of $CD3^+/CD4^+$ T cells was also variable across donors, ranging from 0,3% (patient 2) to 6,7% (patient 5). The percentage of blasts at the time of cell collection as well as the type of sample (bone marrow or PBMCs) seemed to dramatically influence the presence of T cells.

(A)

Sample number	Type of material	Sex	% of blasts	Karyotype	Molecular genetic
1	Bone-Marrow	f	91%	46,XX	NPM1-, DNMT3A-mutated, FLT3-ITD
2	PBMCs	m	97%	47,XY,+8[15]/46,XY[2]	IDH1-mutated
3	Bone-Marrow	m	68%	46,XY	WT1-mutated, FLT3-ITD
4	PBMCs	m	60%	46,XY,del(17)(p11.2)[1]/46,sl,del(5)(q13q33)[9]/46,XY[10]	TP53-, NRAS-, TET2- and PHF6-mutated
5	Bone-Marrow	m	87%	46,XY,add(9)(p13),add(11)(p13),add(12)(q22),add(18)(q21), add(20)(q13.2)[8]/46,XY,del (18)(q21q21)[2]/ 46,XY[10]	EZH2-, RUNX1-mutated FLT3-ITD

(B)

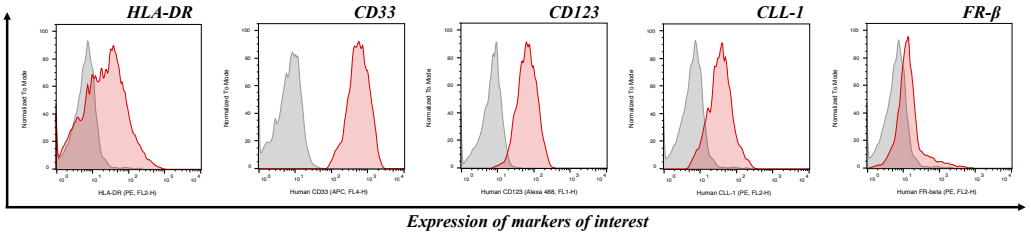

(C)

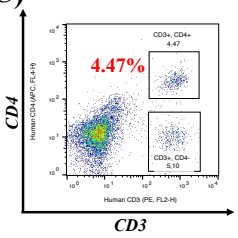

(D)

Sample number	Analysed markers on AML blasts					After thawing	
	HLA-DR	CD33	CD123	CLL-1	FR-β	% $CD3^+/CD4^+$	% blasts
1	Low	+	Low	+	-	1,99%	93,0%
2	Low	+	+	+	Low	0,31%	96,5%
3	+	+	+	+	+	4,47%	75,4%
4	+	+	+	+	+	0,49%	69,1%
5	+	+	+	+	+	6,71%	70,0%

Figure 25: Characteristics of the AML patients enrolled in the present study
(A) Summary of the available clinical data for the five patients involved in the *ex vivo* study. FLT3-ITD: Internal tandem duplication in FLT3.
(B-D) Patient samples were thawed and stained for markers of interest (HLA-DR, CD33, CD123, CLL-1 and FR-β). Expression of these markers on AML blasts, as well as the frequency of $CD3^+/CD4^+$ and AML blasts were measured in flow cytometry. Observations for patient 3 are shown in **(B)** and **(C)**. The summary for all five patients is shown in **(D)**.

2.2.3.2. Antigen-armed antibodies can activate $CD4^+$ T cells from AML patients and redirect anti-EBV cytotoxicity

The previous *ex vivo* assessment of antigen-armed antibodies was based on a two-step process [216]. First, the authors generated LCLs by infecting donor B cells with Epstein-Barr virus, and further used these LCLs to stimulate T cells from the matching donor. Subsequently, these T cells were used in assays at controlled E:T ratios with primary CLL cells. However, the limited amount of biological material, the very low number of B cells (below 1% in the tested samples – *data not shown*) as well as the poor survival of AML cells in long-term culture limited the feasibility of such an approach.

Instead, an "immediate killing-assay" was designed, where the freshly thawed cells from patients were directly pulsed with a mix of AgAbs (targeting one of the four markers of interest), or native antibodies. This approach was tested with the cells from patients 2 to 5. Unfortunately, the sample 1 could not be tested at all, due to a very poor viability at baseline.

Samples from patients 2-5 were treated every fourth day with 10ng native antibodies or a mix of 10ng AgAbs (5 long AgAbs for each target – 2ng per EBV conjugate). In addition, combination with 5µg/mL anti-PD-1, anti-PD-L1 or both antibodies was assessed, since the T cell reactivity from some AML patients has previously been described to be reversibly dampened [219]. The cells were collected after 9 and 15 days and both the T cell activation and AML cell viability were assessed. For the former assessment, the cells were stained with CD3/CD4 antibodies in order to evaluate the T cell proliferation in response to AgAb-treatment. CD69 expression was also measured on $CD4^+$ T cells in order to evaluate the percentage of activated cells in this subset.

Strikingly, the treatment of AML blasts with antigen-armed antibodies (without immune checkpoint inhibitors) triggered a robust T cell activation and expansion in all tested donors. After 15 days, CD3/CD4 T cells were found to be expanded between 3- and 10-fold in response to AgAb-cocktails, compared to native antibodies (example of patient 3 in figure 26). Furthermore, the percentage of $CD4^+$ cells expressing CD69 was markedly increased, confirming the activation and proliferation of $CD4^+$ T cells in response to AgAb-treatment. Interestingly, all four AgAb-cocktails drove comparable T cell expansion and CD69 expression, excepting FR-β cocktail in patient 2 (consistently with a very low expression of this marker on the blasts from this patient).

Of note, a T cell expansion was also visible in the HLA-DR^{low} patient 2, and this, in spite of the very low basal frequency of T cells (1,2% $CD3^+/CD4^+$ T cells in response to CD33 AgAbs, versus 0,2% in response to CD33 native antibody).

In addition, ELISA of culture supernatants showed release of IFNγ and granzyme B by $CD4^+$ T cells.

In order to verify that the expanded T cells could kill AML blasts, the collected cells were stained with an antibody targeting a myeloid lineage-specific marker (CD33 excepting for cells pulsed with CD33 native or AgAbs which were stained with anti-CLL-1 antibody) and Live/Dead dye. Then, the percentage of $Live/Dead^+$ events among $CD33^+$ or $CLL\text{-}1^+$ was measured in flow cytometry. Unfortunately, sample 4 and 5 displayed a very high mortality among AML blasts, already in control conditions. This observation underlined the high

discrepancies in terms of the *ex vivo* survival of blasts between samples, and prevented me from accurately evaluating the ability of expanded T cells to kill blasts in 2 samples. In the other samples, expansion of T cells was accompanied with a dramatic reduction in the AML cell viability. Strikingly, expanded T cells from patient 3 killed more than 90% of AML blasts in response to all AgAb-cocktails (Figure 26).

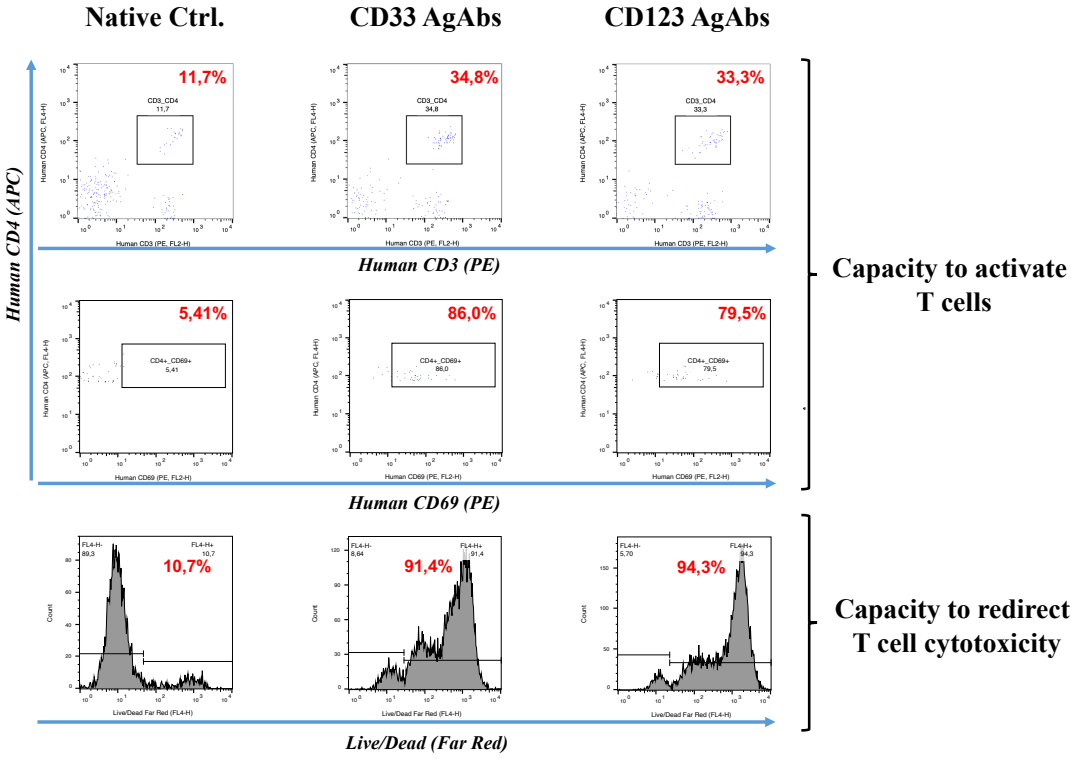

Figure 26: Large antigen armed antibodies can activate cytotoxic CD4$^+$ T cells from AML patients *(example of patient 3)*

Freshly thawed bone marrow cells from an AML patient (patient 3) were cultured in AML medium in the presence of a cocktail of AgAbs (here shown CD33 and CD123) or native antibodies (Native control). Fresh antibodies were dispensed every four days (10ng/1,5.10^5 cells). The percentage of CD3$^+$/CD4$^+$ among lymphocytes, as well as the frequency of CD69$^+$ cells among CD4$^+$ population were evaluated in flow cytometry on day 16.

Treated cells were also stained with a Live/Dead dye and the viability of target AML cells was evaluated in flow cytometry.

Although PD-1 and PD-L1 were found to be overexpressed on CD4$^+$ T cells (and on blasts for PD-L1) in response to AgAbs, addition of the corresponding immune checkpoint inhibitors had a variable effect upon combination with AgAb-cocktails. In patient 3, the addition of either anti-PD-1 or anti-PD-L1 did not consistently influence the proliferation of CD3/CD4 T cells after 16 days. Indeed, the percentage of CD4$^+$ T cells was always mildly increased when combining anti-PD-1 and anti-PD-L1 with all four AgAb-cocktails. However, the effects of single immune checkpoint inhibitors in combination with AgAb did not evenly impact the CD4$^+$

T cell percentage across target markers (mostly unchanged, slightly increased or decreased). The example of patient 3 is shown in figure 27. Nevertheless, for all the AgAb cocktails, antibodies blocking these immune checkpoints further increased the percentage of activated $CD4^+$ T cells, with no impact on T cell activation in response to native antibodies. Lastly, only a very mild although non-significant effect was seen on the viability of AML blasts in patient 3. However, the addition of immune checkpoint inhibitors increased both the T cell frequency and the killing efficacy in response to AgAbs in patient 2 (At day 10, AML cell elimination: 11,5% with CD33 AgAbs versus 21% with CD33 AgAbs + anti-PD-1; $CD4^+$ T cells: 0,22% with CD33 AgAbs versus 1,11% CD33 AgAbs + anti-PD-1).

Altogether, the effects of immune checkpoint inhibitors on the T cell response seemed to be patient-dependent, and is influenced by the efficacy of AgAbs in monotherapy.

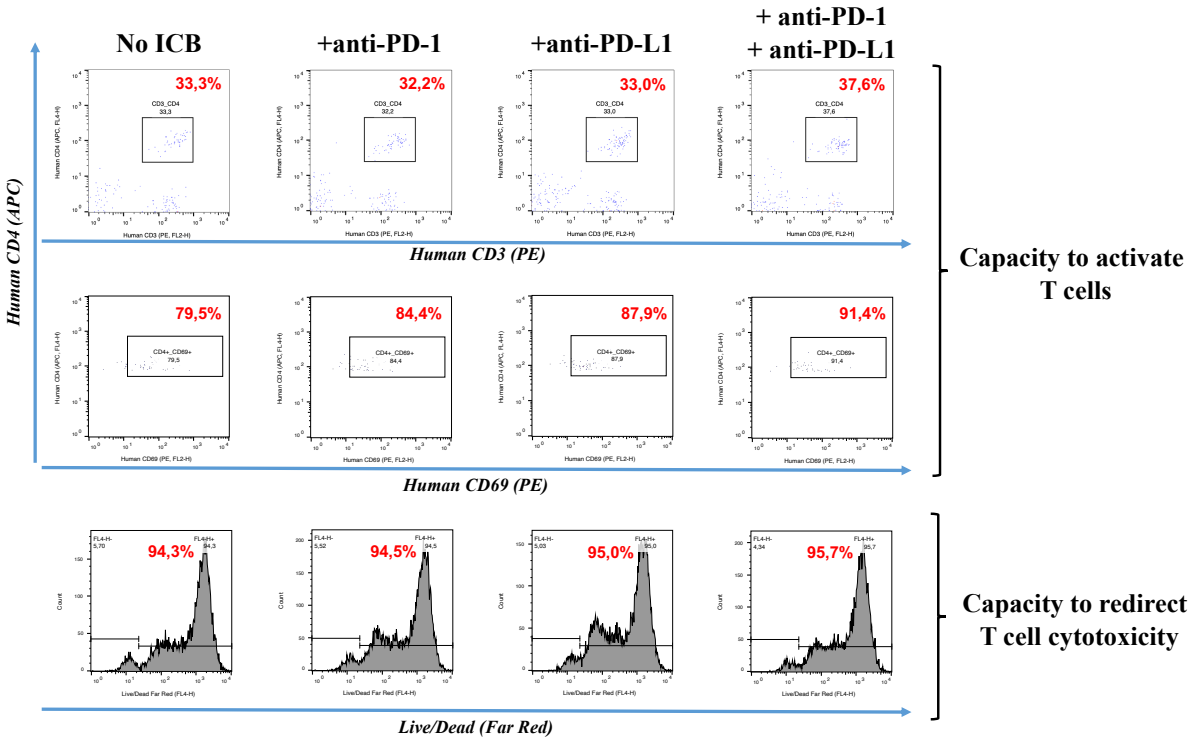

Figure 27: Immune checkpoint inhibitors only mildly increase the T cell activation and killing efficacy mediated by large AgAbs *(example of patient 3)*

Freshly thawed bone marrow cells from an AML patient (patient 3) were cultured in AML medium in the presence of a cocktail of CD123 AgAbs (10ng/1,5.10^5 cells) with or without anti-PD-1 and/or anti-PD-L1 (5µg/1,5.10^5 cells). Fresh antibodies were dispensed every four days. The percentage of $CD3^+/CD4^+$ among lymphocytes, as well as the frequency of $CD69^+$ cells among $CD4^+$ population were evaluated in flow cytometry on day 16.

Treated cells were also stained with a Live/Dead dye and the viability of target AML cells was evaluated in flow cytometry.

In conclusion, antigen-armed antibodies seem to be capable of stimulating EBV-specific memory $CD4^+$ T cells from AML patients. These T cells proliferate, display activation markers and are capable of killing AML blasts presenting the EBV epitopes. Although very promising, these results are preliminary, and further samples will be needed to generate more solid data. In particular, the variations in viability between samples, will increase the overall number of samples needed for a scientifically sound analysis.

2.3. Assessment of AgAbs in a murine model of acute myeloid leukemia

2.3.1. Development of a suitable model for *in vivo* assessments

2.3.1.1. Modification of murine AML cell lines

Most of the current *in vivo* investigations in the field of anti-AML therapy involve human leukemia cell lines in humanized mice, or patient-derived xenografts (PDX) in NOD SCID gamma (NSG) mice. These mice are either severely immunocompromised or have a reconstituted human immune system. In order to study the effects of AgAbs on redirecting a pre-existing immunity toward cancer cells, a full-murine model appeared to be the most suitable and relevant approach. WEHI-3 and C1498 are the two best documented murine AML cell lines. WEHI-3 is a cell line isolated from a BALB/c mouse which underwent paraffin injection, initially intended to induce the development of plasma cell tumour. This myelomonocytic cell line fulfils all the criteria of a human acute myeloid leukemia [298]. C1498 has been generated in 1941 from the blood of a 10-month old C57BL/6J mouse which spontaneously developed an acute myeloid leukemia [299].

Both cell lines were stained for the four previously studied markers (murine counterparts of CD33, CD123, CLL-1 and FR-β), as well as murine MHC-II ($I^{A/E}$). None of these two AML cell lines was found to be positive for MHC-II, although its expression was inducible on WEHI-3 cells with murine IFNγ. Moreover, none of the four myeloid markers was found to be expressed on C1498, while WEHI-3 slightly expressed CLL-1 (Figure 28A). In the literature, only one sequence coding for the variable parts of an anti-mouse FR-β was available, none of the cell lines expressed this marker, though. Since both a targetable marker and MHC-II were

needed for subsequent AgAb assessments, I decided to express them in the cell lines using lentiviral transduction. For the induction of $I^{A/E}$ expression, the DNA sequence encoding the isoform 8 of the class-II major histocompatibility transactivator (CIITA) was cloned into a pLKO-1 vector. In order to select transformed cells after lentiviral infection, the puromycin-N-acetyltransferase gene (*PAC*) was also added under the control of the same promoter as the *CIITA* gene (separated with an IRES). In summary, the construct *CIITA*-IRES-*PAC* was inserted into the lentiviral pLKO-1 vector (Clone B2186). For the induction of murine FR-β, the cDNA sequence of the murine *FOLR2* mRNA was cloned in the same lentiviral vector, with no selection gene (Clone B2098). Both lentiviruses were produced in HEK293T cells, by co-transfecting each lentiviral construct (either B2098 or B2186) with packaging plasmids (B653 and B654). Each supernatant was collected and filtered five days after transfection.

WEHI-3 and C1498 cells were first infected with the CIITA-carrying lentivirus. Both cell lines were spinoculated with lentiviral supernatant in the presence of Polybrene®. After five days, the infected cells were selected with G418. At that point, only 40% of the survivor cells expressed murine MHC-II. Nevertheless, these cells were infected with the second lentivirus, in order to induce the expression of murine folate receptor beta. After five days, around 15% of the total WEHI-3 and C1498 populations were positive for mFR-β (Figure 28B). Both heterogeneous populations were finally stained with anti-$I^{A/E}$ and anti-mouse FR-β antibodies, and subsequently sorted with a BD FACS Aria IIIu cell sorter. Sorted populations were homogeneously double positive for MHC-II and mouse FR-β (Figure 28B).

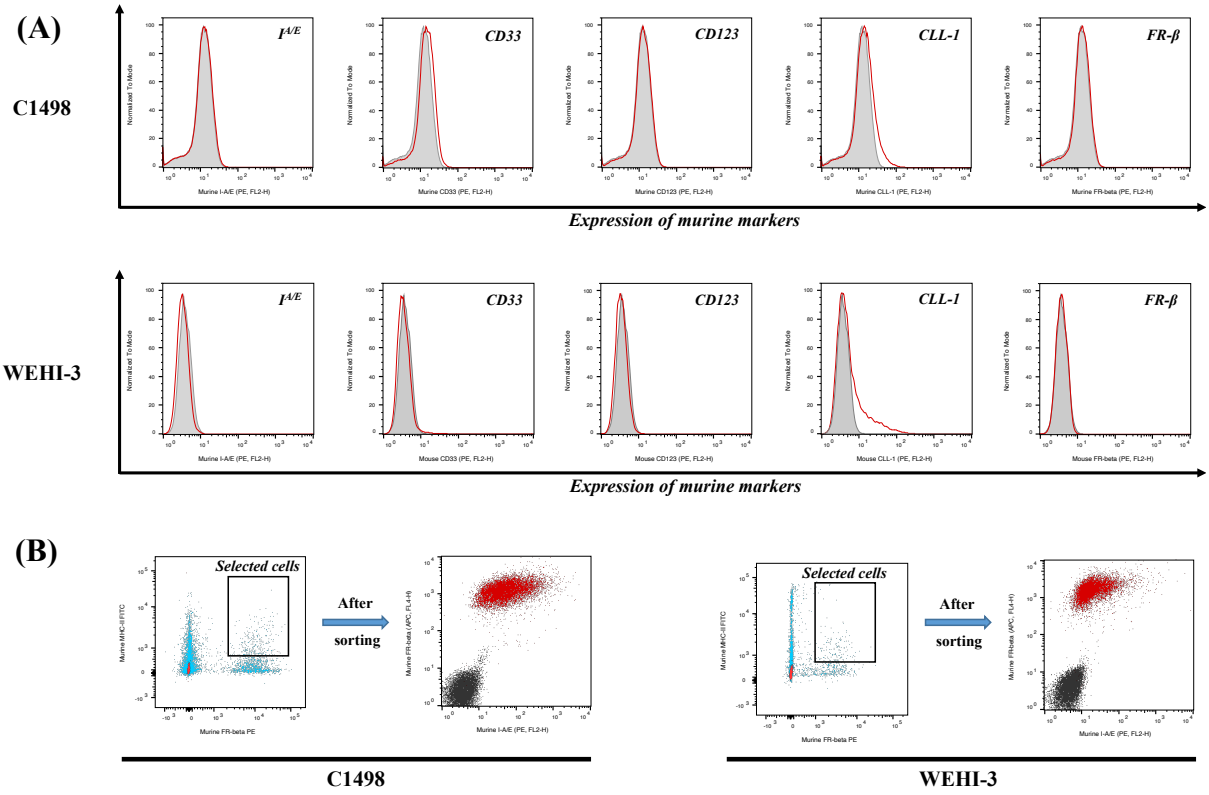

Figure 28: Modification of C1498 and WEHI-3 cells for subsequent AgAb assessments
(A) C1498 and WEHI-3 murine AML cell lines were stained with antibodies specific for the murine counterparts of the four target markers investigated in the previous parts of the study. Stainings for murine MHC-II ($I^{A/E}$) were also conducted. The signal was analysed in flow cytometry.
(B) C1498 and WEHI-3 cell lines were infected with lentiviruses to induce the expression of $I^{A/E}$ and FR-β. For each cell line, the double positive population was identified by conduction a co-staining with specific commercial antibodies and were selected in cell sorting with a BD FACS Aria III (population of interest indicated with a black frame on both pre-sorting panels). Isolated populations were purely double positive for the analysed markers (Isotype controls in black, $I^{A/E}$ /FR-β double staining in red).

2.3.1.2. In vivo behaviour of the modified cell lines

WEHI-3 and C1498 have been reported to invasively grow in syngeneic mice (BALB/c and C57BL/6J, respectively) [299, 300]. However, the behaviour of the modified WEHI-3 and C1498 had to be assessed.

Furthermore, *in vivo* assessment of AgAbs required a pre-existing immunity (similarly to EBV-immunity in humans). Since Epstein-Barr virus does not infect mice, murine cytomegalovirus, a beta-herpes virus, was used instead as a source of epitopes. The behaviour of both WEHI-3 and C1498 cell lines in mCMV-infected mice was also unknown, underlying the importance of a preliminary *in vivo* experiment.

The vast majority of the previous studies involving C1498 are based on an intravenous injection of the cells. However, intraperitoneal injections have been described in a few papers [301]. Conversely, both intraperitoneal and intravenous injections of WEHI-3 cells are regularly performed in published studies [300, 302].

As a result, I decided to assess both intravenous and intraperitoneal injections of both AML cell lines in mCMV-infected mice. Eight-week old female BALB/c and C57BL/6J mice were ordered from Janvier Labs® (France) and infected with 2.10^5 pfu mCMV, strain Smith (Mainz). 28 days after infection, the mice received the tumour cells either intraperitoneally or intravenously. The animals were monitored daily and humanely sacrificed when one of the sacrifice criteria was met. Humane endpoints avoiding excessive pain and distress were defined as follows: clinical sign of tumor development (pathological mass increase, sizable abdominal enlargement paralysis) or significant behavorial change (reduced mobility, rough hair coat, hunched posture, lethargy). Survival data for all the mice is shown in figure 29A.

Both intravenous or intraperitoneal injections of WEHI-3 cells led to a neoplastic infiltration of the spleen (splenomegaly). However, stainings of splenocytes could not confirm FR-β expression. Moreover, no sign of tumour development could be observed in any of the analysed tissues (blood, bone marrow, liver, lungs), possibly due to the loss of FR-β and MHC-II expression.

Intraperitoneal injection of C1498 cells led to an infiltration in the intestine and the peritoneum by MHC-II and FR-β positive tumor cells. However, no sign of tumour development could be observed in any of other analysed tissues. Conversely, intravenous injection of C1498 cells led to the infiltration of all the analysed tissues, including blood, bone marrow, lungs, spleen, and liver. These infiltrating tumour cells maintained their MHC-II and FR-β expression (Figure 29B). Thus, the latter model seemed to better recapitulate a human acute myeloid leukemia, with tumour development in the bone marrow and the blood, but also infiltration of solid organs.

(A)

Mice (inj. route)	Cell line	Population	Number of cells	Survival (days post injection)
BALB/c *(i.p.)*	WEHI-3	FR-β$^+$, I$^{A/E+}$	1.10^6	19
			1.10^5	25
		Parental	1.10^6	15
BALB/c *(i.v.)*	WEHI-3	FR-β$^+$, I$^{A/E+}$	1.10^6	30
C57BL/6J *(i.p.)*	C1498	FR-β$^+$, I$^{A/E+}$	5.10^6	26
			5.10^5	33
		Parental	5.10^6	15
C57BL/6J *(i.v.)*	C1498	FR-β$^+$, I$^{A/E+}$	1.10^6	31

(B)

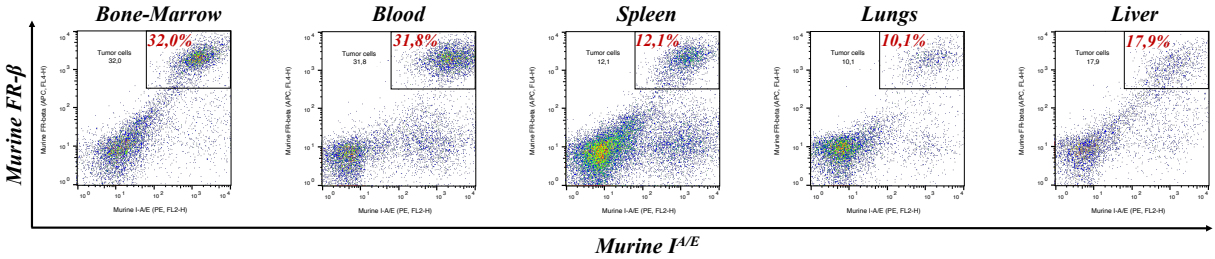

Figure 29: *In vivo* tumour formation by injected modified C1498 and WEHI-3 cells
C57BL/6J or BALB/c mice were intraperitoneally infected with mCMV and injected intraperitoneally (i.p.) or intravenously (i.v.) with either C1498 or WEHI-3 cells, respectively. Two doses i.p. and one dose i.v. were assessed for each modified cell line, and the parental population was also tested at the highest dose only. The doses were defined according to the literature. The survival time for each mouse (i.e. each condition) is given in the table in **(A)**.
(B) The mouse which received the C1498 cells intravenously showed infiltration of tumour cells in several hematopoietic tissues (blood, bone marrow, spleen) and organs (lungs, liver). Organs were collected and processed immediately after sacrifice, and the isolated cells were subjected to a murine I$^{A/E}$ and FR-β co-staining. Signal was analysed in flow cytometry, and tumour cell populations were defined as double positive for the analysed markers. Percentages of tumor cells are indicated in dark red.

2.3.2. Generation of murine antigen-armed antibodies for *in vivo* assessments

Native anti-mouse folate receptor beta was constructed by conjugating variables parts (V_H and V_L) to constant regions (C_H from a murine IgG2a with no Fc mutation, and C_L from a murine kappa light chain) in PCR, similarly to what was performed for anti-human antibodies in part 2.1.3. For the cloning of AgAbs, a KpnI restriction site was added at the 3'-end of the heavy chain sequence. Five previously described mCMV class-II antigens were chosen for the development of anti-mouse AgAbs. These epitopes were $M25_{409-425}$, $M25_{721-740}$, $M112_{36-50}$, $M139_{560-574}$ and $M142_{26-40}$. Some of these antigens included two overlapping epitopes, and all of them were shown to induce a strong CD4$^+$ T cell response in mCMV-infected C57BL/6 mice [283, 284]. To minimise the potential effects on the yield for later production of AgAbs, I

decided to incorporate these antigens into two AgAbs. As a result, one AgAb contained three antigens ($M25_{721-740}$, $M112_{36-50}$ and $M139_{560-574}$) and the second AgAb contained the two other antigens ($M25_{409-425}$ and $M142_{26-40}$). These antigenic regions were PCR-amplified with specific primers containing the KpnI restriction sequence in 5' (forward primer) and the HindIII restriction sequence in 3' (reverse primer). Subsequently, the antigenic sequences were inserted at the 5'-end of the native heavy chain.
In addition to the previous antibodies with native Fc, Fc-null counterparts were also engineered. For that purpose, L235A/L235A and D265A (LALA+DA) mutations were inserted through site-directed PCR mutagenesis in the Fc regions of both native and antigen-armed antibodies. These three mutations have been reported to alter FcγR binding, reducing antibody-dependant cell-mediated cytotoxicity (ADCC), complement-dependant cytotoxicity (CDC) and antibody-dependant cellular phagocytosis (ADCP) [303].

These antibodies were produced in HEK293T cells, similarly to the protocol used for human AgAbs (Figure 30A). I confirmed in a binding assay that anti-mouse FR-β antibodies could all bind C1498 cells expressing the cognate target, but did not bind to the untransduced C1498 cells (Figure 30B).

Finally, the anti-mouse FR-β AgAbs were assessed in a T cell assay. This allowed to check their successful internalisation after recognising FR-β at the cell surface, and that induced MHC-II presentation is functional. Both modified and untransduced C1498 cells were pulsed either with native anti-mouse FR-β or with one of the two AgAbs (LALA+DA). Interestingly, when the modified C1498 cells (FR-β^+, MHC-II^+) were pulsed with one AgAb and co-incubated with hybridoma specific for an epitope included in the same AgAb, IL-2 was released by the T cell hybridoma cells (Figure 30C). However, when hybridoma cells were incubated with C1498 cells pulsed with the native antibody, or with an AgAb including unmatched epitopes, no IL-2 could be detected in the supernatants. Importantly, co-incubation of hybridomas with unmodified C1498 (FR-β and MHC-II negative) did not result in any IL-2 secretion, even when these cells were pulsed with AgAbs containing epitopes matching the T cells.

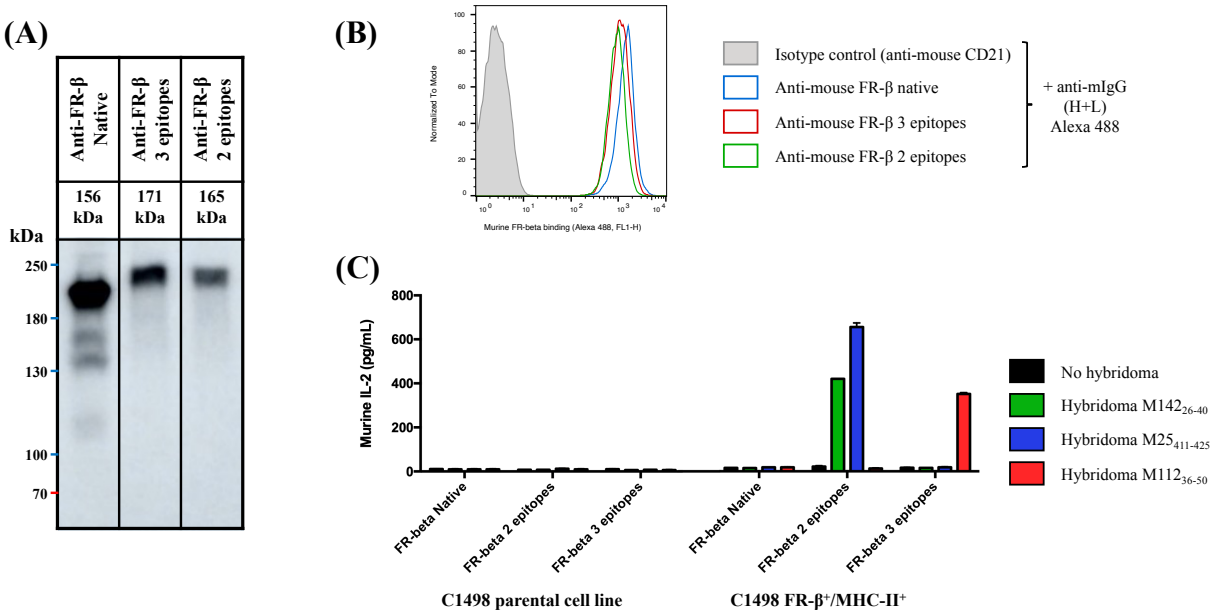

Figure 30: Anti-mouse FR-β AgAbs are correctly produced, can bind their target on modified C1498 cells, and mCMV epitopes can be processed and activate mCMV specific CD4$^+$ T cell hybridomas

(A) 5µL of transfection supernatants were mixed with protein loading buffer (non-reducing conditions) and loaded onto a 7.5% acrylamide gel. Antibodies were detected on the membrane with an anti-mouse IgG (H+L) HRP antibody. The membrane was exposed for 5 minutes in a chemiluminescence imager.
(B) Modified C1498 cells were incubated with anti-mouse FR-β mIgG2a (LALA+DA), unconjugated or conjugated to 2 or 3 mCMV epitopes. The shaded curves represent the signal obtained with the anti-mouse CD21 (LALA+DA) which was used as an isotype control. Binding of the respective antibodies was detected using a secondary anti-mouse IgG (H+L) antibody and the fluorescence was detected in flow cytometry.
(C) Parental or modified C1498 cells were pulsed overnight with 100ng AgAbs (either 2 or 3 epitopes) or native antibody (LALA+DA). The following day, the cells were washed before co-incubation with different CD4$^+$ T cell hybridomas at an E:T ratio = 1:1. After 18 hours, the supernatants were collected and mouse IL-2 titers were checked in ELISA. Of note, the AgAb with 2 epitopes included M25$_{411-425}$ and M142$_{26-40}$, while the AgAb with 3 epitopes included M112$_{36-50}$.
This assay was performed in triplicates with means and standard deviations displayed in the graphs.

In conclusion, transduced C1498 can be targeted by anti-mouse FR-β AgAbs, which can be processed, resulting in a specific activation of T cells.

2.3.3. *In vivo* assessment of anti-mouse folate-receptor beta AgAbs

For *in vivo* assessments, large number of transfections were conducted (in average 3 litres of supernatants for each antibody). These supernatants were first concentrated using the

Minimate™ Tangential Flow Filtration Capsule system (Pall®) before purification on Äkta™ Pure 25 (GE Healthcare) equipped with a HiTrap™ Protein G HP (Cytiva). The eluted antibody was finally dialysed and filter-sterilized.

For the first assessment, seventeen 8-week old C57BL/6J were ordered from Charles River (France). After a one-week resting period, each mouse received 2.10^5 pfu mCMV, strain Smith (100µL intraperitoneal injection), in order to induce a pre-existing immunity for this pathogen. One month later, all the mice received 1.10^6 modified C1498 cells – expressing both FR-β and MHC-II – through intravenously injection (tail vein). Injection of tumour cells set the day 0 of the experiment. The mice were then allocated to two different groups, depending on subsequent treatment. The animals received either native antibodies (n=6 mice) or AgAbs (n=6 mice), both with mutated Fc, or PBS only (n=5 mice). The PBS control group was added to this experiment to verify the absence of effect of native antibodies with triple Fc-mutation. The native- and AgAb-treated mice received 100ng of antibodies (50ng for each AgAb, 100ng total). All groups received as a vehicle solution sterile PBS (total volume 150µL – intraperitoneal injection). Altogether, five injections were performed, respectively on day 1, 5, 10, 15 and 20 (Figure 31A).

In order to assess the immune reaction triggered by the different treatments, some blood was withdrawn from each mouse (blood collection from the submandibullar vein) one day after the last intraperitoneal injection (day 21). PBMCs were isolated and stained for T cell and activation markers (CD4, CD69 and PD-1). While most $CD4^+$ T cells from PBS- or FR-β native-injected mice uniformely expressed low levels of PD-1, a second population up-regulating PD-1 could be detected among $CD4^+$ T cells from AgAbs-treated mice (Figure 31B). The same trend was visible for CD69, evidencing an increased T cell activation specifically in AgAb-treated mice.

The animals were monitored daily during the observation period (110 days). As in the preliminary experiment, humane endpoints avoiding excessive pain and distress were defined as follows: clinical sign of tumor development (pathological mass increase, sizable abdominal enlargement paralysis), behavorial change (reduced mobility, rough hair coat, hunched posture, lethargy). The mice were sacrificed when one of these criteria was met, evidencing leukemia development.

Strikingly, the mouse survival was significantly extended upon treatment with antigen-armed antibodies (Figure 31C). Furthermore, no difference was found between the PBS-treated mice

and the native-treated mice, confirming the absence of therapeutical effect mediated by the Fc domain of the antibody (ADCC, ADCP, CDC).

After sacrifice, blood and bone marrow samples, as well as the liver and the spleen were collected. PBMCs (blood), BMMC (bone marrow), splenocytes (spleen) and liver cells (hepatocytes and other cell types) were isolated. These cells were stained and analysed in flow cytometry to assess the percentage of $CD3^+$ T cells (both $CD4^+$ and $CD8^+$), but also the expression of immune markers evidencing T cell activation (CD69, PD-1, PD-L1).

Remarkably, the T cell frequencies in the blood, bone marrow and liver were increased in the AgAb-treated mouse. Furthermore, the fraction of both $CD4^+$ and $CD8^+$ T cells expressing activation markers (CD69 and PD-1) were heightened in the liver, the spleen, the blood and the bone marrow of AgAb-treated mouse (Figure 31D for liver, figure 31E for bone marrow). Furthermore, a significant upregulation of PD-L1 was visible on tumor cells infiltrating the liver, the blood and the bone marrow in AgAb-treated mice in comparison to PBS or FR-β native mice (*data not shown*). Of note, C1498 cells have previously been reported to upregulate PD-L1 upon *in vivo* injection, which was also observed in the present study, but the upregulation was to a greater extent in AgAb-treated mice.

These observations suggest an intense immune activation triggered by antigen-armed antibodies, even in mice which developed leukemia. No statistical analysis could be conducted though, due to the low amount of available data from AgAb-treated mice (2 animals succumbed in this group)

These findings support the rational for further experimentations of AgAbs in the *in vivo* model of acute myeloid leukemia I developed. Furthermore, preliminary stainings support the interest for future combinations of AgAbs with immune checkpoint inhibitor, including PD-1.

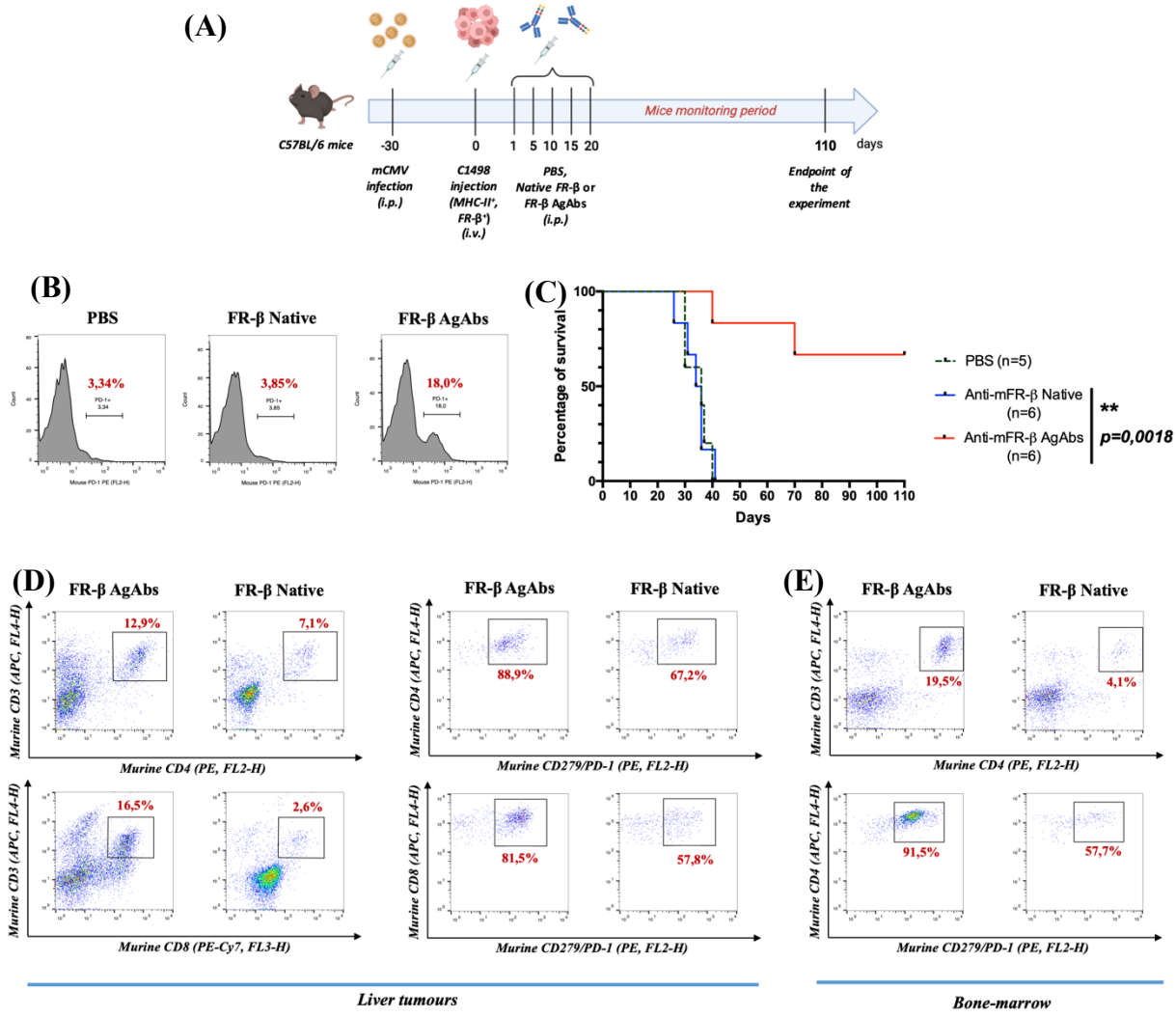

Figure 31: Anti-mouse FR-β AgAbs induce a significant immune activation *in vivo* and extend the survival of AML-bearing mice in Fc-mutated framework

(A-E) 8-week old C57BL/6J mice were first infected with murine Cytomegalovirus (mCMV). 30 days later (day 0), the mice were intravenously injected with 1.10^6 C1498 AML cells (modified to express murine FR-β and murine MHC-II). Every fifth day between day 1 and day 20, the mice were intraperitoneally injected with PBS (n=5), 100µg native anti-mouse FR-β (n=6), or 100µg of anti-mouse FR-β AgAbs (fused to 5 mCMV epitopes, n=6), both with triple Fc-mutation ($L_{234}A$,$L_{235}A$+$D_{265}A$).

(A) Timeline of the murine experiment assessing the effects of mCMV AgAbs in the C1498 AML model.

(B) Blood samples were collected on day 21, the PBMCs were isolated and PD-1 expression was measured on $CD4^+$ T cells in flow cytometry. The fraction of $PD\text{-}1^+$ cells among $CD4^+$ T cell population is indicated in dark red. For each group, a mouse representative of the average PD-1 level expression is shown.

(C) The animals were monitored daily and humanely sacrificed when displaying a sign of tumour development. Statistical significance was calculated with a Log-rank (Mantel-Cox) test.

(D-E) Liver tumours and bone marrow were collected upon sacrifice of leukemia-positive animals. The cells were isolated after organ collection and stained for CD4, CD8 and PD-1. The signals were analysed in flow cytometry. For each group, a mouse representative of the average CD3/CD4 percentage and PD-1 level expression is shown.

3. Discussion

In the present doctoral work, the potency of antibodies armed with EBV epitopes to redirect EBV $CD4^+$ T cell immunity toward acute myeloid leukemia cells was studied. The idea of using antibodies as shuttles to deliver epitopes to antigen-presenting cells has already been applied in previous studies. Although these antibodies were firstly developed in vaccine strategies, more recently, they have been assessed in anti-cancer treatment in the laboratory. In vaccine strategies, these antibodies were often designed to target dendritic cells, while the target cells in cancer were tumour B cells (B-CLL and BCL). The present work is a first-in-class study of anti-tumour AgAbs in the treatment of a myeloid disease.

Although extensive research has already been conducted for the development of AgAbs in BCL and B-CLL models, the strategy needed to be adapted to a very distinct disease. As the pre-existing infection with a pathogen is a cornerstone of the AgAb approach, Epstein-Barr virus was chosen as the preferred source of epitope for this work. Even if the bone marrow and other hematopoietic compartments are invaded by AML blasts, EBV-specific memory T cells are maintained and functional in AML patients as most patients experience EBV or CMV reactivation under iatrogenic immunosuppression (conditioning regimen for HSCT), but not earlier [304]. This supports the potency of anti-EBV T cells in non-immunosuppressed AML patients.

Another prerequisite for the development of antigen-armed antibodies is the presence of targetable markers. Before being able to generate antibodies, the expression of several previously reported markers was studied *in vitro* on a panel of twelve human AML cell lines. Although the eight FAB classes could not be represented in the panel of cell lines, CD33, CD123, CD371 (also referred as CLL-1) and FR-β were well distributed with frequencies close to those observed in patients (with the exception of FR-β which was under-represented in comparison to its expressions in patients [271]). Marker analysis with patient samples also supported the use of CD33, CD123, CLL-1 and FR-β as target for the antibodies. Indeed, the former three markers were expressed at high levels on AML cells from the five studied patients and the latter was significantly expressed on three patients.
These four markers have the advantage of not being expressed on effector cells, neither on T and NK cells, nor on B cells, as confirmed by the staining of peripheral blood cells from healthy

donors. Thus, AgAb therapy is unlikely to eliminate the immune cells that act in the fight against the leukemic cells. Although CD33 and CD123 have the major drawback of being expressed on some late bone marrow progenitors, they are mostly absent from hematopoietic stem cells, and are expressed on almost all patient samples (each sample expressed at least one of the two molecules) [240]. On the contrary, CLL-1 and FR-β are absent from hematopoietic progenitors, but their expression rate is slightly lower. Not only highly expressed on AML blasts, CD123 and CLL-1 are also expressed at significant levels on leukemic stem cells [238, 260].

These four markers are expressed on mature myeloid blood cells. However, these mature populations are dramatically reduced in AML patients due to their blocked production resulting from the leukemia. Additionally, intensive chemotherapies used as standard of care in AML patients not only kill AML blasts, but also affect the viability of mature blood populations (including myeloid and lymphoid populations) but also progenitors (including hematopoietic stem cells) [42]. While CD33 and CLL-1 are restricted to hematopoietic lineages, another general concern about CD123 or FR-β is their expression in solid tissues (CD123 expression detected in the brain, muscles or lungs; FR-β is expressed in placenta) [236–238, 270]. However, AgAbs require the expression MHC-II to exert their therapeutic effect, and most of the non-hematologic healthy cells are MHC-II negative, which provides AgAbs with a selective advantage over other immunotherapies which target all the cells expressing the marker of interest (including ADC, CAR-T cells, , …) [305]. Importantly, data released from pre- and clinical studies involving anti-CD33, -CD123, -CLL-1 or FR-β, described potential side effects of such immunotherapies [79]. CD33 is the most investigated target with varying side effects depending on the therapy. In addition to the investigations in AML, CD123 is already targeted in BPDCN by tagraxofusp (IL-3/diphtheria toxin fusion protein), with moderate side effects [244]. CLL-1 and FR-β are also under investigations with promising safety profiles.

Altogether, the focus on these four markers for the development of AgAbs in AML seems legitimate.

Expression of MHC-II on target cell is the third cornerstone of AgAb therapy. Indeed, as it helps preventing off-target effect on non-hematopoietic cells with no MHC-II expression, the absence of expression on target cells would lead to the tumour escape. Among the screened cell lines, nine were clearly positive and the three others had at least a low expression that could be increased upon IFN-γ exposure. In the clinics, 85% of the AML patients have been shown to

express MHC-II at diagnosis [288]. This reinforces the validity of an AgAb-approach in these AML patients. However, the frequency of MHC-II expression in patients at relapse (after several rounds of treatment – mainly chemotherapy or allo-HSCT) seems to decrease [221]. As a result, this could restrict the application of AgAbs to a narrower group of candidates.

In the present study, I first investigated the ability of human AML cell lines to be targeted by antigen-armed antibodies *in vitro*. Similar to what could be observed in the BCL model, the AgAbs loaded with short EBV epitopes were shown to activate matched $CD4^+$ T cells (IFNγ and granzyme B release). This epitope delivery is specifically dependent on the internalisation of the target marker and does not occur through non-specific antigen uptake. Indeed, $CD19^-$ AML cells failed to activate matched $CD4^+$ T cells in the presence of CD19 AgAbs (data not shown in the study). This corroborates previous findings from the laboratory, where concanamycin A suppressed T cell activation mediated by AgAbs [216].
However, a low expression of a target marker has been shown in this study to be sufficient for triggering a significant T cell activation at high dose (CLL-1 targeting on MV4-11 cells).

Furthermore, the activation of these effector $CD4^+$ T cells culminated in the elimination of AML target cells. Strikingly, both cytokine titers and killing efficacies were equal or slightly superior with AML cells as APCs (with an identical T cell clone), although MHC-II levels were significantly higher on BCL cells [215].
Of note, CD33 AgAbs yielded a higher T cell activation compared to the other three investigated AML markers. This may be related to the template CD33 antibody, which is the clone from the Gemtuzumab (used in clinics as ADC). As a result, it is highly likely that this antibody has increased internalisation properties compared to the three other template antibodies.
In this study, we focused on the perforin/granzyme B pathway. Indeed, previous studies from the laboratory demonstrated that this latter is the main cytotoxic pathway involved in the elimination of target cells by EBV-specific memory $CD4^+$ T cells [215, 216]. Furthermore, the performed assessments mainly focused on short-term cytotoxicity. While granzyme B pathway has been reported to exert cytotoxic effects within minutes to a few hours after T cells activation, TNF-α/TNF-receptor and Fas/FasL pathway may take 24 hours to trigger the death of the target cell [306].

Although *in vitro* experiments demonstrated a potent anti-tumour effect of antigen-armed antibodies, these assessments were performed with preliminarly stimulated $CD4^+$ T cell clones. Additionally, the human AML cell line cells derive from tumours isolated and grown *in vitro* for decades. Their behaviour may strongly differ from primary cells. As a result, one could debate about the clinical significance of these observations.

The previous assessment of AgAb with patient samples was performed in chronic lymphocytic leukemia (CLL). In this study, CLL cells were pulsed with CD19-CD22 AgAbs, fused to large domains from EBNA3C. Lymphoblastoid cell lines were also generated for each donor and used as APCs, in order stimulate and exapnd $CD4^+$ T cells. In actual T cell and killing assays, CLL cells were used as antigen-presenting cells with amplified $CD4^+$ T cells, in very controlled E:T ratios (up to 30:1). In the AML model, the number of B cells which could be used for LCL generation is very limited (below 2% across all tested donors). Together with the limited overall amount of material, this precluded the possibility of adopting the same approach as in the CLL model. AgAbs were shown to induce the proliferation of memory $CD4^+$ T cells from healthy donors, both in this study and in previous assessments [215]. Thus, I decided to adopt a more physiological "approach", where blood or bone marrow samples (containing AML blasts but also T cells and other immune cells) were pulsed with cocktails of EBNA1, EBNA2 and EBNA3C AgAbs. EBNA1 and EBNA2 were used as additional sources of epitopes, due to the very high prevalence of memory $CD4^+$ T cells specific for epitopes among these proteins [98]. Importantly, these antibodies showed a potent ability to activate T cells, which was comparable to short antigen-armed antibodies.

While a significant T cell proliferation was visible across donors, the direct cytotoxicity was significantly more difficult to study. The main limitation of this approach is the spontaneous death of AML blasts in culture, in spite of a complex medium with cytokines favouring the survival of the patient cells [307]. These discrepancies between samples may be linked to the time between collection of cells and freezing, cell processing, storage, but also genetic abnormalities and patient characteristics. The ability of AgAbs to eliminate AML cells could only be tested only in two samples (out of five – including one sample excluded due to low initial viability). It is noteworthy that the very high killing efficacy mediated by AgAbs in these two samples was accompagnied with a low background cell mortality in control conditions (patient 3 – up to 95% in 16 days). The second sample yielded a lower killing efficacy than sample 3, possibly reflecting the extreme percentage of blasts (97%) and the very low percentage of T cells (0,2%). Although the ability of antigen-armed antibodies to induce the proliferation of $CD4^+$ T cells from AML samples was clearly established, which supports

further the validity of the AgAb-approach in AML, more samples are needed to study in details the cytotoxic potential of these $CD4^+$ T cells *ex vivo*.

In order to have a comprehensive view on the AgAb-potency at the scale of a whole organism, a murine model of acute myeloid leukemia had to be developed. Not only involving AML blasts and effector T cells, the potency of immunotherapies is very dependent on the immunosuppressive leukemic micro-environment [79, 308]. Furthermore, it seemed crucial to study the recall of anti-pathogen immunity at the scale of the organism, and not only with effector and target cells within a small volume of very controlled medium. Last but not least, the accessibility of AML cells to the AgAb is imperative and can be assessed in such models.
Most of the *in vivo* studies in the field of acute myeloid leukemia are performed with patient-derived or human AML cell lines xenografts in NSG mice. These mice are severely immunocompromised to allow engraftment of human cells, which reduces the possibility to study the recall of memory immunity against a pathogen. Other models exist for the generation of tumour-bearing mice, such as viral (e.g. MuLV) of chemical induction (e.g. 3-methylcholantrene) of leukemia, but these models are often highly heterogeneous, with a strong inter-individual discrepancy [309]. Thus, it was decided to explore the potential of antigen-armed antibodies in a fully murine model, involving a murine AML cell line and a murine pathogen.
The two studied cell lines were found negative for all tested markers, in parallel from a low to absent expression of MHC-II. As a result, both cell lines were modified to ectopically induce $I^{A/E}$ and FR-β. This latter target was chosen since the sequence of an anti-mouse FR-β was publically available. Generating an antibody specific for another marker would have been very time-demanding. One could argue that this model is artificial, but the levels of expression for both MHC-II and target marker are comparable to what could be observed on patient samples. Furthermore, C1498 cells kept their leukemic properties and intravenous injection was found to recapitulate a human leukemia, with the invasion of hematopoietic compartments (bone marrow and blood, but also spleen), and organomegalies (liver, lungs).
The use of AgAbs - with mutations in the Fc - demonstrated a striking effect in increasing mice survival, in comparison to native counterpart. Furthermore, evidence of T cell proliferation and activation was visible in several tissues from AgAb-treated mice. The present experiments were conducted with Fc-null antibodies, since the use of constructs without mutations was thought to lead to a reduced difference between AgAb and native anti-FR-β. This would mainly be due

to the potent ADCC, ADCP and CDC mechanisms in C57BL/6 mice [310, 311]. However, the overall efficacy of anti-FR-β could be further enhanced by these mechanisms.

These *in vivo* experiments constitute a first proof of principle that antigen-armed antibodies can vehicle epitopes to disseminated AML cells, leading to the recall of a memory immune response culminating in a T cell proliferation and elimination of the malignant cells. Nonetheless, further investigation is needed. In particular, the characterisation of the anti-CMV immune response in AgAb-treated mice versus native antibody-treated mice would be extremely enriching. Furthermore, it would be very informative to assess the immune response toward tumoral epitopes. Indeed, several observations seem to support such an immune response. In preliminary assessments, the mice injected with modified tumour cells experienced an extended survival compared to parental C1498 cells. Additionally, AgAbs not only triggered $CD4^+$ T cell proliferation, but $CD8^+$ T cells were also found to be expanded. This may indicate that by increasing AML cell killing, the AgAbs can also favour the release and the presentation of tumour-associated antigens. In human leukemia, the mutational burden is in average very low, but an increased tumour cell lysis could also theoretically favour the proliferation of potential TAA-specific T cells. Aside from an analysis of the TCR specificity in the T cell pool in mice, the re-challenge of surviving AgAb-treated mice with tumour cells (without a second AgAb treatment) would elucidate this aspect.

The major limitation of this murine model is the poor knowledge of FR-β expression in healthy murine tissues. None of the checked tissues in the present study expressed FR-β. Importantly, the expression profile of this marker seems to differ from its human counterpart, human FR-β being expressed on hematopoietic compartments, whereas no binding of anti-mouse FR-β could be detected on healthy murine blood/bone marrow cells. As a result, a direct translation of the safety data from this experiment is impossible.

The need of both MHC-II and expressed marker for the AML cells to present the epitopes to $CD4^+$ T cells can be seen as a limitation for the present therapeutic strategy (on the other hand it allows a supplementary safety level to avoid off-tumour cytotoxicity). Indeed, the loss of a target marker or MHC-II would lead to the absence of cytotoxic reaction toward the tumour cell. Furthermore, due to the tumour heterogeneity, rare clones with a reduced or silenced expression of a surface molecule is not to be excluded [295, 312]. Recent study highlighted the potency of Th1 cytokines (IFNγ, TNFα) to induce the senescence and ultimately the cell death of AML blasts [297]. Indeed, bystander experiments conducted in this study showed that

unmatched, unpulsed, AML cells benefited from the T cell activation in response to the AgAb treatment of other target AML cells. In contrast, no striking effect of Th1 cytokines could be seen on healthy PBMCs. This bystander effect is very promising and will have to be further assessed *in vivo* (for example, MHC-II negative C1498 cells co-injected with MHC-II positive cells).

This study paves the way for further research in order to develop relevant AgAbs for AML therapy. Several questions will have to be addressed for subsequent optimisation and assessments.

In the present study, only "conventional" markers have been tested as targets for the antigen-armed antibodies. Although these markers present the tremendous advantage of being expressed on a vast majority of patient samples, they are also expressed on some healthy cells (albeit a low toxicity was visible on healthy PBMCs in this study). A few markers have recently emerged as potential markers for the development of immunotherapies. Among them, membrane expression of PRAME (Preferentially expressed antigen in melanoma – cancer testis antigen) or HDM2 (human homolog of murine double minute 2 – p53 E3-ubiquitin ligase) would be more specific since these proteins are either intracellularly expressed in healthy cells (HDM2) or restricted to some very specific lineages (PRAME expressed on some germ line cells only) [313, 314]. Furthermore, I already cloned antibodies for these markers and promising results have been obtained in T cell assays *in vitro*. PRAME expression was also found on blasts from some patients.

Multiple antigen-targeting may also have to be considered, to further reduce the risk of selecting some tumour clones [315].

The optimisation of the constant region of the shuttle antibody is a factor which tremendously influences the mode of action of antigen-armed antibodies. First of all, the species as well as the isotype determine many properties, such as the half-life, or the immune mechanisms (ADCC, CDC, ADCP), due to the interactions of the Fc domain with Fc-receptors [291, 316]. A specific isotype can subsequently have its properties modulated through specific mutations [303]. In this study, murine IgG2a were used but they were modified with a double mutation to prevent Fc-binding (triple mutation for *in vivo* experiments). In a therapeutic setting, an unmutated Fc would theoretically increase the cytotoxic effect of the AgAbs, by involving innate immunity in the reaction toward cancer cells, as observed in the first *in vivo* experiment. On the other hand, it would also increase the risk of off-tumour, on-target binding as well as

decrease the available amount of antibody for the tumour (due to a direct Fc binding). As a result, a right balance has to be found between high efficacy and a favourable safety profile.

While short epitopes were very interesting for the initial *in vitro* assessments with AML cell lines, the diversity of MHC-II haplotypes would implicate the development of tailored therapy for each patient if AgAbs were fused with single peptides.
The use of long antigenic segments from EBV proteins, namely EBNA1, EBNA2 and EBNA3C seems a more feasible approach for a one-size-fits-all therapy. However, using full-length domains from viral proteins presents a risk in terms of potential bioactivity of these fragments. In addition, neutralizing antibodies specific for epitopes in these domains may exist in the hosts, which would aggregate with the AgAbs and block their binding to malignant targets [317].
Furthermore, most of the long AgAbs were produced with strongly reduced yields in comparison to native counterparts, probably due to inhibitory effects in the antibody assembly through steric hindrance.
One or several long polypeptides gathering epitopes from the aforementioned EBV proteins may circumvent these limitations and should be tested.
To increase the diversity of the epitope repertoire, other sources of epitopes may also be considered. Human cytomegalovirus (HCMV) is also a life-persistent virus with a very high seroprevalence (70% of the human population being seropositive of anti-HCMV antibodies), together with a strong induction of $CD4^+$ cytotoxic T cells [318, 319].
Lastly, the implication of $CD8^+$ T cells would theoretically further enhance the magnitude of the response triggered by AgAbs. While some APCs (mostly dendritic cells, and B cells to a lower extent) are endowed with the ability to do cross-presentation and could theoretically present class-I epitopes delivered by antigen-armed antibodies, AML cells lack this property [320]. However, new approaches are being developed to allow the endosomal evasion of endocytosed antibodies, in order to favour a class-I presentation [321]. This kind of vector seems promising and may supplement $CD4^+$ T involvement with $CD8^+$ memory immunity.

Current knowledge on AML, as well as the results from this work, open new perspectives in terms of potential combinations of AgAbs with other immunotherapies. In this study, the hypothesis of a synergistic effect between antigen-armed antibodies and immune checkpoint inhibitors was assessed. Indeed, T cells from AML patients have been shown to proliferate in response to TCR signal in addition to the inhibition of either PD-1, CLTA-4 or Tim-3 [219]. However, the low mutagenic burden of AML cells limits the number of TAA-specific T cells,

and thus, the efficacy of immune checkpoint inhibitors in the clinics [18, 19, 78]. In *in vitro* assays, several immune checkpoints (both stimulatory and inhibitory) have been found to be expressed in response to AgAb-treatment and T cell activation, with the PD-1/PD-L1 axis being a promising candidate. However, the additive effect of anti-PD-1/anti-PD-L1 antibodies was minor, which may be associated to the short duration of the experiment. *Ex vivo*, the addition of these immune checkpoint inhibitors increased the T cell proliferation across all donors, although to different extents. The effect on AML-cell elimination was also significantly different between the two samples where this property could be assessed. While only a minor effect was visible in patient 3, a much dramatic increase was seen in patient 2. As a result, the effect of immune checkpoint inhibitors may strongly differ between patients, but addition of such antibodies should be beneficial for individuals with immunosuppressed T cells.
The initial observations of *in vivo* experiments seem to confirm the upregulation of immune checkpoints in response to AgAbs, which highlights the potential synergistic effect that ICB (particularly PD-1) could exert in combination with AgAbs. Such experiments will also be conducted in the future.

In this study, a striking *ex vivo* proliferation of $CD4^+$ T cells was visible in response to antigen-armed antibodies for all the tested patients. This highlights the potential use of AgAbs to stimulate T cells from AML patients *ex vi*vo, which could subsequently be re-injected in patients to increase the EBV-reactive T cell pool. The adoptive T cell transfer of EBV-specific T cells is already used in the treatment of EBV-related lymphomas, underlying the feasibility and the potency of such an approach [322]. This strategy would also strengthen the reaction toward cancer cells in patients with a low initial percentage of T cells. Furthermore, the *ex vivo* proliferation of T cells could be supported by the addition of exogenous cytokines (e.g. IFNγ, IL-2) while being potentially not as expensive as CAR-T cells.
Last but not least, it has been demonstrated that a high frequency of EBV-specific T cells in the donor cells upon allo-HSCT is associated with a lower risk of leukemia relapse [323]. In that prospect, addition of antigen-armed antibodies in the therapy regimen after allo-HSCT could be beneficial to engrafted patients.

In conclusion, antigen-armed antibodies appear throughout this study as a promising tool to increase the basal immunogenicity of AML cells, and to redirect a non-tumour immunogenicity toward cancer cells. The present results pave the way for future studies on potential bystander cells, but also among combination strategies. Further optimisation may also be conducted to

increase the specificity of the antibodies, to modulate some of their properties (Fc binding, …) and to enhance the immunogenicity of the viral payload (e.g. other viruses or CD8 epitopes), while keeping an excellent safety profile.
One could also conceive a potential application of this concept to other diseases in the future.

4. Material and Methods

4.1. Material

4.1.1 Cells, virus and mice

Organism	Name	Description	Use
E. coli	DH5α	Chemically competent cells; F- *Φ80lacZ*ΔM15 Δ(*lacZYA-argF*) U169 *rec*A1 *end*A1 *hsd*R17 (rK–, mK+) *pho*A *sup*E44 λ - *thi*-1 *gyr*A96 *rel*A1 (Invitrogen™)	Cloning
H. sapiens	HEK293T	Derivative from human embryonic kidney cells (HEK293), containing SV40 T antigen (ATCC® CRL-1573).	Transfections
	5637	Derivative from human bladder carcinoma (DSMZ ACC 35)	Medium conditioning
	KG-1	AML (FAB M0), FGFR1OP2-FGFR1 fusion, TP53- and NRAS-mutated [324].	Stainings and functional studies *(in vitro)*.
	HL-60	AML (FAB M2), tetraploid cells, amplified Myc [324]	
	Kasumi-1	AML (FAB M2), RUNX1-RUNX1T1 (AML1-ETO) fusion gene; $KIT^{N822\ 322}$	
	GDM-1	AML (FAB M4), AML secondary to CML with Ph^+ [325]	
	Mutz-3	AML (FAB M4), inv(3), KRAS-mutated [324]	
	OCI-AML2	AML (FAB M4), t(6;11)(q27;q23) KMT2A-MLLT4 and $DNMT3A^{R635W}$ [326]	
	OCI-AML3	AML (FAB M4), NPM1-mutated and $DNMT3A^{R882C}$ [326]	
	MV4-11	AML (FAB M5), t(4,11)(q21, q23) KMT2A-AFF1 and FLT3-ITD. [327]	
	NOMO-1	AML (FAB M5a), t(9;11)(p22;q23) KMT2A-MLLT3 [328]	
	MOLM-14	AML (FAB M5a) secondary to MDS with RAEB, t(9;11)(p22;q23) KMT2A-MLLT3 and FLT3-ITD [329]	
	MonoMac6	AML (FAB M5b) t(9;11)(p22;q23) KMT2A-MLLT3 and RUNX1-ATP8A2 fusion, TP53-mutated [324]	
	THP-1	AML (FAB M5b), t(9;11)(p22;q23) KMT2A-MLLT3, CSNK2A1-DDX39B fusion, TP53 and NRAS-mutated. [324]	
	GB and AS LCLs	Human lymphoblastoid cell lines (B cells immortalized with EBV). They were kindly provided by Prof. Josef Mautner (Helmholz-Zentrum, München, Germany).	Maintenance of human T cell lines/clones.
	gp350 1D6 and EBNA3C 3H10 $CD4^+$ T cell clones	$CD4^+$ T-cell clones were generated through ex vivo stimulation of PBMCs from healthy donors with peptide. They were kindly provided by Prof. Josef Mautner (Helmholz-Zentrum, München, Germany)	Functional studies *(in vitro)*.
M. musculus	C1498	Murine AML cell line (C57BL/6J) (ATCC TIB-49)	Functional studies (*in vitro* and *in vivo*)
	WEHI-3	Murine AML cell line (BALB/c) (ATCC TIB-68)	
	$CD4^+$ T cell hybridoma	Immortalized $CD4^+$ T cells specific for mCMV epitopes. They were kindly provided by Prof. Annette Oxenius (ETH, Zurich, Switzerland)	Functional studies (*in vitro*)

Table 4: List of cell lines used in the present study

Virus	Description	Use
mCMV	Murine Cytomegalovirus (mCMV), strain Smith	Infection of mice (*in vivo* experiments)

Table 5: List of viruses used in the present study

Mice (Strain)	Description	Supplier
C57BL/6J	Black mice used for *in vivo* experiments with C1498 cells.	Janvier Labs (France)
BALB/c	White mice used for *in vivo* experiments with WEHI-3 cells.	

Table 6: List of mouse strains used in the present study

4.1.2. Media for eukaryotic and bacteria cell culture

4.1.2.1 Commercial media

Name	Supplier	Catalogue number	Use
RPMI-1640 Medium	Gibco™ by life technologies™	11875093	Cell maintenance, assays
IMDM		12440053	
AIM-V™ Medium		12055091	
RPMI-1640 Medium, no phenol red		11835063	Calcein-release assay
Opti-MEM™		31985070	DNA complex formation
FreeStyle™ 293 Expression medium		12338018	Antibodies production

Table 7: List of commercial media used in the present study

4.1.2.2 Supplements for the formulation of complete media

Name	Supplier	Catalogue number	Use
GlutaMax™ Supplement	Gibco™ by life technologies™	35050038	Eukaryotic cell culture
HEPES Buffer Solution 1M		15630056	
MEM NEAA Solution 100X		11140050	
Gentamicin (50mg/mL)		12055091	
Amphotericin B (250µg/mL)		15290026	
Penicillin-Streptomycin (10.000 U/ml)		15140122	
Sodium Pyruvate solution 100mM	Sigma-Aldrich®	S8636-100ML	
Foetal bovine serum (FBS)		F9665-500ML	
β-mercaptoethanol (14.3M)	Carl Roth	4227.3	

Ciprofloxacin	BioChemica	A4589,0001	T cell culture
Recombinant human IL-2	Kindly provided by Prof. Josef Mautner (Munich, Germany)		
Phytohemagglutinin (PHA)			
Recombinant human IL-3	Shenandoah Biotechnology Inc™	100-80	*Ex vivo* culture of AML and healthy cells
Recombinant human G-CSF		100-72	
Recombinant human FLT3L		100-21	
Recombinant human SCF		100-04	
BIT 9500 Serum Substitute	StemCell™ Technologies	09500	
SR1		72342	
UM729		72332	
Ampicilin	Serva	13399.02	Bacteria culture
Geneticin™ (G418 Sulfate) (50 mg/mL)	Gibco™ by life technologies™	10131035	Selection of infected cells

Table 8: List of cell culture supplements used for the formulation of complete

4.1.2.3. Complete media

Name	Composition	Use
LCL Medium	RPMI-1640 Medium supplemented with 10% (v/v) FBS, 1% (v/v) GlutaMax™, 1% (v/v) NEAA, 1mM sodium pyruvate (1% v/v), 1µg/mL amphotericin B, 50µg/mL gentamicin	LCL culture
T cell Medium	AIM-V™ Medium supplemented with 10% (v/v) human serum, 1% (v/v) GlutaMax™, 10mM HEPES (1% v/v), 10µg/mL ciprofloxacin, 50µg/mL gentamicin. 10U/mL and 250ng/mL were added freshly.	T cell culture (*in vitro*)
AML Medium	IMDM, 15% BIT, 20ng/mL IL-3 and G-CSF, 50ng/mL FLT3L, 100ng/mL SCF, 50µg/mL Gentamicin, 10µg/mL ciprofloxacin, 0.1mM β-mercaptoethanol, 500nM SR1 and UM729. 0.22µM filter-sterilized.	Maintenance of AML cells and healthy PBMCs (*ex vivo*)
LB Medium	10g/L tryptone, 5g/L yeast extract, 10g/L sodium chloride in deionized water (pH adjusted to 7.0) Sterilized through autoclaving.	Liquid bacteria culture
LB agar	32g/L LB-agar, 5g/L sodium chloride in deionized water. Sterilized through autoclaving, kept at 52˚C until poored.	Solid bacteria culture

Table 9: List of complete media used in the present study

4.1.2.4 Other chemicals/solutions for cell culture

Name	Supplier	Catalogue number	Use
1D6 and 3H10 peptides	Kindly provided by Prof. Josef Mautner (Munich, Germany)		LCL pulse for T cell stimulation
Recombinant human TNFα	PeproTech®	300-01A	*In vitro* assessments
Recombinant human IFNγ	Bio-Rad	PHP050	MHC-II induction / assessments
Recombinant murine IFNγ	Bio-Rad	PMP43A	MHC-II induction

Ultra-LEAF™ Purified anti-human CD279 (PD-1) (Isotype EH12.2H7)	BioLegend®	329926	*In vitro*/*Ex vivo* assessments
Ultra-LEAF™ Purified anti-human CD274 (PD-L1) (Isotype 29E.2A3)		329716	
Trypsin-EDTA (0,05 %)	Gibco™ by life technologies™	25300062	Passage of adherent cells
DNAse I (50U/µL)	Thermo Scientific™	EN0523	Thawing medium AML
Metafectene®	Biontex	T020-5.0	Lentivirus production
Polybrene®	Santa Cruz Biotechnology®	sc-134220	Infection with lentivirus

Table 10: List of other chemicals used in the present study

4.1.3. Clonings

4.1.3.1. Plasmids

The table contains all the plasmids used for the cloning and the production of mouse anti-human antibodies (native and AgAbs). B200/B233 were used as templates and were already present in the lab. Plasmids in pEX vectors have been ordered for synthesis from Eurofins.

Human antibodies

Lab ID	Name	Description
B200	pRK5-MoAHuCD21 kappa LC	Kappa light chain of mouse anti-human CD21
B233	pRK5-MoAHuCD21 IgG2a HC	IgG2a heavy chain of mouse anti-human CD21
B1783	pEX-A128-antiHuCD123.VH	Variable part (heavy chain) of anti-human CD123
B1784	pEX-A128-antiHuCD123.VL	Variable part (light chain) of anti-human CD123
B1785	pEX-A128-antiHuCLL-1.VH	Variable part (heavy chain) of anti-human CLL-1
B1786	pEX-A128-antiHuCLL-1.VL	Variable part (light chain) of anti-human CLL-1
B1852	pEX-A128-antiHuCD33.VH	Variable part (heavy chain) of anti-human CD33
B1855	pEX-A128-antiHuCD33.VL	Variable part (light chain) of anti-human CD33
B1877	pRK5-MoAHuCLL-1 IgG2a	IgG2a heavy chain of mouse anti-human CLL-1
B1891	pRK5-MoAHuCLL-1 kappa LC	Kappa light chain of mouse anti-human CLL-1
B1902	pRK5-MoAHuCLL-1 IgG2a LALA	IgG2a heavy chain (LALA mutations) of mouse anti-human CLL-1
B1904	pRK5-MoAHuCD21 IgG2a LALA	IgG2a heavy chain (LALA mutations) of mouse anti-human CD21
B1911	pEX-A128-antiHuFR-β.VH	Variable part (heavy chain) of anti-human FR-β
B1912	pEX-A128-antiHu FR-β.VL	Variable part (light chain) of anti-human FR-β
B1913	pRK5-MoAHuCD123 IgG2a LALA	IgG2a heavy chain (LALA mutations) of mouse anti-human CD123
B1914	pRK5-MoAHuCD123 IgG2a LALA E3C 3H10	IgG2a heavy chain (LALA mutations) of mouse anti-human CD123 with EBNA3C 3H10 epitope

B1916	pRK5-MoAHuCD123 IgG2a LALA gp350 1D6	IgG2a heavy chain (LALA mutations) of mouse anti-human CD123 with gp350 1D6 epitope
B1917	pRK5-MoAHuCD123 kappa LC	Kappa light chain of mouse anti-human CD123
B1923	pRK5-MoAHuCLL-1 IgG2a LALA E3C 3H10	IgG2a heavy chain (LALA mutations) of mouse anti-human CLL-1 with EBNA3C 3H10 epitope
B1925	pRK5-MoAHuCLL-1 IgG2a LALA gp350 1D6	IgG2a heavy chain (LALA mutations) of mouse anti-human CLL-1 with gp350 1D6 epitope
B2018	pRK5-MoAHuCD33 IgG2a LALA	IgG2a heavy chain (LALA mutations) of mouse anti-human CD33
B2019	pRK5-MoAHuCD33 IgG2a LALA E3C 3H10	IgG2a heavy chain (LALA mutations) of mouse anti-human CD33 with EBNA3C 3H10 epitope
B2021	pRK5-MoAHuCD33 IgG2a LALA gp350 1D6	IgG2a heavy chain (LALA mutations) of mouse anti-human CD33 with gp350 1D6 epitope
B2022	pRK5-MoAHuCD33 kappa LC	Kappa light chain of mouse anti-human CD33
B2023	pRK5-MoAHuFR-β IgG2a LALA	IgG2a heavy chain (LALA mutations) of mouse anti-human FR-β
B2024	pRK5-MoAHuFR-β IgG2a LALA E3C 3H10	IgG2a heavy chain (LALA mutations) of mouse anti-human FR-β with EBNA3C 3H10 epitope
B2026	pRK5-MoAHuFR-β IgG2a LALA gp350 1D6	IgG2a heavy chain (LALA mutations) of mouse anti-human FR-β with gp350 1D6 epitope
B2027	pRK5-MoAHuFR-β kappa LC	Kappa light chain of mouse anti-human FR-β
B2029	pRK5-MoAHuCD33 IgG2a LALA EBNA1	IgG2a heavy chain (LALA mutations) of mouse anti-human CD33 with EBNA1 (aa 400-622) domain
B2030	pRK5-MoAHuCLL-1 IgG2a LALA EBNA1	IgG2a heavy chain (LALA mutations) of mouse anti-human CLL-1 with EBNA1 (aa 400-622) domain
B2031	pRK5-MoAHuCD123 IgG2a LALA EBNA1	IgG2a heavy chain (LALA mutations) of mouse anti-human CD123 with EBNA1 (aa 400-622) domain
B2032	pRK5-MoAHuFR-β IgG2a LALA EBNA1	IgG2a heavy chain (LALA mutations) of mouse anti-human FR-β with EBNA1 (aa 400-622) domain
B2034	pRK5-MoAHuCD33 IgG2a LALA EBNA2	IgG2a heavy chain (LALA mutations) of mouse anti-human CD33 with EBNA2 (aa 278-293) domain
B2035	pRK5-MoAHuCLL-1 IgG2a LALA EBNA2	IgG2a heavy chain (LALA mutations) of mouse anti-human CLL-1 with EBNA2 (aa 278-293) domain
B2036	pRK5-MoAHuCD123 IgG2a LALA EBNA2	IgG2a heavy chain (LALA mutations) of mouse anti-human CD123 with EBNA2 (aa 278-293) domain
B2037	pRK5-MoAHuFR-β IgG2a LALA EBNA2	IgG2a heavy chain (LALA mutations) of mouse anti-human FR-β with EBNA2 (aa 278-293) domain
B2039	pRK5-MoAHuCD33 IgG2a LALA EBNA3C #1	IgG2a heavy chain (LALA mutations) of mouse anti-human CD33 with EBNA3C (aa 1-341) domain
B2040	pRK5-MoAHuCLL-1 IgG2a LALA EBNA3C #1	IgG2a heavy chain (LALA mutations) of mouse anti-human CLL-1 with EBNA3C (aa 1-341) domain
B2041	pRK5-MoAHuCD123 IgG2a LALA EBNA3C #1	IgG2a heavy chain (LALA mutations) of mouse anti-human CD123 with EBNA3C (aa 1-341) domain
B2042	pRK5-MoAHuFR-β IgG2a LALA EBNA3C #1	IgG2a heavy chain (LALA mutations) of mouse anti-human FR-β with EBNA3C (aa 1-341) domain
B2044	pRK5-MoAHuCD33 IgG2a LALA EBNA3C #2	IgG2a heavy chain (LALA mutations) of mouse anti-human CD33 with EBNA3C (aa 322-679) domain
B2045	pRK5-MoAHuCLL-1 IgG2a LALA EBNA3C #2	IgG2a heavy chain (LALA mutations) of mouse anti-human CLL-1 with EBNA3C (aa 322-679) domain
B2046	pRK5-MoAHuCD123 IgG2a LALA EBNA3C #2	IgG2a heavy chain (LALA mutations) of mouse anti-human CD123 with EBNA3C (aa 322-679) domain

B2047	pRK5-MoAHuFR-β IgG2a LALA EBNA3C #2	IgG2a heavy chain (LALA mutations) of mouse anti-human FR-β with EBNA3C (aa 322-679) domain
B2049	pRK5-MoAHuCD33 IgG2a LALA EBNA3C #3	IgG2a heavy chain (LALA mutations) of mouse anti-human CD33 with EBNA3C (aa 653-992) domain
B2050	pRK5-MoAHuCLL-1 IgG2a LALA EBNA3C #3	IgG2a heavy chain (LALA mutations) of mouse anti-human CLL-1 with EBNA3C (aa 653-992) domain
B2051	pRK5-MoAHuCD123 IgG2a LALA EBNA3C #3	IgG2a heavy chain (LALA mutations) of mouse anti-human CD123 with EBNA3C (aa 653-992) domain
B2052	pRK5-MoAHuFR-β IgG2a LALA EBNA3C #3	IgG2a heavy chain (LALA mutations) of mouse anti-human FR-β with EBNA3C (aa 653-992) domain

Table 11: List of plasmids (human antibodies) used in the present study

Murine antibodies

Lab ID	Name	Description
B1921	pEX-A128-antiMoFR-β.VH	Variable part (heavy chain) of anti-mouse FR-β
B1922	pEX-A128-antiMoFR-β.VL	Variable part (light chain) of anti-mouse FR-β
B2097	pRK5-MoAMoFR-β kappa LC	Kappa light chain of mouse anti-mouse FR-β
B2102	pEX-A128- mCMV epitopes	Codon-optimised antigenic sequences encoding C57BL/*6* and BALB/*c* mCMV epitopes
B2139	pRK5-MoAMoFR-β IgG2a with $M25_{6-24}$, $M44_{43-62}$, $M55_{232-252}$ and $M55_{325-342}$	IgG2a heavy chain (LALA mutations) of mouse anti-mouse FR-β with mCMV $M25_{6-24}$, $M44_{43-62}$, $M55_{232-252}$ and $M55_{325-342}$ (BALB/*c* background)
B2180	pRK5-MoAMoFR-β IgG2a Unmutated	IgG2a heavy chain (native Fc) of mouse anti-mouse FR-β
B2181	pRK5-MoAMoFR-β IgG2a LALA+DA	IgG2a heavy chain (LALA and DA mutations) of mouse anti-mouse FR-β
B2182	pRK5-MoAMoFR-β IgG2a Unmutated with $M142_{26-40}$ and $M25_{409-425}$	IgG2a heavy chain (native Fc) of mouse anti-mouse FR-β with mCMV $M142_{26-40}$ and $M25_{409-425}$ (C57BL/6 background)
B2183	pRK5-MoAMoFR-β IgG2a LALA+DA $M142_{26-40}$ and $M25_{409-425}$	IgG2a heavy chain (LALA and DA mutations) of mouse anti-mouse FR-β with mCMV $M142_{26-40}$ and $M25_{409-425}$ (C57BL/6 background)
B2184	pRK5-MoAMoFR-β IgG2a Unmutated with $M139_{560-574}$, $M25_{721-740}$ and $M112_{36-55}$	IgG2a heavy chain (native Fc) of mouse anti-mouse FR-β with mCMV $M139_{560-574}$, $M25_{721-740}$ (2 ep) and $M112_{36-55}$ (2 ep) (C57BL/6 background)
B2185	pRK5-MoAMoFR-β IgG2a LALA+DA with $M139_{560-574}$, $M25_{721-740}$ and $M112_{36-55}$	IgG2a heavy chain (LALA and DA mutations) of mouse anti-mouse FR-β with mCMV $M139_{560-574}$, $M25_{721-740}$ (2 ep) and $M112_{36-55}$ (2 ep) (C57BL/6 background)

Table 12: List of plasmids (murine antibodies) used in the present study

Lentiviruses

Lab ID	Name	Description
B653	pCMV-Gag.Pol (deltaR8.91)	Lentivirus packaging helper plasmid (Gag + Pol)
B654	pCMV-VSV-G	Lentivirus packaging helper plasmid (Envelope protein VSV-G)
B671	pLKO.1 Puro Empty	Lentivirus empty backbone

B734	p-pTet.M81.BZLF1.with.intron-pTet.NGFR.IRES.GFP-CMVp.CD2-B95.8.EBNA1.oriP	Plasmid containing NGFR-GFP construct with IRES (template for IRES extraction)
B1782	pcDNA3-CIITA8	pcDNA plasmid containing isoform 8 of CIITA
B1905	pEX-A128-FOLR2	Murine FOLR2 mRNA cDNA sequence
B2098	pLKO.1-hPGKp.FOLR2	Lentivirus genome with FOLR2 mRNA cDNA
B2186	pLKO.1-hPGKp.CIITA IRES Puro	Lentivirus genome with CIITA-IRES-PuroR construct

Table 13: List of plasmids (lentiviruses) used in the present study

4.1.3.2. Primers

Primers for antibody clonings (and sequencing)

Lab ID	Name	Sequence
289	pRK5 insert sequencing **fwd**	ACCCCCTTGGCTTCGTTAG
856	pRK5 insert sequencing **rev**	CCTAACCAAGTTCCTCTTTCAG
1838	aCD33/CD123/ CLL-1/HuFR-β/MoFR-β HC **fwd**	TCGATTGAATTCATGGCTGTCCTGGTGCTGTT
1990	IgG2a CH (OL with EBNA3C 1/3) **rev**	CTGTCCTTCAAATGATTCTTTACCCGGAGTCCGGGA
1993	EBNA3C 1/3 Ag (OL with CH IgG2a) **fwd**	TCCCGGACTCCGGGTAAAGAATCATTTGAAGGACAGGG
1998	EBNA3C 3/3 Ag (OL with CH IgG2a) **rev**	TGAGCAAGCTTTCAATCTAGCTCACTTTCAGTG
2000	IgG2a CH (OL with EBNA3C 2/3) **rev**	TGGATTTTCATTAGGTGGTTTACCCGGAGTCCGGGA
2002	IgG2a CH (OL with EBNA3C 3/3) **rev**	AATTTCACGACCAGCCCGTTTACCCGGAGTCCGGGA
2006	EBNA3C 1/3 Ag (OL with CH IgG2a) **rev**	TGAGCAAGCTTTCAGTTCTGGATTACGTGTTCTT
2007	EBNA3C 2/3 Ag (OL with CH IgG2a) **fwd**	TCCCGGACTCCGGGTAAACCACCTAATGAAAATCCA
2014	EBNA3C 2/3 Ag (OL with CH IgG2a) **rev**	TGAGCAAGCTTTCAGCGAGGCGTTGTAGG
2015	EBNA3C 3/3 Ag (OL with CH IgG2a) **fwd**	TCCCGGACTCCGGGTAAACGGGCTGGTCGTG
2391	IgG2a CH (OL with EBNA1) **rev**	AAATGGCCTTCTACCTGGTTTACCCGGAGTCCGGGA
2392	EBNA1 Ag (OL with CH IgG2a) **fwd**	TCCCGGACTCCGGGTAAACCAGGTAGAAGGCCATTTTT CCAC
2393	EBNA1 Ag (OL with CH IgG2a) **rev**	TGAGCAAGCTTTCAATCACCCTCCGCGGCAGC
3609	aCLL-1 VH **fwd**	CGAGCGAATTCGAGGTCCAGCTGCAG

3610	IgG2a CH (OL VH aCLL-1) **fwd**	GTCACCGTCTCCTCAGCCAAAACAACAGCC
3611	aCLL-1 VH (OL IgG2a CH) **rev**	GGCTGTTGTTTTGGCTGAGGAGACGGTGAC
3612	IgG2a CH short **rev**	CGGCGAAGCTTTCATTTACCCGGAGTCC
3613	IgG2a CH **rev** (long for SP insertion – native antibody)	CGCGCGCGCGCAAGCTTTCATTTACCCGGAGTCCGGGAGAAG
3614	Signal peptide for CLL-1 HC **fwd**	CATTAGAATTCATGGCTGTCCTGGTGCTGTTCCTCTGCCTGGTTG CATTTCCAAGCTGTGTCCTGTCCGAGGTCCAGCTGCAGCAGTCTG
3615	aCLL-1 VL **fwd**	CGCGCGAATTCGACATCCAGATGACCC
3616	Kappa CL (OL VL aCLL-1) **fwd**	GCAGCATCAGCCCGGCGTTTTATTTCCAGCTTGG
3617	aCLL-1 VL (OL kappa CL) **rev**	CAAGCTGGAAATAAAACGCCGGGCTGATGCTG
3618	Kappa CL short **rev**	CGGCGAAGCTTTCAACACTCATTCCTGTTGAAG
3619	Kappa CL **rev** (long for SP insertion)	GCGCCGCGCGCGCGCAAGCTTTCAACACTCATTCCTGTTGAAGC TCTTGACAATG
3620	Signal peptide for aCLL-1 LC **fwd**	CGTATGAATTCATGGATTTTCAAGTGCAGATTTTCAGCTTCCTGC TAATCAGTGCCTCAGTCATAATATCCAGAGGAGACATCCAGATG ACCCAGTCTCCATCC
3723	LALA mutagenesis **fwd**	GCAAATGCCCAGCACCTAACGCCGCGGGTGGACCATCCGTCTTC ATC
3724	LALA mutagenesis **rev**	GATGAAGACGGATGGTCCACCCGCGGCGTTAGGTGCTGGGCATT TGC
3740	aCD123/hFR-β VH **fwd**	GCGCTCGAATTCGAGGTGCAGCTGGTG
3741	Signal peptide for aCD123/hFR-β HC **fwd**	CATTAGAATTCATGGCTGTCCTGGTGCTGTTCCTCTGCCTGGTTG CATTTCCAAGCTGTGTCCTGTCCGAGGTGCAGCTGGTGC
3742	aCD33/CD123/hFR-β VH (OL IgG2a CH) **rev**	GGGCTGTTGTTTTGGCGCTGCTCACGGTCA
3743	IgG2a CH (OL VH aCD33/CD123/hFR-β) **fwd**	TGACCGTGAGCAGCGCCAAAACAACAGCCC
3744	IgG2a CH **rev** (long for SP insertion – addition of EBNA3C 3H10)	GCTATAAGCTTTCAGGACTGGGGGAGCTGTCGCTCCCTCATAAA CATACGTACGACTTTACCCGGAGTCCGGG
3748	IgG2a CH **rev** (long for SP insertion – addition of gp350 1D6)	GCTATAAGCTTTCATCGAGGTTGGTAGACAGCCTTCGTATGGGG TGTCAGCTGGCCAAATTTACCCGGAGTCCGGG
3769	aCD123 VL **fwd**	CGCGCGAATTCGACTTCGTGATGACCC
3770	aCD33/CD123 VL (OL kappa CL) **rev**	GCAGCATCAGCCCGCCTCTTGATCTCCAGC
3771	Kappa CL (OL VL aCD33/CD123) **fwd**	GCTGGAGATCAAGAGGCGGGCTGATGCTGC
3772	Signal peptide for aCD123 LC **fwd**	CGTATGAATTCATGGATTTTCAAGTGCAGATTTTCAGCTTCCTGC TAATCAGTGCCTCAGTCATAATATCCAGAGGAGACTTCGTGATG ACCCAGAGCCC
3773	aHuFR-β VL **fwd**	CGCGCGAATTCAGCAGCGAGCTGAC
3774	aHuFR-β VL (OL kappa CL) **rev**	GCAGCATCAGCCCGCAGCACGGTCAGC

3775	Kappa CL (OL VL aHuFR-β) **fwd**	GCTGACCGTGCTGCGGGCTGATGCTGC
3776	Signal peptide for aHuFR-β LC **fwd**	CGTATGAATTCATGGATTTTCAAGTGCAGATTTTCAGCTTCCTGC TAATCAGTGCCTCAGTCATAATATCCAGAGGAAGCAGCGAGCTG ACCCAGG
3929	aCD33 VH **fwd**	GCGCTCGAATTCCAGGTGCAGCTGCAG
3930	Signal peptide for aCD33 HC **fwd**	CATTAGAATTCATGGCTGTCCTGGTGCTGTTCCTCTGCCTGGTTG CATTTCCAAGCTGTGTCCTGTCCCAGGTGCAGCTGCAGC
3931	aCD33 VL **fwd**	CGCGCGCGAATTCAACATCATGCTGACCC
3932	Signal peptide for aCD33 LC **fwd**	CGTATGAATTCATGGATTTTCAAGTGCAGATTTTCAGCTTCCTGC TAATCAGTGCCTCAGTCATAATATCCAGAGGAAACATCATGCTG ACCC
4076	EBNA2 (832-977) Ag **Rev**	GCTATAAGCTTTCAGCTAGGAGGCAGAGGCATAGGAGGGATGTT GTAGAACACGGTAGGGCTTTTACCCGGAGTCCGGG
4125	aMoFR-β VH **fwd**	CTGCGTCCTGTCCGAGGTGCAGCTGGTC
4126	aMoFR-β VH (OL kappa CH) **rev**	GGGCTGTTGTTTTGGCGCTGGACACTGTCAC
4127	Kappa CH (OL VH aMoFR-β) **fwd**	GTGACAGTGTCCAGCGCCAAAACAACAGCCC
4128	Signal peptide for aMoFR-β HC **fwd**	CATTAGAATTCATGGCTGTCCTGGTGCTGTTCCTCTGCCTGGTTG CATTTCCAAGCTGCGTCCTGTCCGAGGTGC
4129	aMoFR-β VL **fwd**	CCTGCTAATCAGTGCCTCAGTCATAATATCCAGAGGAGATATCG TGATGACCCAG
4130	aMoFR-β VL (OL kappa CL) **rev**	GCAGCATCAGCCCGGGCCCGCTTGATTTC
4131	Kappa CL (OL VL aMoFR-β) **fwd**	GCAGCATCAGCCCGGGCCCGCTTGATTTC
4132	Signal peptide for aMoFR-β LC **fwd**	CGTATGAATTCATGGATTTTCAAGTGCAGATTTTCAGCTTCCTGC TAATCAGTGCCTCAGTCATAATATCCAG
4341	BALB/c antigenic regions (OL with IgG2a CH) **fwd**	CTCCCGGACTCCGGGTAAAGATAACAAGTACGACCAGCACAAG
4343	BALB/c antigenic regions **rev**	GCTAGCAAGCTTTCACATATCTTCCCGCTCCAGGAAGG
4348	IgG2a CH (OL with BALB/c antigenic regions) **rev**	CTTGTGCTGGTCGTACTTGTTATCTTTACCCGGAGTCCGGGAG
4410	D265A mutagenesis **fwd**	GTCACATGTGTGGTGGTGGCTGTGAGCGAGGATGACCC
4411	D265A mutagenesis **rev**	GGGTCATCCTCGCTCACAGCCACCACCACACATGTGAC
4415	C57BL/6 3 epitopes HindIII **rev**	GTATAAAGCTTTCAGATCATTCCTCTCAGCTCTTC
4417	C57BL/6 2 epitopes KpnI **fwd**	CATTAGGTACCAGAAGCAGATACCTGACAG
4418	C57BL/6 2 epitopes HindIII **rev**	GTATAAAGCTTTCAGATGTCGATCACCATGGC
4419	C57BL/6 3 epitopes KpnI **fwd**	CATTAGGTACCACCAGACCCTACCGG
4420	aMoFR-β IgG2a KpnI **rev**	GTATAGGTACCTTTACCCGGAGTCCGGGAGAAG

Table 14: List of primers (cloning of antibodies) used in the present study

Primers for the lentiviruses cloning

Lab ID	Name	Sequence
3544	IRES BglII **rev**	GCAGCTCGAGCTCGAGCAGATCTAATCCAATTCGCTTTATGATA ACAATCTG
3688	B671 EcoRI **fwd**	GCTCGAGCTCGAGCGAATTCTCGACCTCGAGACAAATG
3689	B671 (OL with CIITA) **rev**	GAGCCAGGCAACGCATGGATCCCCCTGGGGAG
3690	CIITA (OL with B671) **fwd**	CTCCCCAGGGGGATCCATGCGTTGCCTGGCTC
3691	CIITA (OL with IRES) **rev**	GTCGTCAAGGGCATCGGTCATCTCAGGCTGATCCGTG
3692	IRES (OL with CIITA) **fwd**	CACGGATCAGCCTGAGATGACCGATGCCCTTGACGAC
3935	CIITA sequencing 1	ATCTACCATGGTGAGGTG
3936	CIITA sequencing 2	GTGATGCGCTACTTTGAG
3937	CIITA sequencing 3	GAGGAGAAGTTCACCATC
4121	Murine FOLR2 for B671 **fwd**	GTCTCGGATCCATGGCCTGGAAACAGACACC
4122	Murine FOLR2 for B671 **rev**	CTGAGGGTACCTCAGCCAGGGAGCCATAATG

Table 15: List of primers (cloning of lentiviruses) used in the present study

4.1.3.3. Enzymes for clonings

Enzyme	Concentration	Supplier	Catalogue number
BamHI	10U/µL	Thermo Fisher Scientific™	ER0051
BglII	10U/µL		ER0081
DpnI	10U/µL		ER1701
EcoRI	10U/µL		ER0271
KpnI	10U/µL		ER0521
HindIII	10U/µL		ER0502
Alkaline phosphatase (AP) from calf intestine	2U/µL	Roche	11097075001
Phusion™ High-Fidelity DNA-polymerase	2U/µL	Thermo Fisher Scientific™	F530S
RNAse A	100mg	Roche	10109169001
T4 DNA Ligase	5U/µL	Thermo Fisher Scientific™	EL0011

Table 16: List of enzymes used in the present study

4.1.4. Antibodies

Antibodies for stainings of human markers

Target	Conjugate	Clone	Isotype	Supplier	Catalogue number
CD3	PE APC	UCHT1	Mouse IgG1	BioLegend®	300408 300412
CD4	APC	RPA-T4			300514
CD19	APC	HIB19			302211
CD20	PE	2H7			302305
CD33	PE APC	WM53			303403 303407
CD56	PE	B159		BD Pharm.	555516
CD69	PE	FN50		BioLegend®	310906
CD123	Al 488	6H6			306036
CD135	PE	BV10A4H2			313305
CLL-1	PE	HB3		Invitrogen™	12-9878-42
FR-β	PE APC	94b/ FOLR2		BioLegend®	391703 391705
HLA-DR	PE	Tü36	Mouse IgG2b		361605
PD-1	PE	EH12.2H7	Mouse IgG1		329905
PD-L1	PE	MIH2			393607
CTLA-4	PE	BNI3	Mouse IgG2a		369604
4-1BB	PE	4B4-1	Mouse IgG1		309804
Lag-3	PE	7H2C65			369206
Tim-3	PE	F38-2E2			345005
TIGIT	Al 488	MBSA43		Invitrogen™	53-9500-41
VISTA	PE	B7H5DS8			12-1088041
OX-40	PE	Ber-ACT35		BioLegend®	350003
GITR	PE	621			311604
Iso IgG1	PE Al488 APC	MOPC-21			400112 400132 400119
Iso IgG2a	PE	MOPC-173	Mouse IgG2a		400213
Iso IgG2b	PE	27-35	Mouse IgG2b		402203

Table 17: List of antibodies (human markers - stainings) used in the present study

Antibodies for the stainings of murine markers

Target	Conjugate	Clone	Isotype	Supplier	Catalogue number
CD3	APC	17A2	Rat IgG2b	BioLegend®	100236
CD4	PE FITC APC	GK1.5			100408 100405 100412
CD8a	APC	53-6.7	Rat IgG2a		100711
CD33	PE	9A11-CD33	Rat IgG2b	Invitrogen	12-0331-80
CD69	PE	H1.2F3	Hamster IgG	BioLegend®	104507
CD123	PE	5B11	Rat IgG2a		106005
CLL-1	APC	5D3/CLEC12A			143405

FR-β	APC	10/FR2			153305
$I^{A/E}$	PE	M5/114.15.2	Rat IgG2b		107607
CD135	PE	A2F10	Rat IgG2a		153305
PD-1	PE	RMP1-30	Rat IgG2b		109103
PD-L1	PE	10F.9G2			124307
Iso IgG2a	PE APC	RTK2758	Rat IgG2a		400507 400511
Iso IgG2b	PE APC	RTK4530	Rat IgG2b		400635 400611
Iso Ham IgG	PE	SHG-1	Hamster IgG		402008

Table 18: List of antibodies (murine markers – stainings) used in the present study

Other dyes used for stainings

Dye	Supplier	Catalogue number	Application
Carboxyfluorescein diacetate succinimidyl ester (CFSE)	BioLegend	423801	Cell Tracking
Calcein-AM		425201	Calcein-release assay
LIVE/DEAD™ Fixable Far Red Dead Cell Stain	Invitrogen™	L10120	O/N killing assay and *ex vivo* assays

Table 19: List of dyes (stainings) used in the present study

Other antibodies

Antibody	Species	Supplier	Catalogue number	Application
Goat anti-Mouse IgG (H+L) Alexa Fluor™ 488	Goat	Invitrogen™	A-11001	Secondary Ab. for binding assays
AffiniPure Goat Anti-Mouse IgG + IgM (H+L)	Goat	Jackson Immuno Research©)	115-005-044	IgG2a ELISA
Mouse IgG2a Standard	Mouse IgG2a	Invitrogen™	39-50420-65	
Anti-mouse IgG (H+L) – HRP conjugated	Goat	Promega™	W4021	IgG2a ELISA and Western-Blot
Anti-mouse IL-2 (clone JES6-1A12)	Rat IgG2a	eBiosciences™ (Invitrogen)	16-7022-81	Murine IL-2 ELISA
Anti-mouse IL-2 biotin (clone JES6-5H4)	Rat IgG2b		13-7021-81	
Streptavidin-HRP	---	Mabtech	3310-9-1000	

Table 20: List of antibodies (other applications than stainings) used in the present study

4.1.5. Commercial kits

Kit	Supplier	Catalogue number	Application
PureLink HiPure Plasmid Maxiprep Kit	Invitrogen™	K210007	Large-scale preparation of DNA
PCR and Gel Extraction Mini Spin column kit	Genaxxon Bioscience	S5380.0250	Purification of DNA fragments from Agarose Gels
ELISA Flex: Human IFN-γ (HRP)	Mabtech	3420-1H-20	Quantification of human IFN-γ
ELISA Flex: Human Granzyme B (HRP)		3486-1H-20	Quantification of human granzyme B

Table 21: List of commercial kits used in the present study

4.1.6. Buffers and solutions

Name of the solution		Composition
ACK Buffer		1 mM $KHCO_3$, 150mM NH_4Cl, 0.1 mM EDTA
Äkta Buffer	Running Buffer	9,3mM NaH_2PO_4, 10,7mM Na_2HPO_4 (20mM sodium phosphate), 150mM NaCl, pH=7.0
	Elution Buffer (Glycine Buffer)	0.1M glycine-HCl, pH=2.7
	Regeneration Buffer (Guanidine Buffer)	6M guanidine-HCl
DNA loading buffer (6X)		0.15 % (w/v) bromphenol blue, 25 % (w/v) sucrose
ELISA buffer		2% (w/v) BSA in PBS 1X
FACS buffer		1% (v/v) FBS in PBS 1X
PBS (1X)		137mM NaCl, 2.7mM KCl, 10mM Na_2HPO_4, 2mM KH_2PO_4
PBS-Tween-20 (1X) (Wash Buffer WB/ELISA)		0.1% Tween-20 (v/v) in PBS 1X
Polyethylenimine (PEI) 1X (1mg/mL)		0.1 g PEI in 100 mL H_2O, pH=7.0, 0.22µm filter-sterilized. Stored at -80˚C.
Protein loading buffer (4X)		250 mM Tris HCl pH 6.8, 10 % (v/v) SDS, 40 % (w/v) glycerol, 0.4% (w/v) bromphenol blue
Skimmed milk buffer		3% (w/v) skimmed milk powder in PBS 1X
TAE (50X)		2.0 M Tris, 0.05 M EDTA, 1.0 M acetic acid
TE buffer (1X)		10 mM Tris, 1 mM EDTA, pH=8.0
Western Blot	Polyacrylamide separating gel (7.5%)	335mM Tris (pH 8.9), 25 % (v/v) acrylamide, 3.3mM EDTA. 60µL 10 % (w/v) APS and 6µL TEMED freshly added in each 6 mL
	Polyacrylamide stacking gel (4.5%)	125mM Tris (pH 6.8), 15 % (v/v) acrylamide, 4mM EDTA. 15µL 10 % (w/v) APS and 8µL TEMED freshly added in each 2mL
	SDS running buffer	250mM Tris, 1.92M glycine, 1 % (v/v) SDS, pH=8.5
	Blotting buffer	25mM Tris, 150mM glycine, 10 % (v/v) methanol

Table 22: List of buffers and solutions used in the present study

4.1.7. Chemicals and other reagents

Chemical	Supplier	Catalogue number
Acetic acid	Sigma-Aldrich®	71251
Agarose	Sigma-Aldrich®	A9539
Ammonium chloride	Sigma-Aldrich®	A9434
Bovine serum albumin (BSA)	Sigma-Aldrich®	A2153
Ammonium peroxodisulfate (APS)	Merck	1012010500
BD OptEIA™ TMB substrate reagent set	BD Biosciences	555214
Bromophenol blue	Serva	15375.01
Dimethyl sulfoxide (DMSO)	Sigma-Aldrich®	D2650
DNAse-free water	Sigma-Aldrich®	W4502
dNTP mix (dATP, dCTP, dGTP, dTTP)	Roche	3622614001
Ethanol absolute	Fisher chemical	BP2818500
Ethidium bromide	Bio-Rad	1610433
Ethylenediaminetetraacetic acid (EDTA)	Sigma-Aldrich®	EDS
Ficoll-Paque™ Plus	Cytiva	17144003
Glycerol	Fisher chemical	G33-1
Glycine	PanReac Applichem	A1067,5000
Glycine hydrochloride	ChemCruz™	sc-263346
Guanidine hydrochloride	Sigma-Aldrich®	G3272
Heparin	Sigma-Aldrich®	H3149
Hydroxychloric acid	Sigma-Aldrich®	H1758
Isopropanol (2-propanol)	Sigma-Aldrich®	190764
LB Agar (Lennox L Agar)	Invitrogen	22700-041
Liberase™ TM	Roche	5401119001
Methanol	Sigma-Aldrich®	322415
Monobasic potassium phosphate (KH_2PO_4)	Sigma-Aldrich®	1551139
Monosodium phosphate (NaH_2PO_4)	Sigma-Aldrich®	S0751
Murine IL-2 (standard)	Invitrogen	29-8021-65
PBS tablets (for cell culture)	Gibco™	18912014
Polyethylenimine, branched (PEI)	Sigma-Aldrich®	408727
Poly I:C (HMW)	InvivoGen	31852-29-6
Potassium acetate ($C_2H_3KO_2$)	Sigma-Aldrich®	236497
Potassium bicarbonate ($KHCO_3$)	Sigma-Aldrich®	60339
Protease inhibitor	Sigma-Aldrich®	P8340
Rotiphorese® Gel 30 (37,5:1)	Carl Roth	3029.1
Sodium chloride (NaCl)	Fisher chemical	7647-14-5
Sodium dodecyl sulfate (SDS) 20%	Serva	20767.02
Sodium hydroxide (NaOH)	Fisher chemical	1310-73-2
Sodium phosphate dibasic anhydrous (Na_2HPO_4)	Sigma-Aldrich®	71640
Spectra™ Multicolor High Range protein ladder	Thermo Scientific™	26625
Skimmed milk powder	Millipore®	70166-500G
Sucrose	Carl Roth	4621.1
Tango Buffer 10X	Thermo Scientific™	BY5
Tetramethylethylenediamine (TEMED)	PanReac Applichem	A1148
Trizma® base	Sigma-Aldrich®	T1503
Triton® X-100	Sigma-Aldrich®	93443

Tween® 20	ChemCruz™	sc-29113
Western Lightning® Plus ECL	PerkinElmer®	NEL103001EA
0.4% trypan blue	Sigma-Aldrich®	93595
1kb Plus DNA ladder	Invitrogen™	10787018
2-mercaptoethanol	Carl Roth	4227.3

Table 23: List of other chemicals/reagents used in the present study

4.1.8. Working consumables and devices

Consumables

Material/consumables	**Supplier**	**Catalogue number**
Amersham™ Protran® Western blotting membranes (nitrocellulose)	GE Healthcare	GE10600002
Cellstar® cell culture flask 50mL	Greiner bio-one	690160
Cellstar® cell culture flask 250mL	Greiner bio-one	658170
Cellstar® 15mL PP tube	Greiner bio-one	188271
Cellstar® 50mL PP tube	Greiner bio-one	227261
EIA/RIA 1x8 Stripwell™ 96 well plate	Corning™	CLS2592
Folded Paper Filters Grade 3hw	Munktell Ahlstrom	E-1415
Greiner Cryo.s™ vials	Greiner bio-one	V3135
HiTrap protein G HP	Cytiva	29048581
Millex GV syringe filter unit, 0.22µm, PVDF	Millipore®	SLGV033RS
Minimate™ Tangential Flow Filtration Capsules with Omega™ Membrane – 30K	Pall®	OA030C12
Omnifix®-F 1.0mL syringe	B-Braun	9161406V
PCR tubes	Eppendorf	0030124359
Safe-lock microcentrifuge tubes 0.5mL/1.5mL/2.0mL	Eppendorf	T8911/T9661/T2795
Scalpel (n˚11)	Swann-Morton	0503
Sterican® needle Ø 0,40 x 20 mm 27G	B-Braun	4657705
Sterile 70µm Cell Strainers	Corning™	431751
Terumo™ Luer-Lock syringe 5mL	Terumo™	1SS05LE1
Terumo™ Luer-Lock syringe 50mL	Terumo™	8SS50LE1
Tissue culture dish 100mm	TPP	93100
Tissue culture dish 150mm	TPP	93150
Tissue culture test plate 6 wells	TPP	92006
Tissue culture test plate 24 wells	TPP	92024
Tissue culture test plate 24 wells (Untreated for low-attachment)	Nunc (Thermo Scientific)	144530
Tissue culture test plate 96 wells U-bottom	TPP	92097
Tissue culture test plate 96 wells flat bottom	TPP	92096
Ultrafree®-CL centrifugal device (0.22µm, PVDF)	Millipore®	UFC40GV00
Vacutainer® safety-lok™ blood collection set	BD	367246
Vivaspin® 20 centrifugal concentrator MWCO 50,000Da	Sartorius	VS2032

14mL PP tube sterile	Greiner bio-one	187261
5mL polystyrene round-bottom tubes	Falcon®	352008
5mL polystyrene round-bottom tubes with cell strainer cap – sterile	Falcon®	351935

Table 24: List of other consumables used in the present study

Devices

Device/software	Supplier	Catalogue number
Äkta Pure 25	GE Healthcare	29-0206-58
Amersham™ Imager 680	GE Healthcare	29270769
Avanti J-E centrifuge (with JLA-16.250 and JA-25.50 rotors)	Beckman Coulter	969352
BD FACSCalibur™	BD Biosciences	342975
BD FACS Aria IIIu	BD Biosciences	23-11539-00
BD FACSDiva™ software	BD Biosciences	-
CellQuest™ Pro software	BD Biosciences	-
Chronos Biosafe®	Messer Griesheim	-
DNA/RNA UV-cleaner box, UVC/T-AR	Biosan	BS-040102-AAA
FlowJo V10.7 software	FlowJo, LLC	-
Gammacell 1000	Atomic Energy of Canada Ltd.	-
GraphPad Prism 9 software	GraphPad Software Inc	-
Heracell™ 150i incubator	Thermo Fisher Scientific™	51026282
Herasafe™ 2030i, class II biological safety cabinet	Thermo Fisher Scientific™	51033761
Heraeus™ Megafuge 1.0	Thermo Fisher Scientific™	75003060
Heraeus™ Megafuge 16R	Thermo Fisher Scientific™	75004270
Heraeus™ Multifuge 3L	Thermo Fisher Scientific™	75004370
Heraeus™ Pico™ 17 centrifuge	Thermo Fisher Scientific™	75002410
Heraeus™ Fresco™ 21 centrifuge	Thermo Fisher Scientific™	75002555
HydroFlex™ plate washer	Tecan	30000820
HT Mulitron shaker	Infors AG	110202
Kern 572 scale	Kern und Sohn GmbH	HKR-572-A03
Infinite® M Nano+ plate reader	Tecan	MIC9264
Light inverted microscope DMI1	Leica Microsystems	11526208
MacVector 17.5 software	MacVector Inc.	-
Micropipets PIPETMAN® Classic P2, P20, P200, P1000	Gilson	F167380
Minimate™ Tangential Flow Filtration System	Pall®	OAPMPUNV
MiniVE vertical electrophoresis system	GE Healthcare	80641877
MultiDoc-It™ Digital imaging system	UVP	UVP97019301
Nanodrop 2000	Thermo Fisher Scientific™	S06497
Owl™ EasyCast™ B2 electrophoresis system	Thermo Fisher Scientific™	B2
pH-meter 766	Knick Electronische™	9774761
Pippetus Akku	Hirschmann	HI9907200
Power Pro 300 power supply	Cleaver Scientific	POWERPRO3AMP
Sonoplus HD2070	Bandelin Electronics	BASO_17007
Thermomixer compact	Eppendorf	5350

Transilluminator Bioview UV light	Biostep®	BU02-W1265
Vortex Genie 2	Scientific Industries	SI-0236
Waterbath WNE7	Memmert	MMWNE7

Table 25: List of other apparatus/softwares used in the present study

4.2. Methods

4.2.1. DNA technics: Generation of native antibodies and AgAbs counterparts, cloning of lentiviruses

4.2.1.1. Template DNA

The sequences coding the variable parts (VH and VL) of the cloned antibodies were found in the literature and in public databases. These sequences were synthetized by Eurofins Genomics. The mRNA sequence encoding murine FOLR2 was found on NCBI under the accession number NM_001303239. The open-reading frame was synthetized by Eurofins Genomics.
The plasmid carrying the sequence coding for CIITA isoform 8 was a kind gift from Peterlin's lab (University of California, San Francisco).
The sequences of mCMV epitopes were found in the literature and synthetized by Eurofins Genomics.

4.2.1.2. Cloning of coding sequences

All the clonings generally involved PCR steps. As a general rule, PCR amplifications were performed in 50µL.
For simple PCRs, the amplification mixes were composed of 31.5µL DNA/DNAse/RNA/RNAse-free water, 10µL 5x Phusion HF Buffer, 1µL dNTPs (10mM total), 1µL of template DNA (20 ng total), 2.5µL of 10µM of forward primer, 2.5µL of 10µM reverse primer (50pmol primers total), 2µL dimethylsulfoxide, 0.5µL (1 U) Phusion™ High Fidelity DNA Polymerase (ThermoFisher Scientific). The reactions were performed in a Biometra TOne Thermo Cycler (Analytik Jena) as follow: 1) 98˚C for 30 seconds; 2a) 98˚C for 10 seconds; 2b) 55-72˚C for 30 seconds; 2c) 72˚C for 30 seconds/kb; 2d) Repetition of steps 2a -

2c 35 times; 3) 72˚C for 10 minutes. The annealing temperature (step 2b) was calculated using the online Tm-determination tool from ThermoFisher. Upon extension of DNA fragments with an overhang segments in the primers (overhang extension PCR), 10 cycles were generally performed with the Tm of the annealed region, then 25 cycles were performed with the Tm of the whole primers.

For overlap-PCRs, mixes were composed of the same chemicals as simple PCRs, with the exception of the two preliminary PCR-extended overlapping DNA fragments (overlap of >20 nucleotides) as template DNA. Also, the primers (forward hybridizing on the 5' DNA fragment and reverse hybridizing on the 3' DNA fragment) were added after 10 cycles. In order to minimise the volume variations, the primers were added as a mix in a total volume of 0.5µL (100µM, 50pmol total). The annealing temperature of step 2b was the Tm of the overlapped region for the first 10 cycles, the Tm of the annealed region for 10 further cycles, and finally the Tm of the whole primers for the last 20 cycles.

- Cloning of native antibodies, short AgAbs (including EBNA2 AgAb)

Native antibodies and short AgAbs were generally cloned together. The variable parts (VH and VL) were first PCR-amplified in order to extend their 3'-end with the first 10-15 nucleotides from the 5'-end sequence of the IgG2a Fc region (VH) or kappa light chain CL (VL) (overhang-extension PCR). Likewise, the IgG2a-Fc and kappa light chain CL regions were amplified from a previously described antibody [216] and their 5'-end were extended with 10-15 nucleotides from the 3'-end sequence of the VH part (IgG2a-Fc) or VL part (kappa light chain CL).

The amplified fragments were purified from 1%-agarose gel. Variable and constant regions for each single heavy and light chains were fused to each other through their overlapping sequences (overlap PCR). The forward primers added for this PCR reaction were always containing six random nucleotides, the EcoRI cutting site and a signal peptide for an efficient secretion. The reverse primers were designed to remove the stop codon at the end of the Fc region, and were containing the sequence encoding an epitope, then a stop codon (for short AgAbs – no additional sequence for native antibodies) as well as the HindIII cutting site and six random nucleotides. After the overlap PCR, the product with the expected size was isolated from a 1% agarose-gel for further processing.

Short anti-human antibodies:

Construct	First Step				Second Step (Overlap)			Clone
	Subpart	Primers	Template	Tm (10/25 cycles)	Primers		Tm (10/10/20 cycles)	
CLL-1 IgG2a HC Native (WT Fc)	VH	3609+3611	B1785	54,9˚C/ 70,5˚C	3613 + 3614		70,3˚C/ 66,8˚C/ 72,0˚C	**B1877**
	CH	3610+3612	B233	52,7˚C/ 70,3˚C				
CLL-1 kappa LC	VL	3615+3616	B1786	51,8˚C/ 70,5˚C	3619 + 3620		70,2˚C/ 68,0˚C/ 72,0˚C	**B1891**
	CL	3617+3618	B200	51,1˚C/ 70,2˚C				
CD21 IgG2a HC (LALA)		3723 + 3724	B233	55˚C (18 cycles)	No second PCR (site-directed mutagenesis)			**B1904**
CLL-1 IgG2a HC (LALA)	VH	3609+3611	B1785	54,9˚C/ 70,5˚C	3614 +	3613	70,3˚C/ 66,0˚C/ 72,0˚C	**B1902** (Nat)
						3744		**B1923** (3H10)
	CH	3610+3612	B1904	52,7˚C/ 70,3˚C		3748		**B1925** (1D6)
CD123 IgG2a HC (LALA)	VH	3740+3742	B1783	56,0˚C/ 72,0˚C	3741 +	3613	72,0˚C/ 66,0˚C/ 72,0˚C	**B1912** (Nat)
						3744		**B1914** (3H10)
	CH	3743+3612	B1904	56,0˚C/ 72,0˚C		3748		**B1916** (1D6)
CD123 kappa LC	VL	3769+3770	B1784	56,0˚C/ 72,0˚C	3619 + 3772		72,0˚C/ 67,0˚C/ 72,0˚C	**B1917**
	CL	3771+3618	B200	56,0˚C/ 72,0˚C				
CD33 IgG2a HC (LALA)	VH	3929+3742	B1852	56,0˚C/ 72,0˚C	3930 +	3613	72,0˚C/ 66,0˚C/ 72,0˚C	**B2018** (Nat)
						3744		**B2019** (3H10)
	CH	3743+3612	B1904	56,0˚C/ 72,0˚C		3748		**B2021** (1D6)
CD33 kappa LC	VL	3931+3770	B1855	56,0˚C/ 72,0˚C	3619 + 3932		72,0˚C/ 67,0˚C/ 72,0˚C	**B2022**
	CL	3771+3618	B200	56,0˚C/ 72,0˚C				
HuFR-β IgG2a HC (LALA)	VH	3740+3742	B1911	56,0˚C/ 72,0˚C	3741 +	3613	72,0˚C/ 66,0˚C/ 72,0˚C	**B2023** (Nat)
						3744		**B2024** (3H10)
	CH	3743+3612	B1904	56,0˚C/ 72,0˚C		3748		**B2026** (1D6)
HuFR-β kappa LC	VL	3773+3774	B1912	56,0˚C/ 72,0˚C	3619 + 3776		72,0˚C/ 67,0˚C/ 72,0˚C	**B2027**
	CL	3775+3618	B200	56,0˚C/ 72,0˚C				

Table 26: PCR conditions for the cloning of short anti-human antibodies

Anti-mouse antibodies

Construct	First Step				Second Step (Overlap)			Final clone
	Subpart	Primers	Template	Tm (10/25 cycles)	Fusion	Primers	Tm (10/10/20 cycles)	
MoFR-β IgG2a HC (Unmutated)	VH	4125 + 4126	B1921	58,0˚C/ 72,0˚C	VH + CH	4128 + 3613	72,0˚C/ 67,0˚C/ 72,0˚C	**B2180** *Native UM*
	CH	3612 + 4127	B233	58,0˚C/ 70,3˚C	VH + CH	4128 + 4420		Vector for Ag insertion (see below)
MoFR-β IgG2a HC AgAb BALB/c epitopes	IgG2a	1838+4348	B2180	58,0˚C/ 68,0˚C	IgG2a + Ag	1838 + 4343	72,0˚C/ 72,0˚C/ 72,0˚C	**B2139**
	Ag domain	4341+4343	B2102					
Antigens C57BL/6	mCMV (M25+ M142)	4417 + 4418	B2102	58,0˚C/ 68,0˚C	No second PCR; Digestion with KpnI and HindIII, and ligation in vector for Ag insertion.			**B2182** *AgAb 2ep UM*
	mCMV (M25+ M112+ M139)	4415 + 4419						**B2184** *AgAb 3ep UM*
MoFR-β IgG2a HCs (LALA) Native, AgAbs 2 and 3 epitopes		3723 + 3724	B2180 B2182 B2184	55˚C (18 cycles)	No second PCR (site-directed mutagenesis)			Template for DA mutation (see below)
MoFR-β IgG2a HC (LALA+DA)		4410 + 4411	B2180 with "LALA"	55˚C (18 cycles)	No second PCR (site-directed mutagenesis)			**B2181**
MoFR-β IgG2a HC 2 epitopes (LALA+DA)			B2182 with "LALA"					**B2183**
MoFR-β IgG2a HC 3 epitopes (LALA+DA)			B2184 with "LALA"					**B2185**

Table 27: PCR conditions for the cloning of anti-mouse antibodies

- Cloning of antibodies with longer antigenic sequences (*ex vivo* and *in vivo* antibodies)

Antibodies with larger antigenic regions were subsequently cloned in a two-step process. The sequence encoding the native heavy chain was amplified and extended with the 5'-end of either EBNA1 or EBNA3C (first, second or third part) or with murine antigenic regions (EBNA2 sequence was short enough to be added as described in the previous part). The extension PCR was designed to remove the stop codon previously localised at the end of the native heavy chain. Antigenic regions were also extended in their 5'-end with 10-15 nucleotides from the 3'-end of the IgG2a heavy chains (with no stop codon). The fragments were then fused through their

overlaps, following a similar protocol to this used to fuse variable parts with their matching constant regions.

Since the antigenic regions were too short for the C57BL/6 AgAbs (dramatic length difference between antigenic sequence and heavy chain), a different approach was adopted. Antigenic domains were first amplified and KpnI and HindIII restriction sites were added in 5' and 3' respectively. A KpnI restriction site was also added at the 3'-end of the mFR-β heavy chain. Subsequently, the antigenic domains were inserted at the 3'-end of mFR-β heavy chain through digestion (KpnI/HindIII) and ligation.

Anti-human long AgAbs

First Step					**Second Step (Overlap)**			**Clone**	
Subpart	**Template**	**Primers**		**Tm (10/25 cycles)**	**Fu-sion**	**Pri-mers**	**Tm (10/30 cycles)**		
IgG2a Fc (OL with antigen)	B1902 *(CLL-1)* B1913 *(CD123)* B2018 *(CD33)* B2023 *(HuFR-β)*	1838 +	2391 *(E1)*	60,0˚C/ 72,0˚C	IgG + E1	1838 + 2393	72,0˚C/ 72,0˚C	**B2029** *(CD33)* **B2030** *(CLL-1)* **B2031** *(CD123)* **B2032** *(HuFR-β)*	**EBNA1**
			1990 *(E3C 1/3)*		IgG + E3C 1/3	1838 + 2006		**B2039** *(CD33)* **B2040** *(CLL-1)* **B2041** *(CD123)* **B2042** *(HuFR-β)*	**EBNA3C 1/3**
			2000 *(E3C 2/3)*						
			2002 *(E3C 3/3)*						
EBNA1 (OL with IgG2a)	B1301	2392+2393			IgG + E3C 2/3	1838 + 2014		**B2044** *(CD33)* **B2045** *(CLL-1)* **B2046** *(CD123)* **B2047** *(HuFR-β)*	**EBNA3C 2/3**
EBNA3C (1/3) (OL with IgG2a)	B1199	1993+2006							
EBNA3C (2/3) (OL with IgG2a)	B1200	2007+2014			IgG + E3C 3/3	1838 + 1998		**B2049** *(CD33)* **B2050** *(CLL-1)* **B2051** *(CD123)* **B2052** *(HuFR-β)*	**EBNA3C 3/3**
EBNA3C (3/3) (OL with IgG2a)	B1201	2015+1998							

CD33 EBNA2	B2018	1838+4076	60,0˚C/ 72,0˚C	*Direct cloning (no overlap)*	**B2034**	**EBNA2**
CLL-1 EBNA2	B1902				**B2035**	
CD123 EBNA2	B1913				**B2036**	
HuFR-β EBNA2	B2023				**B2037**	

Table 28: PCR conditions for the cloning of long anti-human AgAbs

- Cloning of lentiviral genomes

Two different lentiviruses were cloned, with two different strategies.

The CIITA lentivirus was designed so that both CIITA and a puromycin resistance genes were under the same promoter, separated with an IRES. Since no compatible cutting site was found in the lentivirus vector (B671) for a 5' insertion, a part of the vector was PCR-amplified up to a unique EcoRI site. This fragment was extended at its 3'-end with nucleotides from the CIITA sequence. The polio IRES sequence was amplified from the vector B and extended at its 5'-end with nucleotides from the end of the CIITA sequence and at its 3'-end with a BglII cutting site and nucleotides from the puromycine resistance gene. The sequence coding the isoform 8 of the human major histocompatibility complex transactivator (CIITA) was PCR amplified and extended at its 5'end to create an overlap with the fragment from B671, and at its 3' end to create an overlap with the IRES fragment. All three fragments were fused through two overlap PCRs.

A different approach was adopted for the cloning of the FOLR2 lentivirus (since infected cells were already resistant to puromycin). The puromycin resistance gene was exchanged with the FOLR2 mRNA sequence in B671. The latter was PCR-amplified with overhang primers, so that BamHI site was added at its 5'-end and the KpnI site at its 3'-end.

<table>
<tr><th rowspan="2">Construct</th><th colspan="4">First Step</th><th colspan="3">Second Step (1st overlap)</th><th colspan="2">Third PCR (2nd overlap)</th><th rowspan="2">Clone</th></tr>
<tr><th>Sub part</th><th>Pri-mers</th><th>Tem-plate</th><th>Tm 10/25 cycles</th><th>Pri-mers</th><th>Tm 40 cycles</th><th>Pro-duct</th><th>Pri-mers</th><th>Tm 40 cycles</th></tr>
<tr><td rowspan="3">CIITA lentivirus</td><td>B671 region</td><td>3688 + 3689</td><td>B671</td><td>64,3˚C/ 72,0˚C</td><td rowspan="2">3688 + 3691</td><td rowspan="2">72,0˚C</td><td rowspan="2">B671 region + CIITA</td><td rowspan="3">3688 + 3544</td><td rowspan="3">72,0˚C</td><td rowspan="3">B2186</td></tr>
<tr><td>CIITA gene</td><td>3690 + 3691</td><td>B1782 (received)</td><td>62,6 ˚C/ 72,0˚C</td></tr>
<tr><td>IRES</td><td>3692 + 3544</td><td>B734</td><td>63,0˚C/ 72,0˚C</td><td colspan="3"></td></tr>
<tr><td>FOLR2 lentivirus</td><td>FOLR 2</td><td>4121 + 4122</td><td>B1905</td><td>64,9 ˚C/ 72,0˚C</td><td colspan="5">Direct PCR (no overlap)</td><td>B2098</td></tr>
</table>

Table 29: PCR conditions for the cloning of lentiviral plasmids

4.2.1.3. Restriction digests of inserts, vector preparation

All the heavy and light chains (native and AgAbs) were designed with EcoRI and HindIII cutting sites, at their 5'- and 3'-ends, respectively. In preparation for the insertion in their vector, the chains were digested with these enzymes for 2 hours at 37˚C. Likewise, the pRK5 vector (from B918) was digested with the same enzymes. Both digestions were conducted in 50µL, with 10µL 10x Tango Buffer, 1.5µL EcoRI (10U/µL), 1.5µL HindIII (10U/µL), 5µg DNA and PCR-grade water up to 50µL.

The CIITA fragment was digested with EcoRI and BglII enzymes for 2 hours at 37˚C in 50µL (10µL 10x Tango Buffer, 1.5µL EcoRI (10U/µL), 1.5µL BglII (10U/µL), 5µg DNA). The B671 vector for the CIITA lentivirus was comparably digested with EcoRI and BamHI. Of note, BglII and BamHI ends are compatible.

The FOLR2 fragment and the B671 vector were digested with BamHI and KpnI enzymes for 2 hours at 37˚C in 50µL (5µL 10x Tango Buffer, 1µL BamHI (10U/µL), 2µL KpnI (10U/µL), 5µg DNA and PCR-grade water up to 50µL).

All the vectors were subsequently dephosphorylated. A mix of 10µL dephosphorylation buffer (10X), 1µL alkaline phosphatase and 39µL PCR-grade water (50µL total) was added to the digestion reactions. These reactions were incubated for 30 minutes and heat-inactivated at 80˚C for 10 minutes. All the reactions were then loaded on a 1% agarose gel for isolation.

4.2.1.4. Purification of DNA fragments from agarose gels

Migrations of PCR and digestion products were routinely performed to isolate the fragments with the expected size and to eliminate secondary products and primers. Agarose-embedded DNA fragments were purified with the PCR and Gel Extraction Mini Spin column kit (Genaxxon Bioscience), according to the manufacturer's indications. To summarise, the gel slices were heated at 50˚C in GB buffer before loading into spin columns. The columns were washed twice with Wash Buffer before elution with pre-heated (70˚C) elution buffer.

4.2.1.5. DNA ligation

All DNA concentrations were measured before further steps using a NanoDrop 2000 device (Thermo Fisher scientific). All the light and heavy chains were inserted in the pRK5 vector. CIITA and FOLR2 fragments were inserted in their matching B671 vectors.
For the ligation, 50µg of plasmid backbone was mixed with the insert of interest (1:3 vector : insert molar ratio – for example 50µg for a native heavy chain since the insert is 3 times shorter than the opened pRK5 vector). 1µL of ligase buffer (10X), 0.4µL T4 DNA ligase (5U/µL) and PCR-grade water up to 10µL. A control with no insert (vector only) was always performed. The reaction was incubated at room temperature for 20 minutes.

4.2.1.6. Site directed-mutagenesis

Point mutations in the constant fragments of antibodies (L234A/L235A or D265A) were inserted with site-directed mutagenesis. Specific complementary primers were designed to introduce, containing the unmatched nucleotides, flanked in 5' and 3' with at least 15-20 matched nucleotides. The PCR reaction mix was similar to a normal PCR (see in Ib). The reaction was run as follow: 1) 98˚C for 30 seconds; 2a) 98˚C for 10 seconds; 2b) 55˚C for 30 seconds; 2c) 72˚C for 3 minutes; 2d) Repetition of steps 2a - 2c 18 times; 3) 72˚C for 10 minutes. Then, 25µL from the PCR reaction were supplemented with 5µL DpnI buffer, 2µL DpnI enzyme (10U/µL) and 18µL of PCR-grade water. The reaction was incubated at 37˚C for 2 hours in order to digest the parental methylated DNA. As a control reaction, the template DNA (unmutated plasmid without PCR) was also digested with DpnI.
After digestion, 10µL from each reaction were directly used for bacterial transformation.

4.2.1.7. Transformation of chemically competent DH5α bacteria and screening of bacterial clones

After ligation (or site-directed mutagenesis), the DNA products were introduced into chemically competent DH5α *E.coli* bacteria for amplification. 100µL bacterial aliquots were slowly thawed on ice. Subsequently, the bacteria were supplied with 10µL of the DNA mixture and incubated on ice for 5 minutes, followed by a heat-shock (42˚C) for 90 seconds. The bacteria were then immediately transferred into a tube with loose cap in 3mL of LB medium with no antibiotics, and incubated at 37˚C with constant agitation (180rpm) for 20 minutes.
The tubes were then centrifuged for 10 minutes (4000rpm), the bacteria were resuspended in 100µL of LB medium and plated on LB agar plates containing ampicillin (1‰ v/v). The plates were next incubated for 16-18 hours at 37˚C, and colonies were counted and compared to the reaction control (either empty vector for ligation or DpnI-digested parental DNA for site-directed mutagenesis) to ensure minimum background.
Three to six random colonies were selected and amplified overnight in 7mL LB medium with ampicillin (1‰ v/v), in tubes with loose cap. Each amplified clone was then subjected to plasmid purification (mini-prep), and isolated plasmids were digested with the same enzymes previously used for the cloning. The correct DNA banding pattern was then verified after migration of the digestion products on a 1% agarose gel. Plasmids with a correct digestion pattern were sent for sequencing. The clones with congruent sequencing results were stored in 25% v/v glycerol at -80˚C (one clone for each construct) for further use.

4.2.1.8. DNA Sequencing

Sequencing of plasmids was performed by Microsynth Seqlab. 1 µg plasmid DNA was mixed with 30pg of a primer allowing the sequencing of the region of interest. The total volume was 15µL. Sequencing results were analysed using the MacVector software.

4.2.1.9. Amplification of plasmids

- Alkaline lysis Mini-Prep

Bacteria were cultured overnight in 5-8 mL LB medium (1‰ v/v ampicilin) in tubes under constant agitation at 37˚C.
The bacteria were first centrifuged (4000rpm), resuspended in 200µL TE buffer (+1µL RNAse A) and transferred into 1.5mL tubes. Then, 200µL freshly prepared 0,2M NaOH + 1% (v/v)

SDS were added to the bacteria and the tubes were carefully mixed twice. After 5 minutes at room temperature, the lysis was neutralized with 200µL 3M potassium acetate (pH=5.5) solution. The tubes were inverted three times before 10 minutes incubation on ice. The debris were then pelleted for 20 minutes at 14.000rpm in a Heraeus™ Pico™ 21 Fresco microcentrifuge. The supernatants were collected and centrifuged again to get rid of smaller debris. The clear supernatant was subsequently transferred into a new tube and DNA precipitation was triggered by adding 500µL ice-cold isopropanol. The tubes were incubated on ice for another 10 minutes before centrifugation at 14.000rpm for 15 minutes. The DNA pellet was washed twice with 1mL 80% ethanol, to get rid of salts. Finally, all ethanol traces were removed and the pellet was resuspended in 50µL PCR-grade water.

- Large scale plasmid preparation ("maxi-prep")

Bacteria were cultured in 200-400mL LB medium containing 1‰ ampicillin (v/v) in 2L Erlenmeyer flasks at 37˚C under constant agitation.
Plasmid preparation was performed with the PureLink™ HiPure Plasmid Maxiprep kit (Invitrogen™), according to manufacturer's instructions.

4.2.2. Eukaryotic cell culture

4.2.2.1. Human and murine cell lines maintenance

All cell lines were maintained at 37°C, 5% CO2, in a humidified incubator. MV4-11 AML cell line was kindly provided by Prof. Diederich's lab (DKFZ). 5637 cells as well as HL-60 and Mutz-3 AML cell lines were kindly provided by Prof. Plass' lab (DKFZ). All other human AML cell lines were a gift of Prof. Krämer's lab. mCMV murine CD4 T cell hybridoma were kindly supplied by Prof. Oxenius' lab (ETH Zurich).
C1498 and WEHI-3 murine cell lines were purchased from ATCC.
HEK293T and 5637 adherent cells were maintained in Roswell Park Memorial Institute (RPMI) 1640 1X medium (Gibco®) supplemented with 10% h.i. foetal bovine serum (FBS).
NOMO-1, KG-1, GDM-1, HL-60, MV4-11, MOLM-14, and THP-1 human AML cells, as well as C1498 murine AML cell line and murine T cell hybridomas, were cultured in RPMI-1640 with 10% FBS. MonoMac6 cells were maintained in RPMI 1640 supplemented with 10% FBS,

2mM GlutaMAX™, 1% (v/v) non-essential amino-acids (NEAA). Kasumi-1, OCI AML-2 and OCI AML-3 were cultured in RPMI 1640 supplemented with 20% FBS.

Mutz-3 AML cells were maintained in 60% Iscove's Modified Dulbecco's Medium (IMDM, Gibco®) with 20% FBS and 20% 5637-conditionned medium. WEHI-3 murine AML cells were cultured in IMDM with 10% FBS and 0.05 mM 2-mercaptoethanol.

LCL cells, generated by transformation of B cells with EBV, were maintained in RPMI 1640 supplemented with 10% FBS, 2mM GlutaMAX™, 1% (v/v) NEAA, 1mM Sodium Pyruvate, 5‰ (v/v) Fungizone and 50 µg/mL Gentamicin (LCL medium). T cell clones were maintained in AIM V™ Medium (Gibco®) supplemented with 10% freshly isolated human serum (see T cell stimulation section), 10 mM HEPES, 2mM GlutaMAX™, 0,4mg/mL Ciprofloxacin and 50µg/mL Gentamicin.

4.2.2.2. Production of recombinant antibodies

AgAbs and native antibodies were produced in HEK293T cells transiently transfected with purified plasmid DNA and Polyethylenimine (PEI). HEK293T cells were plated in 10cm culture dishes one day prior to the transfection, at a confluency of 3.10^6, in 6mL RPMI 1640 with 10% FBS. For native antibodies and short human AgAbs, heavy and light chain were transfected at DNA ratio of 1:2 (light chain limiting). Conversely, for long human AgAbs and murine AgAbs, heavy and light chain were transfected at a DNA ratio of 2:1 (heavy chain limiting). Transfection complexes were formed in 800µL Opti-MEM™ (Gibco®), with 30µg DNA total (HC+LC mixed according to the aforementioned ratios), and 90µg PEI. After 20 minutes, the complexes were gently transferred onto the cells. Finally, the supernatants were removed after 6 hours, transfected cells were carefully rinsed once with sterile PBS 1X, and 10mL of pre-warmed FreeStyle™ 293 Expression Medium (Gibco®) were added to the cells.

The culture supernatants were collected after 5-7 days (at 37˚C), centrifuged and filtered through a 0.45µm low-protein binding filter (Merck Millipore) in order to get rid of cell fragments. The filtrated supernatants were then concentrated to 500µL with a Vivaspin® 20 centrifugal filter (Cut-off 50KDa, Sartorius). The concentrate antibodies were finally filter-sterilized with 0.22µm Ultrafree®-CL centrifugal filter (Merck Millipore).

For animal experiments, the supernatants were concentrated (1-2 litres at once) and the buffer was exchanged for PBS using a Minimate™ Tangential Flow Filtration Capsule system (Pall®) up to a final volume of 50mL. This concentrated solution was subsequently loaded into an

Äkta™ Pure 25 (GE Healthcare) equipped with a HiTrap™ Protein G HP (Cytiva). The eluted antibody is then dialysed with Vivaspin® 20 centrifugal filter (Sartorius) and filter-sterilized with 0.22µm Ultrafree®-CL centrifugal filter (Merck Millipore).

4.2.2.3. Production of recombinant lentiviruses

HEK293T cells were plated in 6-well plates (2.10^5 cells/well) in 2mL RPMI-1640 10% FBS, one day prior to the transfection. For each well, 100µL RPMI were supplemented with 1µg plasmid DNA with the gene of interest, 0.5µg of both packaging helper DNA-plasmids (B653 – pCMV gag/pol – and B654 – pCMV VSV-G). 100µL containing 6µL Metafectene® (Biontex) were then added to the DNA mix and the reaction was subsequently incubated for 20 minutes, before addition onto the HEK293T cells. The following day, the supernatants were replaced with fresh RPMI-1640 with 10%FBS. 3 days later, the supernants containing the lentiviruses were centrifuged (1500rpm) and filtered with a 0.45µm low-protein binding filter (Merck Millipore).

4.2.2.4. Modification of murine AML cells

WEHI-3 and C1498 murine cell lines were modified with lentiviruses to induce the surface expression of murine MHC-II and folate receptor beta. Cloning and production of both lentiviruses is detailed in part.

For the infection, 5.10^5 murine cells were washed and resuspended in 500µL RPMI-1640 (C1498) or IMDM (WEHI-3) with 10% FBS and 500µL lentivirus-containing supernatant, complemented with 8 µg/mL Polybrene® (Santa Cruz), in a 6 well-plate. The plate was then centrifuged for 2 hours at 1200xg (spinoculation). 1mL culture medium was then added (RPMI-1640 or IMDM) and the plate was incubated for 18 hours at 37˚C. The following day, the cells were washed with sterile PBS and resuspended in their respective culture medium.

The first infection was performed with the CIITA lentivirus, in order to induce MHC-II expression. Infected cells were selected with 0.4mg/mL G418 in the culture media (dose determined in a preliminary dose response experiment). Survivor cells were then infected with the FOLR2 lentivirus in order to induce folate receptor-beta expression.

Selection of MHC-II^+/FR-β^+ cells was conducted performing fluorescence-activated cell sorting (FACS). Briefly, 10^7 infected cells were collected, and resuspended in a sterile staining solution (PBS + 1% FBS, anti-mouse FR-beta and anti-mouse MHC-II antibodies, 0.22µm-

filter sterilized) and incubated on ice and in the dark for 30 minutes. Finally, the cells were washed and resuspended in sterile staining PBS+1% FBS and immediately subjected to cell sorting on a FACSAria™ IIIu Cell Sorter (Beckton Dickinson). The sorted cells were subsequently cultured in their respective culture medium with Penicilin/Streptomycin.

4.2.2.5. Maintenance of human T cell clones

- Production of human serum

Venous blood was freshly collected from healthy donors (minimum 2 per round), and left for clotting for 4 hours at room temperature. The clotted blood was then centrifuged at 2100rpm for 30 minutes with no brake. The serum phase was subsequently collected and centrifuged for another 10 minutes to get rid of small clots. The clear serum was then heat-inactivated for 30 minutes at 52˚C, aliquoted and frozen at -20˚C.

- Isolation of PBMCs from healthy donors

Peripheral blood mononuclear cells were isolated from buffy-coats, provided by the "Institut für Klinische Transfusionsmedizin und Zelltherapie (IKTZ)" (Blood bank Mannheim). Blood from 2 donors was used for each stimulation. 30mL concentrated blood was diluted with 50mL PBS+1% (v/v) Heparin in 250mL conic centrifugal tubes, underlaid with 50mL Ficoll-Paque Plus™ (Cytiva) and centrifuged at 500g for 30 minutes (Heraeus 3L centrifuge, with no break). The white interphase was then carefully collected and washed three times with sterile PBS 1X (centrifugations at 80g for 10 minutes).
Finally, the PBMCs were resuspended in T cell medium at a concentration of 10^6 cells/mL and equally mixed so that half of the total PBMC count was coming from each donor. The cells were then irradiated at 40 Grays before being used as feeder cells in T cell cultures.

- Stimulation of T cells

HLA-matched lymphoblastoid cell line cells (LCLs, EBV-immortalised B cells) were used as APCs. The cells were pulsed for 4-6 hours in LCL medium at a concentration of 1.10^6 cells/mL (1µg/peptide for each 10^6 cells). GB LCLs were used to stimulate EBNA3C 3H10 T cells and AS LCLs were used to stimulate gp350 1D6 T cells.
The cells were then irradiated at 80 Grays. Subsequently, the irradiated LCLs were washed twice in PBS 1X to get rid of unbound peptide. Finally, the T cells were mixed with the LCLs

and the PBMCs in a 24-well plate. For each 10^6 T cells, $1{,}8.10^5$ LCLs and 10^6 PBMCs were mixed in 2mL T cell medium (supplemented with 10U/mL of IL-2 and 250 ng/mL of PHA). After 48 hours, the supernatants were carefully replaced for T cell medium without PHA. The stimulation was repeated every 10-14 days.

4.2.2.6. Ex vivo culture of donor cells

Healthy PBMCs were freshly collected as described in part 4.2.2.5.
Malignant PBMCs or bone marrow cells from AML patients were provided by Dr. med. Caroline Pabst from the *Universitätsklinikum* Heidelberg as frozen vials. To optimise the quality of the thawed sample, thawing medium (IMDM, 20% FBS, 100µg/mL DNAse I) was warmed at 37˚C. The vial was thawed in a waterbath and its content was carefully transferred into 10mL thawing medium. The cells were then washed once with pre-warmed maintenance/expansion medium (IMDM, 15% BIT, 20ng/mL IL-3 and G-CSF, 50ng/mL FLT3L, 100ng/mL SCF, 50µg/mL Gentamicin, 10µg/mL Ciprofloxacin, 0.1mM β-mercaptoethanol, 500nM SR1 and UM729).
AML cells were cultured for maintenance in the maintenance/expansion medium in platsicware with hydrophobic (non-treated) surface to avoid cell-attachment. In 24-well plates, 2.10^5 cells were seeded in 1mL. The volume between the wells was filled with sterile water to limit medium evaporation.
Healthy PBMCs and AML cells from patients were cultured either in AML medium or T cell medium for assessments of T cell proliferation.

4.2.3. Assessment technics

4.2.3.1. Western-blotting

Expression and correct assembly of recombinant native antibodies as well as antigen-armed antibodies were checked in Western-Blot. 10-50ng of antibody were diluted in 4X protein loading buffer without β-mercaptoethanol (15µL total sample volume) and boiled at 95˚C for 10 minutes. The samples were then loaded onto a biphasic SDS-polyacrylamide gel (4,5%-acrylamide stacking gel and 7,5%-acrylamide separation gel). 5µL Spectra™ Multicolor High Range Protein Ladder (40-300KDa) were loaded as a protein standard. The migration was first performed at 80V until the samples reached the separation gel and the voltage was increase up

to 120V. The proteins were then blotted onto a Amersham™ Protran® nitrocellulose membrane (0,45µm pores, GE), for 90 minutes at 45V. Subsequently, the membrane was blocked with PBS + 3% (m/v) skim milk for 1h at room temperature. A goat-anti mouse IgG-HRP antibody (Promega) was then used to detect the antibodies on the membrane (1:20.000 dilution in PBS+milk, incubation for 1h at room temperature). Finally, the membrane was washed 3 times in PBS-0.05% Tween 20 before the addition of 2mL pre-mixed Western Lightning® Plus –ECL substrate. The chemiluminescence was detected using an Amersham™ 680 Imager (General Electrics).

4.2.3.2. Antibody quantification

The exact quantification of produced and concentrated antibodies was determined with a murine IgG ELISA. Corning® 1 x 8 Stripwell™ 96-Well plates were coated over-night with 50µL/well capture antibody (10µg/mL, AffiniPure Goat Anti-Mouse IgG + IgM (H+L), Jackson ImmunoResearch©), diluted in PBS 1X. The plates were washed with the washing buffer (PBS + 0.1% Tween-20) and blocked overnight at 4˚C with 300µL/well blocking solution (PBS + 2% BSA (m/v)). The samples were then distributed into the wells in triplicates, along with the IgG2a standard (Invitrogen™) which ranged from 10ng/mL to 0,156ng/mL, and a blank condition. After a 1-hour incubation at room temperature with constant agitation, the plates were washed and 50µL of pre-diluted anti-mouse IgG HRP (Promega, 0.5µg/mL) was dispensed into the wells. Finally, the plates were washed and 100µL of pre-mixed (1:1 solution A and B) BD OptEIA™ TMB Substrate. The reaction was stopped with 100µL of 2M sulfuric acid and the OD_{450nm}, with a wavelength correction at 540nm, was measured with a microplate photometer (Tecan Infinite M Nano Plus).

4.2.3.3. Marker screening in flow cytometry

To assess the expression of cell-surface markers, flow cytometry stainings were performed. The cells to stain were collected and washed once in PBS + 1% FBS (staining buffer). 2.10^5 cells were then resuspended in 100µL staining buffer and antibodies against the markers of interest (or isotype controls) were added according to the recommendations from the manufacturer (most often 5µL/antibody). In case of multiple stainings (2 antibodies in the same staining), compatible dyes were chosen to minimise compensation (PE – channel 2 – or FITC/Alexa Fluor™ 488 – channel 1 – in combination with APC – channel 4). In some conditions,

discrimination between live and dead cells was performed with LIVE/DEAD™ Fixable Far Red Dead Cell Stain Kit (Invitrogen™), which is compatible with PE and FITC dyes with minimal compensation. The stainings were then incubated in the dark, on ice, for 30 minutes before being washed once with staining buffer. The stained cells were finally resuspended in 300µL staining buffer and analyzed with a FACSCalibur™ Flow Cytometer (Becton Dickinson Biosciences), using CellQuest software. Between 10.000 and 50.000 events were generally recorded.
Flow cytometry data was subsequently analyzed using FlowJo V10.7.

4.2.3.4. Binding assays

To assess the binding of preliminarily cloned antibodies (native or AgAbs), binding assays in flow cytometry were conducted. 2.10^5 cells of interest (expressing the marker of interest) were collected and washed once in staining buffer. The cells were then resuspended in 100µL staining buffer and incubated with 100ng of the antibody to test for 30 minutes. An isotype control was always added with a produced antibody targeting a marker absent from the surface of stained cells. Afterwards, the cells were washed and resuspended in 100µL staining buffer with 2µL Goat anti-Mouse IgG (H+L) Alexa Fluor™ 488 (Invitrogen™). After further 30 minutes, the cells were washed and the fluorescence evidencing the binding of the native antibody/AgAb was measured on the flow-cytometer, similarly to part 4.2.3.3.

4.2.3.5. Cytokine-release assays

- Co-culture of effector and target cells

T-cell activation induced by the presentation of EBV epitopes (peptide or from AgAbs) was assessed through the release of pro-inflammatory cytokines, namely IFNγ and Granzyme B.
On day 1, antigen-presenting cells (LCL or AML cells) were counted, resuspended at 5.10^5 cells/mL in their respective culture medium, and pulsed either with peptide or AgAbs (ranging from 0,1ng to 100ng per 5.10^4 cells, e.g. 1ng-1µg/mL) or native antibody (highest concentration only 100ng per 5.10^4 cells, e.g. 1µg/mL) for 16 hours.
On day 2, the cells were washed twice in sterile PBS 1X to get rid of unbound antibodies/peptides. The APCs were subsequently incubated with matching T cells (unless specified, E:T = 2:1, e.g. 5.10^4 APCs with 10^5 T-cells), in 200µL RPMI-1640 + 10% FBS, in U-bottom 96-well plates, and at 37°C for 16 hours.

On day 3, the plates were centrifuged at 1200rpm and the supernatants were collected. The presence of IFNγ and Granzyme B was then assessed in ELISA specific for these cytokines.
A very similar co-culture was performed to assess the presentation of mCMV epitopes to murine T cell hybridomas by murine C1498 and WEHI-3 cells. Murine AML cells were pulsed with anti-FR-β AgAbs or native antibodies, before being washed and co-incubated with matching murine T cell hybridomas (E:T=2:1). On day 3, the supernatants were collected and IL-2 concentration was measured.

- Human IFNγ and Granzyme B ELISA

Cytokine release was assessed using IFNγ and Granzyme B ELISA kits (Mabtech) according to the manufacturer's instructions. Briefly, Corning® 1 x 8 Stripwell™ 96-Well plates were coated over-night with the provided coating antibodies (Clone MT34B6 for GzmB and 1-D1K for IFNγ) overnight at 4˚C before blocking with PBS + 2% BSA (ELISA buffer). Samples were then distributed along with respective standard ranges and incubated for 2 hours at room temperature under constant agitation. Biotinylated detection antibodies (Clone MT28 for GzmB and 7-B6-1 for IFNγ) and Streptavidin-HRP diluted in ELISA buffer were subsequently added and incubated for 1 hour each. Finally, BD OptEIA™ TMB Substrate was used to reveal HRP activity, the reaction was stopped with 2M sulfuric acid and the OD_{450nm}/OD_{540nm} were read with a microplate reader, comparably to the IgG2a ELISA (III-B).

- Murine IL-2 ELISA

Corning® 1 x 8 Stripwell™ 96-Well plates were coated over-night with the anti-mouse IL-2 monoclonal antibody (Clone JES6-1A12, eBiosciences™), diluted 1:200 in PBS, overnight at 4˚C before blocking with PBS + 2% BSA (ELISA buffer). Samples were then distributed along with standard range (highest concentration equal to 400pg/mL, then 1:2 dilutions) and incubated for 2 hours at room temperature under constant agitation. Biotinylated anti-IL-2 detection antibody (Clone JES6-5H4, eBiosciences™), then Streptavidin-HRP (Mabtech), both diluted 1:1000 in ELISA buffer, were subsequently added and incubated for 1 hour each. Finally, BD OptEIA™ TMB Substrate was used to reveal HRP activity, the reaction was stopped with 2M sulfuric acid and the OD_{450nm}/OD_{540nm} were read with a microplate reader, comparably to the IgG2a ELISA (III-B).

4.2.3.6. Killing assays

- Calcein-release assay

To assess short-term killing of target cells by effector cells, calcein-release assays were performed. Preparation of target cells (incubation with peptide/native antibodies/AgAbs) was similar to that of cytokine release assays (100ng/5.10^4 APCs).

On day 2, the cells were washed twice with sterile PBS and stained with Calcein-AM (BioLegend, 1µM) in RPMI-1640 without phenol red (Gibco®) for 30 minutes at 37˚C. The cells were then carefully washed and mixed with matched T cells at different E:T ratios (from 1:1 to 15:1) with a fix number of APCs (5.10^4) in 200µL clear RPMI-1640 in U-bottom 96-well plates. To determine the maximum and spontaneous lysis, some APCs were treated with 1% Triton X-100 (maximum) or mock medium (spontaneous).

After 4 hours, the supernatants were harvested and transferred into a flat-bottom 96 well. The fluorescence was measured with a microplate fluorescence reader (Tecan Infinite M Nano Plus, Excitation = 485/9nm / Emission = 535/20nm). The percentage of specific lysis was evaluated as follows:

$$Specific\ lysis_{(Condition\ A)} = \frac{(Fluorescence_{Condition\ A} - Fluorescence_{Spontaneous\ lysis})}{(Fluorescence_{Maximum\ lysis} - Fluorescence_{Spontaneous\ lysis})}$$

- Overnight killing assay

To assess the elimination of target cells by effector cells over a longer time span, overnight killing assay based on a flow cytometric approach were performed.

On day 1, the cells were washed twice with sterile PBS and stained with 1µM CFSE (5-Carboxyfluorescein diacetate succinimidyl ester, BioLegend®) in PBS for 20 minutes at 37˚C. RPMI-1640 + 10% FBS was then added to quench the fluorophore for 10 minutes at 37˚C. The cells were subsequently washed twice with RPMI-1640 + 10% FBS and either pulsed with peptide, native antibodies or AgAbs (see protocol T cell assay, 100ng/5.10^4 APCs)

The following day, the cells were washed and mixed with either matched or unmatched T cells (5.10^4 APCs and 5.10^4 T cells, E:T=1:1) in 200µL RPMI-1640 + 10% FBS in U-bottom 96 well plates. In some experiments, immune checkpoint inhibitors were also added.

After 16-18 hours, the pellets were collected and stained with 0,5µL LIVE/DEAD™ Fixable Far Red Dead Cell Stain Kit (Invitrogen™), in 100µL staining buffer. The cells were finally washed and resuspended in staining buffer for flow-cytometric analysis. The specific T cell cytotoxicity

was calculated based on the percentage of $CFSE^+$ cells, positive for the LIVE/DEAD marker, as follow:

$$Specific\ lysis_{(Condition\ A)} = \frac{(\%L/D^+{}_{Condition\ A} - \%L/D^+{}_{Unstimulated})}{(100 - \%L/D^+{}_{Unstimulated})}$$

- Long-term T-cell/killing assays *(ex vivo)*

To assess the ability of long AgAbs to stimulate T cells from healthy or AML donors *ex vivo*, long-term T cell and killing assays were conducted.

Donor cells were cultivated in AML medium or T cell medium (compositions see in table 9). PBMCs from healthy donors or PBMCs/BM cells from AML donors were prepared as previously explained (see 4.2.2.6.). 1.10^5 cells/well were incubated in 200µL in U-bottom 96 well-plates with native antibodies or a mix of 10ng AgAbs (EBNA1, EBNA2, EBNA3C – 5 antibodies for each target) with or without immune checkpoint inhibitors (anti-PD-1/anti-PD-L1 – 1µg/well). The cells were then kept at 37˚C and supplied every 4 days with fresh antibodies. At different time points, supernatants were collected for cytokine ELISA (protocol see p) and for stainings in flow cytometry. For the latter assessment, CD3+CD4, CD3+CD69 and CD33+LIVE/DEAD stainings were routinely performed to track the activation and the proliferation of the T cells as well as the elimination of target cells.

4.2.3.7. Bystander assay

In order to evaluate the effects of T cell activation on non-target malignant cells, bystander assays were performed. Mutz-3 or MV4-11 AML cells were respectively pulsed with 100ng 3H10 or 1D6 CD33 AgAbs or peptide, or native CD33 antibody, comparably to previously detailed T cell assays. The cells were then washed and co-incubated with their matching T cells (EBNA3C 3H10 or gp350 1D6) and with preliminarily CFSE-stained unmatched AML cells (CFSE staining protocol see overnight killing assay). Altogether, 5.10^4 matched AML cells were mixed with 5.10^4 T cells and 5.10^4 CFSE+ unmatched AML cells (E:T:Bystander = 1:1:1) in 200µL RPMI-1640 + 10% FBS.

After 72h, the cells were collected and stained with LIVE/DEAD™ Fixable Far Red Dead Cell Stain Kit (Invitrogen™) according to the previously detailed protocol, and the viability of $CFSE^+$ bystander cells was evaluated in flow cytometry.

4.2.4. Mice experiments

4.2.4.1. Preliminary assessment of murine cell lines

Since both C1498 and WEHI-3 cell lines have been modified *in vitro*, their behaviour *in vivo* had to be verified. 8-week C57BL/6J and BALB/c mice were ordered from Janvier Labs® (France). The mice were hosted in the S2 area of the *Zentrales Tierlabor* (animal house) in DKFZ. The mice were first infected with 2.10^5 pfu WT mCMV strain Smith (100µL intraperitoneal injection). 28 days post-infection, the mice were injected with different doses of C1498 (C57BL/6J) or WEHI-3 cells (BALB/c), intraperitoneally (one additional mouse injected intravenously with C1498). The mice were then monitored and humanely sacrificed when moribund.
Blood (intracardiac puncture), bone marrow (femoral bones), spleen, liver, lungs and eventual visible tumour masses were collected immediately after sacrifice, and processed as detailed in the next point.

4.2.4.2. Processing of organs and cell isolations

Blood, bone marrow, spleen, liver, lungs and visible tumour masses were processed to isolate cells for subsequent stainings.

- *Blood:*

Blood was collected in EDTA tubes, diluted 1:2 with PBS and underlaid with 2mL Ficoll-Paque Plus™ (Cytiva). After 30 minutes at 400xg, the white interphase was collected and the PBMCs were washed twice in PBS.

- *Bone marrow:*

PBS was carefully injected with a syringe and a 27G-needle in the medullary canal of the femur. The cells were centrifuged and resuspended in 500µL PBS + 500µL ACK lysis buffer to get rid of red blood cells. The tube was then centrifuged for 5 minutes in a table-top centrifuge at 3000rpm, the supernatant was removed and the cells were washed once with PBS.

- *Spleen:*

The spleen was crushed in a 70µm-cell strainer with a plunger in PBS. The recovered splenocytes were then centrifuged at 1500rpm (Heraeus centrifuge) and resuspended in 1mL

PBS + 1mL ACK lysis buffer. The tube was centrifuged again at 1500rpm for 5 minutes, the supernatant was discarded and the cells were washed once in PBS.

- *Lungs, liver and tumour masses:*

The organs were cut into small pieces with a scalpel and incubated at 37˚C for 1 hour in PBS + Liberase™ TM (20µg/mL, Roche). The digested pieces were then crushed in a 70µm-cell strainer with a plunger in PBS. The recovered cells were then centrifuged at 1500rpm (Heraeus centrifuge) and resuspended in 2mL PBS + 2mL ACK lysis buffer. The tube was centrifuged again at 1500rpm for 5 minutes, the supernatant was discarded and the cells were washed once in PBS.

4.2.4.3. Design of the murine experiments

To evaluate the potency of AgAbs to redirect anti-viral immunity toward AML cells, modified C1498 cells were injected in C57BL/6J mice. The mice were intraperitoneally injected with $2{,}0.10^5$ pfu of mCMV (strain Smith) to induce a memory response toward this pathogen. 30 days after infection, 5.10^5 cells modified C1498 cells were intravenously injected in the tail vein of the mice (day 0 of the experiment). Starting on day 1 and every 5 days, the mice received an intraperitoneal injection of either PBS, native antibodies or AgAbs, depending on their experimental group.
The mice were then monitored for survival and were humanely sacrifice when showing a sign of tumour development or behavioural change. Organs were collected and cells were isolated according to the protocol given in the previous part. Stainings for different markers (AML cell markers, T cell markers and immune checkpoints) were performed according to the protocol given in 4.2.3.3.

4.2.5. Ethical approvals

4.2.5.1. Use of material from healthy donors (serum, PBMCs)

Peripheral blood mononuclear cells (PBMCs) were isolated from healthy donors that provided written informed consent (ethical approval granted by the *Ethikkommission of the Medizinische Fakultät Heidelberg* (S-603/2015)) or from anonymous buffy coats purchased from the *Institut*

für Klinische Transfusionsmedizin und Zelltherapie (IKTZ) in Heidelberg and did not require ethical approval. Ethical approval to use sera from voluntary donors was obtained from the *Ethikkommission of the Medizinische Fakultät Hei*delberg (S-36/2011).

4.2.5.2. Recruitment of AML patient PBMC or bone marrow samples

Peripheral blood mononuclear cells (PBMCs) from blood samples, or bone marrow mononuclear cells (BMMCs) from bone marrow aspirates were obtained as frozen vials and were retrieved from the AML bank of Medical Department V, Hematology and Oncology, University of Heidelberg. Ethical approval to use materials from acute myeloid leukemia donors was obtained from the *Ethikkommission of the Medizinische Fakultät Hei*delberg (S-169, S-686).

4.2.5.3. Murine protocol

Mice were housed in hygiene-restricted S2-area of the *Zentral Tierlabor* (ZTL) in DKFZ, under a 12-hour light-dark cycle and with regular chow. All animal experiments conformed to the German Animal Welfare Act and were approved by the *Regierungspräsidium* of Karlsruhe with the reference G-339/19.

5. List of figures

6. List of tables

7. List of abbreviations

Abbreviation	Description
ADC	Antibody-drug conjugate
ADCC	Antibody dependant cell cytotoxicity
ADCP	Antibody dependant cell phagocytosis
ADP	Adenosine diphosphate
AgAb	Antigen-armed antibody
AML	Acute myeloid leukemia
AMP	Adenosine monophosphate
APC *(dye)*	Allophycocyanin
APC	Antigen-presenting cell
APL	Acute promyelocytic leukemia
APS	Ammonium persulfate
ARG1	Arginase-1
ATP	Adenosine triphosphate
ATRA	All-trans retinoic acid
B-CLL	B-chronic lymphocytic leukemia
BiKE	Bi-specific NK cell engager
BiTE	Bi-specific T cell engager
BL	Burkitt's lymphoma
BM	Bone marrow
BMMC	Bone marrow mononuclear cells
(k)bp	(kilo) base pairs
BPDCN	Blastic plasmacytoid dendritic cell neoplasm
CAR	Chimeric antigen receptor
CCL	CC chemokine ligands
CD	Cluster of differentiation
CDC	Cell dependant cytotoxicity
CDK	Cyclin-dependent kinase
cDNA	Complementary DNA
CFU-G	Colony forming unit granulocytes
CFU-GEMM	Colony forming unit granulocytes, erythrocytes, monocytes, megakaryocytes
CFU-GM	Colony forming unit granulocytes, monocytes
CFSE	Carboxyfluorescein succinimidyl ester
C_H/C_L	Constant heavy / constant light
CIITA	class II, major histocompatibility complex, transactivator
CLEC	C-type lectin
CLL-1	C-type lectin molecule 1
CML	Chronic myeloid leukemia
(m/H)CMV	Murine/human cytomegalovirus

CTL	Cytotoxic T lymphocyte
CTLA-4	Cytotoxic T lymphocyte associated protein-4
(c/p)DC	(Conventional/plasmacytoid) dendritic cell
DLBCL	Diffuse large B cell lymphoma
DNA	Deoxyribonucleic acid
dNTP	Deoxyribonucleotid triphosphate
E-BFU	Erythroid burst forming unit
EBNA	Epstein-Barr virus nuclear antigen
EBV	Epstein-Barr virus
ECTV	Ectromelia virus
EDTA	Ethylenediaminetetraacetic acid
ELISA	Enzyme-linked immunosorbent assay
ELN	European leukemia net
E:T	Effector to target
E.U	European Union
FISH	Fluorescence in situ hybridisation
FAB	*French-American-British*
FasL	Fas ligand
FBS	Fetal bovine serum
FC	Flow cytometry
Fc	Fragment cristallisable
FcγR	Fragment cristallisable gamma receptor
FDA	Food and drug administration
FITC	Fluorescein isothiocyanate
FR-β	Folate receptor beta
G-CSF	Granulocyte colony-stimulating factor
GITR	glucocorticoid-induced TNFR-related protein
GITRL	glucocorticoid-induced TNFR-related protein ligand
GO	Gemtuzumab ozogamycin
gp	Glycoprotein
GPI	Glycosylphosphatidylinositol
H+L	Heavy + light
HC	Heavy chain
HDAC	Histone Deacetylase
HEK	Human embryonic kidney
HIV	Human immunodeficiency virus
HL	Hodgkin's lymphoma
HLA	Human leukocyte antigen
HRP	Horseradish peroxydase
HSC	Hematopoietic stem cell
HSCT	Hematopoietic stem cell transplantation
I.p.	Intraperitoneal(ly)

ITIM	Immunoreceptor tyrosine-based inhibitory motif
I.v.	Intravenous(ly)
ICB	Immune checkpoint blockade
IDAC	Idarubicin and cytarabin
IDO	Indoleamine-pyrrole 2,3-dioxygenase
IFNγ	Interferon gamma
IL	Interleukine
IM	Infectious mononucleosis
IMDM	Iscove's modified Dulbecco's medium
IRES	Internal ribosome entry site
Iso	Isotype
$\lambda_{(ex/em)}$	Wavelength (excitation/emission)
L/D	Live/Dead
LB	Lysogeny broth
LC	Light chain
LCL	Lymphoblastoid cell line
LSC	Leukemic stem cell
MDS	Myelodysplastic syndrome
MDSC	Myeloid-derived suppressor cell
MEM	Minimum essential medium
MFI	Mean of fluorescence
MHC(-I/-II)	Major histocompatibility complex (-I/-II)
MHV68	Murine gammaherpesvirus 68
mIgG	Murine IgG
MTX	Methotrexate
MuLV	Murine leukemia virus
NEAA	Non-essential amino acid
NK	Natural Killer
NOD SCID	Non-obese diabetic/severe combined immunodeficiency
NOS	Nitric oxide synthase
NPC	Nasopharyngeal carcinoma
NSG	Non-obese diabetic/severe combined immunodeficiency gamma
PARP	Poly-(ADP-ribose) polymerase
PBMC	Peripheral blood mononuclear cells
PBS	Phosphate buffer saline
PCR	Polymerase chain reaction
PD-1	Programmed cell death 1
PD-L1	Programmed cell death ligand 1
PE	Phycoerythrin
PEI	Polyethylenimine
Pfu	Plaque-forming unit
PHA	Phytohemagglutinin

PSGL-1	P-selectin glycoprotein ligand-1
PTLD	post-transplant lymphoproliferative disorder
R/R	Relapsed or refractory
ROS	Reactive oxygen species
RPMI	Roswell Park Memorial Institute medium
SCF	Stem cell factor
scFv	Single chain variable fragment
SDS	Sodium dodecyl sulphate
TAA	Tumour associated antigen
TCR	T-cell receptor
TEMED	Tetramethylethylenediamine
TGF-β	Transforming growth factor beta
Th	Helper T cell
TIGIT	T cell immunoreceptor with Ig and ITIM domains
TILs	Tumour infiltrating lymphocytes
TLR	Toll-like receptor
TME	Tumour microenvironment
TNFα	Tumour necrosis factor alpha
TNFSF	Tumour necrosis factor superfamily
TNFRSF	Tumour necrosis factor receptor superfamily
Treg	Regulatory T cell
U.S	United States (of America)
VEGF	Vascular endothelial growth factor
V_H/V_L	Variable heavy/variable light
VISTA	V-domain Ig suppressor of T cell activation
WHO	World Health Organisation
6MP	6-mercaptopurin

8. Bibliography

[1] De Kouchkovsky I, Abdul-Hay M. 'Acute myeloid leukemia: a comprehensive review and 2016 update'. *Blood Cancer J* 2016; 6: e441.

[2] Short NJ, Rytting ME, Cortes JE. Acute myeloid leukaemia. *The Lancet* 2018; 392: 593–606.

[3] DiNardo CD, Garcia-Manero G, Pierce S, et al. Interactions and relevance of blast percentage and treatment strategy among younger and older patients with acute myeloid leukemia (AML) and myelodysplastic syndrome (MDS). *Am J Hematol* 2016; 91: 227–232.

[4] Estey E, Hasserjian RP, Döhner H. Distinguishing AML from MDS: a fixed blast percentage may no longer be optimal. *Blood* 2022; 139: 323–332.

[5] Khoury JD, Solary E, Abla O, et al. The 5th edition of the World Health Organization Classification of Haematolymphoid Tumours: Myeloid and Histiocytic/Dendritic Neoplasms. *Leukemia* 2022; 36: 1703–1719.

[6] Döhner H, Wei AH, Appelbaum FR, et al. Diagnosis and management of AML in adults: 2022 recommendations from an international expert panel on behalf of the ELN. *Blood* 2022; 140: 1345–1377.

[7] Pimenta DB, Varela VA, Datoguia TS, et al. The Bone Marrow Microenvironment Mechanisms in Acute Myeloid Leukemia. *Frontiers in Cell and Developmental Biology*; 9, https://www.frontiersin.org/article/10.3389/fcell.2021.764698 (2021, accessed 28 June 2022).

[8] Estey EH. Acute myeloid leukemia: 2012 update on diagnosis, risk stratification, and management. *Am J Hematol* 2012; 87: 89–99.

[9] Haferlach T, Schmidts I. The power and potential of integrated diagnostics in acute myeloid leukaemia. *British Journal of Haematology* 2020; 188: 36–48.

[10] Shallis RM, Wang R, Davidoff A, et al. Epidemiology of acute myeloid leukemia: Recent progress and enduring challenges. *Blood Rev* 2019; 36: 70–87.

[11] Yi M, Li A, Zhou L, et al. The global burden and attributable risk factor analysis of acute myeloid leukemia in 195 countries and territories from 1990 to 2017: estimates based on the global burden of disease study 2017. *Journal of Hematology & Oncology* 2020; 13: 72.

[12] Ahmed A, Jani C, Bhatt P, et al. EPR22-104: A Comparison of the Burden of Leukemia Amongst Various Regions of the World, 1990-2019. *Journal of the National Comprehensive Cancer Network* 2022; 20: EPR22-104.

[13] Kantarjian H, Kadia T, DiNardo C, et al. Acute myeloid leukemia: current progress and future directions. *Blood Cancer J* 2021; 11: 1–25.

[14] Oran B, Weisdorf DJ. Survival for older patients with acute myeloid leukemia: a population-based study. *Haematologica* 2012; 97: 1916–1924.

[15] Bennett JM, Catovsky D, Daniel MT, et al. Proposals for the classification of the acute leukaemias. French-American-British (FAB) co-operative group. *Br J Haematol* 1976; 33: 451–458.

[16] Schiffer CA, Stone RM. Morphologic Classification and Clinical and Laboratory Correlates. *Holland-Frei Cancer Medicine 6th edition*, https://www.ncbi.nlm.nih.gov/books/NBK13452/ (2003, accessed 7 November 2022).

[17] Kumar CC. Genetic Abnormalities and Challenges in the Treatment of Acute Myeloid Leukemia. *Genes Cancer* 2011; 2: 95–107.

[18] Lawrence MS, Stojanov P, Polak P, et al. Mutational heterogeneity in cancer and the search for new cancer-associated genes. *Nature* 2013; 499: 214–218.

[19] Gröbner SN, Worst BC, Weischenfeldt J, et al. The landscape of genomic alterations across

childhood cancers. *Nature* 2018; 555: 321–327.

[20] Cancer Genome Atlas Research Network, Ley TJ, Miller C, et al. Genomic and epigenomic landscapes of adult de novo acute myeloid leukemia. *N Engl J Med* 2013; 368: 2059–2074.

[21] Vardiman JW, Harris NL, Brunning RD. The World Health Organization (WHO) classification of the myeloid neoplasms. *Blood* 2002; 100: 2292–2302.

[22] Arber DA, Orazi A, Hasserjian R, et al. The 2016 revision to the World Health Organization classification of myeloid neoplasms and acute leukemia. *Blood* 2016; 127: 2391–2405.

[23] Villgran V, Agha M, Raptis A, et al. Leukapheresis in patients newly diagnosed with acute myeloid leukemia. *Transfus Apher Sci* 2016; 55: 216–220.

[24] Rowe JM. The "7+3" regimen in acute myeloid leukemia. *Haematologica* 2022; 107: 3–3.

[25] Yates JW, Wallace HJ, Ellison RR, et al. Cytosine arabinoside (NSC-63878) and daunorubicin (NSC-83142) therapy in acute nonlymphocytic leukemia. *Cancer Chemother Rep* 1973; 57: 485–488.

[26] Lancet JE, Uy GL, Newell LF, et al. CPX-351 versus 7+3 cytarabine and daunorubicin chemotherapy in older adults with newly diagnosed high-risk or secondary acute myeloid leukaemia: 5-year results of a randomised, open-label, multicentre, phase 3 trial. *The Lancet Haematology* 2021; 8: e481–e491.

[27] McCurdy SR, Luger SM. Dose intensity for induction in acute myeloid leukemia: what, when, and for whom? *Haematologica* 2021; 106: 2544–2554.

[28] Shin S-H, Cho B-S, Park S-S, et al. Comparison of the modified low-dose cytarabine and etoposide with decitabine therapy for elderly acute myeloid leukemia patients unfit for intensive chemotherapy. *Oncotarget* 2017; 9: 5823–5833.

[29] Thol F, Schlenk RF, Heuser M, et al. How I treat refractory and early relapsed acute myeloid leukemia. *Blood* 2015; 126: 319–327.

[30] Stein EM, DiNardo CD, Fathi AT, et al. Ivosidenib or Enasidenib Combined with Induction and Consolidation Chemotherapy in Patients with Newly Diagnosed AML with an IDH1 or IDH2 Mutation Is Safe, Effective, and Leads to MRD-Negative Complete Remissions. *Blood* 2018; 132: 560.

[31] Levis M. Midostaurin approved for FLT3-mutated AML. *Blood* 2017; 129: 3403–3406.

[32] Fleischmann M, Schnetzke U, Hochhaus A, et al. Management of Acute Myeloid Leukemia: Current Treatment Options and Future Perspectives. *Cancers (Basel)* 2021; 13: 5722.

[33] Löwenberg B, Huls G. The long road: improving outcome in elderly "unfit" AML? *Blood* 2020; 135: 2114–2115.

[34] Freeman SD, Hills RK, Russell NH, et al. Induction response criteria in acute myeloid leukaemia: implications of a flow cytometric measurable residual disease negative test in refractory adults. *Br J Haematol* 2019; 186: 130–133.

[35] Mayer RJ, Davis RB, Schiffer CA, et al. Intensive postremission chemotherapy in adults with acute myeloid leukemia. Cancer and Leukemia Group B. *N Engl J Med* 1994; 331: 896–903.

[36] Reville PK, Kadia TM. Maintenance Therapy in AML. *Frontiers in Oncology*; 10, https://www.frontiersin.org/articles/10.3389/fonc.2020.619085 (2021, accessed 12 July 2022).

[37] Takami A. Hematopoietic stem cell transplantation for acute myeloid leukemia. *Int J Hematol* 2018; 107: 513–518.

[38] Wei AH, Döhner H, Pocock C, et al. Oral Azacitidine Maintenance Therapy for Acute Myeloid Leukemia in First Remission. *New England Journal of Medicine* 2020; 383: 2526–2537.

[39] Ravandi F, Estey E, Jones D, et al. Effective treatment of acute promyelocytic leukemia with all-trans-retinoic acid, arsenic trioxide, and gemtuzumab ozogamicin. *J Clin Oncol* 2009; 27:

504–510.

[40] Lancet JE, Moseley AB, Coutre SE, et al. A phase 2 study of ATRA, arsenic trioxide, and gemtuzumab ozogamicin in patients with high-risk APL (SWOG 0535). *Blood Adv* 2020; 4: 1683–1689.

[41] Heuser M, Ofran Y, Boissel N, et al. Acute myeloid leukaemia in adult patients: ESMO Clinical Practice Guidelines for diagnosis, treatment and follow-up. *Ann Oncol* 2020; 31: 697–712.

[42] Crossnohere NL, Richardson DR, Reinhart C, et al. Side effects from acute myeloid leukemia treatment: results from a national survey. *Curr Med Res Opin* 2019; 35: 1965–1970.

[43] Darici S, Alkhaldi H, Horne G, et al. Targeting PI3K/Akt/mTOR in AML: Rationale and Clinical Evidence. *J Clin Med* 2020; 9: 2934.

[44] Rodrigues ACB da C, Costa RGA, Silva SLR, et al. Cell signaling pathways as molecular targets to eliminate AML stem cells. *Crit Rev Oncol Hematol* 2021; 160: 103277.

[45] Carter JL, Hege K, Yang J, et al. Targeting multiple signaling pathways: the new approach to acute myeloid leukemia therapy. *Sig Transduct Target Ther* 2020; 5: 1–29.

[46] San José-Enériz E, Gimenez-Camino N, Agirre X, et al. HDAC Inhibitors in Acute Myeloid Leukemia. *Cancers (Basel)* 2019; 11: 1794.

[47] Lee DJ, Zeidner JF. Cyclin-dependent kinase (CDK) 9 and 4/6 inhibitors in acute myeloid leukemia (AML): a promising therapeutic approach. *Expert Opin Investig Drugs* 2019; 28: 989–1001.

[48] Khurana A, Shafer DA. MDM2 antagonists as a novel treatment option for acute myeloid leukemia: perspectives on the therapeutic potential of idasanutlin (RG7388). *Onco Targets Ther* 2019; 12: 2903–2910.

[49] Brunner AM, Blonquist TM, DeAngelo DJ, et al. Phase II Clinical Trial of Alisertib, an Aurora a Kinase Inhibitor, in Combination with Induction Chemotherapy in High-Risk, Untreated Patients with Acute Myeloid Leukemia. *Blood* 2018; 132: 766.

[50] Zhong L, Li Y, Xiong L, et al. Small molecules in targeted cancer therapy: advances, challenges, and future perspectives. *Sig Transduct Target Ther* 2021; 6: 1–48.

[51] Lv M, Wang K, Huang X. Myeloid-derived suppressor cells in hematological malignancies: friends or foes. *Journal of Hematology & Oncology* 2019; 12: 105.

[52] Mougiakakos D, Jitschin R, von Bahr L, et al. Immunosuppressive CD14+HLA-DRlow/neg IDO+ myeloid cells in patients following allogeneic hematopoietic stem cell transplantation. *Leukemia* 2013; 27: 377–388.

[53] Corzo CA, Cotter MJ, Cheng P, et al. Mechanism regulating reactive oxygen species in tumor-induced myeloid-derived suppressor cells. *J Immunol* 2009; 182: 5693–5701.

[54] Frumento G, Rotondo R, Tonetti M, et al. Tryptophan-derived catabolites are responsible for inhibition of T and natural killer cell proliferation induced by indoleamine 2,3-dioxygenase. *J Exp Med* 2002; 196: 459–468.

[55] Corm S, Berthon C, Imbenotte M, et al. Indoleamine 2,3-dioxygenase activity of acute myeloid leukemia cells can be measured from patients' sera by HPLC and is inducible by IFN-gamma. *Leuk Res* 2009; 33: 490–494.

[56] Bronte V, Zanovello P. Regulation of immune responses by L-arginine metabolism. *Nat Rev Immunol* 2005; 5: 641–654.

[57] Mendez LM, Posey RR, Pandolfi PP. The Interplay Between the Genetic and Immune Landscapes of AML: Mechanisms and Implications for Risk Stratification and Therapy. *Front Oncol* 2019; 9: 1162.

[58] Mussai F, De Santo C, Abu-Dayyeh I, et al. Acute myeloid leukemia creates an arginase-dependent immunosuppressive microenvironment. *Blood* 2013; 122: 749–758.

[59] Mehta RS, Chen X, Antony J, et al. Myeloid Derived Suppressor Cells (MDSC)-like Acute Myeloid Leukemia (AML) Cells Are Associated with Resistance to Cytotoxic Effects of Autologous (Auto) T-Lymphocytes (CTLs). *Biology of Blood and Marrow Transplantation* 2015; 21: S191–S192.

[60] Vaisitti T, Arruga F, Guerra G, et al. Ectonucleotidases in Blood Malignancies: A Tale of Surface Markers and Therapeutic Targets. *Frontiers in Immunology*; 10, https://www.frontiersin.org/articles/10.3389/fimmu.2019.02301 (2019, accessed 12 July 2022).

[61] Medeiros BC, Fathi AT, DiNardo CD, et al. Isocitrate dehydrogenase mutations in myeloid malignancies. *Leukemia* 2017; 31: 272–281.

[62] Xu T, Stewart KM, Wang X, et al. Metabolic control of TH17 and induced Treg cell balance by an epigenetic mechanism. *Nature* 2017; 548: 228–233.

[63] Benites BD, da Silva Santos Duarte A, Longhini ALF, et al. Exosomes in the serum of Acute Myeloid Leukemia patients induce dendritic cell tolerance: Implications for immunotherapy. *Vaccine* 2019; 37: 1377–1383.

[64] van Luijn MM, Chamuleau MED, Ossenkoppele GJ, et al. Tumor immune escape in acute myeloid leukemia. *Oncoimmunology* 2012; 1: 211–213.

[65] Le Dieu R, Taussig DC, Ramsay AG, et al. Peripheral blood T cells in acute myeloid leukemia (AML) patients at diagnosis have abnormal phenotype and genotype and form defective immune synapses with AML blasts. *Blood* 2009; 114: 3909–3916.

[66] Williams P, Basu S, Garcia-Manero G, et al. The distribution of T-cell subsets and the expression of immune checkpoint receptors and ligands in patients with newly diagnosed and relapsed acute myeloid leukemia. *Cancer* 2019; 125: 1470–1481.

[67] Szczepanski MJ, Szajnik M, Czystowska M, et al. Increased frequency and suppression by regulatory T cells in patients with acute myelogenous leukemia. *Clin Cancer Res* 2009; 15: 3325–3332.

[68] Ustun C, Miller JS, Munn DH, et al. Regulatory T cells in acute myelogenous leukemia: is it time for immunomodulation? *Blood* 2011; 118: 5084–5095.

[69] Togashi Y, Shitara K, Nishikawa H. Regulatory T cells in cancer immunosuppression — implications for anticancer therapy. *Nat Rev Clin Oncol* 2019; 16: 356–371.

[70] Tian T, Yu S, Liu L, et al. The Profile of T Helper Subsets in Bone Marrow Microenvironment Is Distinct for Different Stages of Acute Myeloid Leukemia Patients and Chemotherapy Partly Ameliorates These Variations. *PLoS One* 2015; 10: e0131761.

[71] Schnorfeil FM, Lichtenegger FS, Emmerig K, et al. T cells are functionally not impaired in AML: increased PD-1 expression is only seen at time of relapse and correlates with a shift towards the memory T cell compartment. *Journal of Hematology & Oncology* 2015; 8: 93.

[72] Li Z, Philip M, Ferrell PB. Alterations of T-cell-mediated immunity in acute myeloid leukemia. *Oncogene* 2020; 39: 3611–3619.

[73] Knaus HA, Berglund S, Hackl H, et al. Signatures of CD8+ T cell dysfunction in AML patients and their reversibility with response to chemotherapy. *JCI Insight* 2018; 3: 120974.

[74] Bross PF, Beitz J, Chen G, et al. Approval summary: gemtuzumab ozogamicin in relapsed acute myeloid leukemia. *Clin Cancer Res* 2001; 7: 1490–1496.

[75] Petersdorf SH, Kopecky KJ, Slovak M, et al. A phase 3 study of gemtuzumab ozogamicin during induction and postconsolidation therapy in younger patients with acute myeloid leukemia. *Blood* 2013; 121: 4854–4860.

[76] Burnett AK, Russell NH, Hills RK, et al. Addition of gemtuzumab ozogamicin to induction chemotherapy improves survival in older patients with acute myeloid leukemia. *J Clin Oncol* 2012; 30: 3924–3931.

[77] Hitzler J, Estey E. Gemtuzumab ozogamicin in acute myeloid leukemia: act 2, with perhaps more to come. *Haematologica* 2019; 104: 7–9.

[78] Perna F, Espinoza-Gutarra MR, Bombaci G, et al. Immune-Based Therapeutic Interventions for Acute Myeloid Leukemia. *Cancer Treat Res* 2022; 183: 225–254.

[79] Isidori A, Cerchione C, Daver N, et al. Immunotherapy in Acute Myeloid Leukemia: Where We Stand. *Front Oncol* 2021; 11: 656218.

[80] Liu Y, Bewersdorf JP, Stahl M, et al. Immunotherapy in acute myeloid leukemia and myelodysplastic syndromes: The dawn of a new era? *Blood Reviews* 2019; 34: 67–83.

[81] Walter RB. Where do we stand with radioimmunotherapy for acute myeloid leukemia? *Expert Opin Biol Ther* 2022; 22: 555–561.

[82] Wolska-Washer A, Robak T. Safety and Tolerability of Antibody-Drug Conjugates in Cancer. *Drug Saf* 2019; 42: 295–314.

[83] Liu S-H, Gu Y, Pascual B, et al. A novel CXCR4 antagonist IgG1 antibody (PF-06747143) for the treatment of hematologic malignancies. *Blood Adv* 2017; 1: 1088–1100.

[84] Schürch CM. Therapeutic Antibodies for Myeloid Neoplasms—Current Developments and Future Directions. *Front Oncol*; 8. Epub ahead of print 18 May 2018. DOI: 10.3389/fonc.2018.00152.

[85] Bewersdorf JP, Stahl M, Zeidan AM. Immune checkpoint-based therapy in myeloid malignancies: a promise yet to be fulfilled. *Expert Rev Anticancer Ther* 2019; 19: 393–404.

[86] Mardiana S, Gill S. CAR T Cells for Acute Myeloid Leukemia: State of the Art and Future Directions. *Front Oncol* 2020; 10: 697.

[87] Agrawal V, Gbolahan OB, Stahl M, et al. Vaccine and Cell-based Therapeutic Approaches in Acute Myeloid Leukemia. *Curr Cancer Drug Targets* 2020; 20: 473–489.

[88] Dolgin E. Bringing down the cost of cancer treatment. *Nature* 2018; 555: S26–S29.

[89] Cohen JI. Epstein-Barr virus infection. *N Engl J Med* 2000; 343: 481–492.

[90] Epstein MA, Achong BG, Barr YM. VIRUS PARTICLES IN CULTURED LYMPHOBLASTS FROM BURKITT'S LYMPHOMA. *Lancet* 1964; 1: 702–703.

[91] Smatti MK, Al-Sadeq DW, Ali NH, et al. Epstein-Barr Virus Epidemiology, Serology, and Genetic Variability of LMP-1 Oncogene Among Healthy Population: An Update. *Front Oncol* 2018; 8: 211.

[92] Fugl A, Andersen CL. Epstein-Barr virus and its association with disease - a review of relevance to general practice. *BMC Fam Pract* 2019; 20: 62.

[93] Chen M-R. Epstein–Barr Virus, the Immune System, and Associated Diseases. *Frontiers in Microbiology*; 2, https://www.frontiersin.org/articles/10.3389/fmicb.2011.00005 (2011, accessed 13 July 2022).

[94] Young LS, Rickinson AB. Epstein–Barr virus: 40 years on. *Nat Rev Cancer* 2004; 4: 757–768.

[95] Shannon-Lowe C, Rickinson A. The Global Landscape of EBV-Associated Tumors. *Front Oncol* 2019; 9: 713.

[96] Dunmire SK, Verghese PS, Balfour HH. Primary Epstein-Barr virus infection. *J Clin Virol* 2018; 102: 84–92.

[97] Cui X, Snapper CM. Epstein Barr Virus: Development of Vaccines and Immune Cell Therapy for EBV-Associated Diseases. *Front Immunol* 2021; 12: 734471.

[98] Taylor GS, Long HM, Brooks JM, et al. The immunology of Epstein-Barr virus-induced disease. *Annu Rev Immunol* 2015; 33: 787–821.

[99] Azzi T, Lünemann A, Murer A, et al. Role for early-differentiated natural killer cells in infectious mononucleosis. *Blood* 2014; 124: 2533–2543.

[100] Lünemann A, Vanoaica LD, Azzi T, et al. A distinct subpopulation of human NK cells restricts B cell transformation by EBV. *J Immunol* 2013; 191: 4989–4995.

[101] Gaudreault E, Fiola S, Olivier M, et al. Epstein-Barr virus induces MCP-1 secretion by human monocytes via TLR2. *J Virol* 2007; 81: 8016–8024.

[102] Fiola S, Gosselin D, Takada K, et al. TLR9 contributes to the recognition of EBV by primary monocytes and plasmacytoid dendritic cells. *J Immunol* 2010; 185: 3620–3631.

[103] Iwakiri D, Zhou L, Samanta M, et al. Epstein-Barr virus (EBV)-encoded small RNA is released from EBV-infected cells and activates signaling from Toll-like receptor 3. *J Exp Med* 2009; 206: 2091–2099.

[104] Rowe M, Zuo J. Immune responses to Epstein-Barr virus: molecular interactions in the virus evasion of CD8+ T cell immunity. *Microbes Infect* 2010; 12: 173–181.

[105] Quinn LL, Zuo J, Abbott RJM, et al. Cooperation between Epstein-Barr virus immune evasion proteins spreads protection from CD8+ T cell recognition across all three phases of the lytic cycle. *PLoS Pathog* 2014; 10: e1004322.

[106] Abbott RJM, Quinn LL, Leese AM, et al. CD8+ T cell responses to lytic EBV infection: late antigen specificities as subdominant components of the total response. *J Immunol* 2013; 191: 5398–5409.

[107] Hislop AD, Kuo M, Drake-Lee AB, et al. Tonsillar homing of Epstein-Barr virus-specific CD8+ T cells and the virus-host balance. *J Clin Invest* 2005; 115: 2546–2555.

[108] Hislop AD, Annels NE, Gudgeon NH, et al. Epitope-specific evolution of human CD8(+) T cell responses from primary to persistent phases of Epstein-Barr virus infection. *J Exp Med* 2002; 195: 893–905.

[109] Woodberry T, Suscovich TJ, Henry LM, et al. Differential targeting and shifts in the immunodominance of Epstein-Barr virus--specific CD8 and CD4 T cell responses during acute and persistent infection. *J Infect Dis* 2005; 192: 1513–1524.

[110] Long HM, Chagoury OL, Leese AM, et al. MHC II tetramers visualize human CD4+ T cell responses to Epstein-Barr virus infection and demonstrate atypical kinetics of the nuclear antigen EBNA1 response. *J Exp Med* 2013; 210: 933–949.

[111] Miyawaki T, Kasahara Y, Kanegane H, et al. Expression of CD45R0 (UCHL1) by CD4+ and CD8+ T cells as a sign of in vivo activation in infectious mononucleosis. *Clin Exp Immunol* 1991; 83: 447–451.

[112] Long HM, Leese AM, Chagoury OL, et al. Cytotoxic CD4+ T cell responses to EBV contrast with CD8 responses in breadth of lytic cycle antigen choice and in lytic cycle recognition. *J Immunol* 2011; 187: 92–101.

[113] Adhikary D, Behrends U, Boerschmann H, et al. Immunodominance of lytic cycle antigens in Epstein-Barr virus-specific CD4+ T cell preparations for therapy. *PLoS One* 2007; 2: e583.

[114] Long HM, Haigh TA, Gudgeon NH, et al. CD4+ T-cell responses to Epstein-Barr virus (EBV) latent-cycle antigens and the recognition of EBV-transformed lymphoblastoid cell lines. *J Virol* 2005; 79: 4896–4907.

[115] Meckiff BJ, Ladell K, McLaren JE, et al. Primary EBV Infection Induces an Acute Wave of Activated Antigen-Specific Cytotoxic CD4+ T Cells. *J Immunol* 2019; 203: 1276–1287.

[116] Marshall NB, Swain SL. Cytotoxic CD4 T cells in antiviral immunity. *J Biomed Biotechnol* 2011; 2011: 954602.

[117] Landais E, Saulquin X, Scotet E, et al. Direct killing of Epstein-Barr virus (EBV)-infected B cells by CD4 T cells directed against the EBV lytic protein BHRF1. *Blood* 2004; 103: 1408–1416.

[118] Haigh TA, Lin X, Jia H, et al. EBV latent membrane proteins (LMPs) 1 and 2 as immunotherapeutic targets: LMP-specific CD4+ cytotoxic T cell recognition of EBV-

transformed B cell lines. *J Immunol* 2008; 180: 1643–1654.

[119] Bhattacharyya ND, Feng CG. Regulation of T Helper Cell Fate by TCR Signal Strength. *Frontiers in Immunology*; 11, https://www.frontiersin.org/articles/10.3389/fimmu.2020.00624 (2020, accessed 17 August 2022).

[120] Wu T, Wieland A, Lee J, et al. Cutting Edge: miR-17-92 Is Required for Both CD4 Th1 and T Follicular Helper Cell Responses during Viral Infection. *JI* 2015; 195: 2515–2519.

[121] Basu A, Ramamoorthi G, Albert G, et al. Differentiation and Regulation of TH Cells: A Balancing Act for Cancer Immunotherapy. *Frontiers in Immunology* 2021; 12: 1577.

[122] Shen J, Xiao Z, Zhao Q, et al. Anti-cancer therapy with TNFα and IFNγ: A comprehensive review. *Cell Prolif* 2018; 51: e12441.

[123] Mojic M, Takeda K, Hayakawa Y. The Dark Side of IFN-γ: Its Role in Promoting Cancer Immunoevasion. *International Journal of Molecular Sciences* 2018; 19: 89.

[124] Jorgovanovic D, Song M, Wang L, et al. Roles of IFN-γ in tumor progression and regression: a review. *Biomark Res* 2020; 8: 49.

[125] Zhou F. Molecular mechanisms of IFN-gamma to up-regulate MHC class I antigen processing and presentation. *Int Rev Immunol* 2009; 28: 239–260.

[126] Mortara L, Balza E, Bruno A, et al. Anti-cancer Therapies Employing IL-2 Cytokine Tumor Targeting: Contribution of Innate, Adaptive and Immunosuppressive Cells in the Anti-tumor Efficacy. *Front Immunol* 2018; 9: 2905.

[127] Sim GC, Radvanyi L. The IL-2 cytokine family in cancer immunotherapy. *Cytokine Growth Factor Rev* 2014; 25: 377–390.

[128] Bos R, Sherman LA. CD4+ T-cell help in the tumor milieu is required for recruitment and cytolytic function of CD8+ T lymphocytes. *Cancer Res* 2010; 70: 8368–8377.

[129] Josephs SF, Ichim TE, Prince SM, et al. Unleashing endogenous TNF-alpha as a cancer immunotherapeutic. *J Transl Med* 2018; 16: 242.

[130] Lu Y, Wang Q, Xue G, et al. Th9 Cells Represent a Unique Subset of CD4+ T Cells Endowed with the Ability to Eradicate Advanced Tumors. *Cancer Cell* 2018; 33: 1048-1060.e7.

[131] Végran F, Apetoh L, Ghiringhelli F. Th9 cells: a novel CD4 T-cell subset in the immune war against cancer. *Cancer Res* 2015; 75: 475–479.

[132] Chen T, Guo J, Cai Z, et al. Th9 Cell Differentiation and Its Dual Effects in Tumor Development. *Front Immunol* 2020; 11: 1026.

[133] Gu-Trantien C, Loi S, Garaud S, et al. $CD4^+$ follicular helper T cell infiltration predicts breast cancer survival. *J Clin Invest* 2013; 123: 2873–2892.

[134] Singh D, Ganesan AP, Panwar B, et al. *CD4+ follicular helper-like T cells are key players in anti-tumor immunity*.

[135] Cabrita R, Lauss M, Sanna A, et al. Tertiary lymphoid structures improve immunotherapy and survival in melanoma. *Nature* 2020; 577: 561–565.

[136] Bailey SR, Nelson MH, Himes RA, et al. Th17 cells in cancer: the ultimate identity crisis. *Front Immunol* 2014; 5: 276.

[137] Guéry L, Hugues S. Th17 Cell Plasticity and Functions in Cancer Immunity. *Biomed Res Int* 2015; 2015: 314620.

[138] Doulabi H, Masoumi E, Rastin M, et al. The role of Th22 cells, from tissue repair to cancer progression. *Cytokine* 2022; 149: 155749.

[139] Li Z, Jiang J, Wang Z, et al. Endogenous interleukin-4 promotes tumor development by increasing tumor cell resistance to apoptosis. *Cancer Res* 2008; 68: 8687–8694.

[140] Nappo G, Handle F, Santer FR, et al. The immunosuppressive cytokine interleukin-4

increases the clonogenic potential of prostate stem-like cells by activation of STAT6 signalling. *Oncogenesis* 2017; 6: e342.

[141] Kidd P. Th1/Th2 balance: the hypothesis, its limitations, and implications for health and disease. *Altern Med Rev* 2003; 8: 223–246.

[142] Acuner-Ozbabacan ES, Engin BH, Guven-Maiorov E, et al. The structural network of Interleukin-10 and its implications in inflammation and cancer. *BMC Genomics* 2014; 15 Suppl 4: S2.

[143] Schmitt E, Williams C. Generation and Function of Induced Regulatory T Cells. *Frontiers in Immunology* 2013; 4: 152.

[144] Tanaka A, Sakaguchi S. Regulatory T cells in cancer immunotherapy. *Cell Res* 2017; 27: 109–118.

[145] Chaudhry A, Samstein RM, Treuting P, et al. Interleukin-10 signaling in regulatory T cells is required for suppression of Th17 cell-mediated inflammation. *Immunity* 2011; 34: 566–578.

[146] Chen M-L, Pittet MJ, Gorelik L, et al. Regulatory T cells suppress tumor-specific CD8 T cell cytotoxicity through TGF-beta signals in vivo. *Proc Natl Acad Sci U S A* 2005; 102: 419–424.

[147] Pandiyan P, Zheng L, Ishihara S, et al. CD4+CD25+Foxp3+ regulatory T cells induce cytokine deprivation-mediated apoptosis of effector CD4+ T cells. *Nat Immunol* 2007; 8: 1353–1362.

[148] Antonioli L, Pacher P, Vizi ES, et al. CD39 and CD73 in immunity and inflammation. *Trends in Molecular Medicine* 2013; 19: 355–367.

[149] Qureshi OS, Zheng Y, Nakamura K, et al. Trans-endocytosis of CD80 and CD86: a molecular basis for the cell-extrinsic function of CTLA-4. *Science* 2011; 332: 600–603.

[150] Wagner H, Starzinski-Powitz A, Jung H, et al. Induction of I region-restricted hapten-specific cytotoxic T lymphocytes. *J Immunol* 1977; 119: 1365–1368.

[151] Feighery C, Stastny P. HLA-D region-associated determinants serve as targets for human cell-mediated lysis. *J Exp Med* 1979; 149: 485–494.

[152] Lukacher AE, Morrison LA, Braciale VL, et al. Expression of specific cytolytic activity by H-2I region-restricted, influenza virus-specific T lymphocyte clones. *J Exp Med* 1985; 162: 171–187.

[153] Maimone MM, Morrison LA, Braciale VL, et al. Features of target cell lysis by class I and class II MHC-restricted cytolytic T lymphocytes. *J Immunol* 1986; 137: 3639–3643.

[154] van Leeuwen EMM, Remmerswaal EBM, Vossen MTM, et al. Emergence of a CD4+CD28- granzyme B+, cytomegalovirus-specific T cell subset after recovery of primary cytomegalovirus infection. *J Immunol* 2004; 173: 1834–1841.

[155] Zaunders JJ, Dyer WB, Wang B, et al. Identification of circulating antigen-specific CD4+ T lymphocytes with a CCR5+, cytotoxic phenotype in an HIV-1 long-term nonprogressor and in CMV infection. *Blood* 2004; 103: 2238–2247.

[156] Appay V, Zaunders JJ, Papagno L, et al. Characterization of CD4(+) CTLs ex vivo. *J Immunol* 2002; 168: 5954–5958.

[157] Aslan N, Yurdaydin C, Wiegand J, et al. Cytotoxic CD4 T cells in viral hepatitis. *J Viral Hepat* 2006; 13: 505–514.

[158] Norris PJ, Moffett HF, Yang OO, et al. Beyond help: direct effector functions of human immunodeficiency virus type 1-specific CD4(+) T cells. *J Virol* 2004; 78: 8844–8851.

[159] Nemes E, Bertoncelli L, Lugli E, et al. Cytotoxic granule release dominates gag-specific CD4+ T-cell response in different phases of HIV infection. *AIDS* 2010; 24: 947–957.

[160] Johnson S, Eller M, Teigler JE, et al. Cooperativity of HIV-Specific Cytolytic CD4 T Cells and CD8 T Cells in Control of HIV Viremia. *J Virol* 2015; 89: 7494–7505.

[161] Casazza JP, Betts MR, Price DA, et al. Acquisition of direct antiviral effector functions by CMV-specific CD4+ T lymphocytes with cellular maturation. *J Exp Med* 2006; 203: 2865–2877.

[162] Omiya R, Buteau C, Kobayashi H, et al. Inhibition of EBV-induced lymphoproliferation by CD4(+) T cells specific for an MHC class II promiscuous epitope. *J Immunol* 2002; 169: 2172–2179.

[163] Brown DM, Lee S, Garcia-Hernandez M de la L, et al. Multifunctional CD4 cells expressing gamma interferon and perforin mediate protection against lethal influenza virus infection. *J Virol* 2012; 86: 6792–6803.

[164] Brown DM, Lampe AT, Workman AM. The Differentiation and Protective Function of Cytolytic CD4 T Cells in Influenza Infection. *Front Immunol* 2016; 7: 93.

[165] Gagnon SJ, Zeng W, Kurane I, et al. Identification of two epitopes on the dengue 4 virus capsid protein recognized by a serotype-specific and a panel of serotype-cross-reactive human CD4+ cytotoxic T-lymphocyte clones. *J Virol* 1996; 70: 141–147.

[166] Kurane I, Brinton MA, Samson AL, et al. Dengue virus-specific, human CD4+ CD8- cytotoxic T-cell clones: multiple patterns of virus cross-reactivity recognized by NS3-specific T-cell clones. *J Virol* 1991; 65: 1823–1828.

[167] Kumar A, Perdomo MF, Kantele A, et al. Granzyme B mediated function of Parvovirus B19-specific CD4(+) T cells. *Clin Transl Immunology* 2015; 4: e39.

[168] Munier CML, van Bockel D, Bailey M, et al. The primary immune response to Vaccinia virus vaccination includes cells with a distinct cytotoxic effector CD4 T-cell phenotype. *Vaccine* 2016; 34: 5251–5261.

[169] Wahid R, Cannon MJ, Chow M. Virus-specific CD4+ and CD8+ cytotoxic T-cell responses and long-term T-cell memory in individuals vaccinated against polio. *J Virol* 2005; 79: 5988–5995.

[170] Coler RN, Hudson T, Hughes S, et al. Vaccination Produces CD4 T Cells with a Novel CD154-CD40-Dependent Cytolytic Mechanism. *J Immunol* 2015; 195: 3190–3197.

[171] Stuller KA, Flaño E. CD4 T cells mediate killing during persistent gammaherpesvirus 68 infection. *J Virol* 2009; 83: 4700–4703.

[172] Verma S, Weiskopf D, Gupta A, et al. Cytomegalovirus-Specific CD4 T Cells Are Cytolytic and Mediate Vaccine Protection. *J Virol* 2016; 90: 650–658.

[173] Verma S, Weiskopf D, Gupta A, et al. Erratum for Verma et al., 'Cytomegalovirus-Specific CD4 T Cells Are Cytolytic and Mediate Vaccine Protection'. *J Virol*; 91. Epub ahead of print 1 September 2017. DOI: 10.1128/JVI.00959-17.

[174] Knudson CJ, Férez M, Alves-Peixoto P, et al. Mechanisms of Antiviral Cytotoxic CD4 T Cell Differentiation. *J Virol* 2021; 95: e0056621.

[175] Takeuchi A, Saito T. CD4 CTL, a Cytotoxic Subset of CD4+ T Cells, Their Differentiation and Function. *Front Immunol*; 8. Epub ahead of print 23 February 2017. DOI: 10.3389/fimmu.2017.00194.

[176] Juno JA, van Bockel D, Kent SJ, et al. Cytotoxic CD4 T Cells-Friend or Foe during Viral Infection? *Front Immunol* 2017; 8: 19.

[177] Thewissen M, Somers V, Hellings N, et al. CD4+CD28null T cells in autoimmune disease: pathogenic features and decreased susceptibility to immunoregulation. *J Immunol* 2007; 179: 6514–6523.

[178] Xie Y, Akpinarli A, Maris C, et al. Naive tumor-specific CD4(+) T cells differentiated in vivo eradicate established melanoma. *J Exp Med* 2010; 207: 651–667.

[179] Quezada SA, Simpson TR, Peggs KS, et al. Tumor-reactive CD4(+) T cells develop cytotoxic activity and eradicate large established melanoma after transfer into lymphopenic hosts. *J*

Exp Med 2010; 207: 637–650.

[180] Porakishvili N, Kardava L, Jewell AP, et al. Cytotoxic CD4+ T cells in patients with B cell chronic lymphocytic leukemia kill via a perforin-mediated pathway. *Haematologica* 2004; 89: 435–443.

[181] Mucida D, Husain MM, Muroi S, et al. Transcriptional reprogramming of mature $CD4^+$ helper T cells generates distinct MHC class II-restricted cytotoxic T lymphocytes. *Nat Immunol* 2013; 14: 281–289.

[182] Eshima K, Chiba S, Suzuki H, et al. Ectopic expression of a T-box transcription factor, eomesodermin, renders CD4(+) Th cells cytotoxic by activating both perforin- and FasL-pathways. *Immunol Lett* 2012; 144: 7–15.

[183] Muraro E, Merlo A, Martorelli D, et al. Fighting Viral Infections and Virus-Driven Tumors with Cytotoxic CD4+ T Cells. *Front Immunol* 2017; 8: 197.

[184] Serroukh Y, Gu-Trantien C, Hooshiar Kashani B, et al. The transcription factors Runx3 and ThPOK cross-regulate acquisition of cytotoxic function by human Th1 lymphocytes. *eLife*; 7: e30496.

[185] Brown DM, Kamperschroer C, Dilzer AM, et al. IL-2 and antigen dose differentially regulate perforin- and FasL-mediated cytolytic activity in antigen specific CD4+ T cells. *Cell Immunol* 2009; 257: 69–79.

[186] Brown DM. Cytolytic CD4 cells: Direct mediators in infectious disease and malignancy. *Cell Immunol* 2010; 262: 89–95.

[187] Sujino T, London M, Hoytema van Konijnenburg DP, et al. Tissue adaptation of regulatory and intraepithelial $CD4^+$ T cells controls gut inflammation. *Science* 2016; 352: 1581–1586.

[188] Lancki DW, Hsieh CS, Fitch FW. Mechanisms of lysis by cytotoxic T lymphocyte clones. Lytic activity and gene expression in cloned antigen-specific CD4+ and CD8+ T lymphocytes. *J Immunol* 1991; 146: 3242–3249.

[189] Xue G, Jin G, Fang J, et al. IL-4 together with IL-1β induces antitumor Th9 cell differentiation in the absence of TGF-β signaling. *Nat Commun* 2019; 10: 1376.

[190] Brien JD, Uhrlaub JL, Nikolich-Zugich J. West Nile virus-specific CD4 T cells exhibit direct antiviral cytokine secretion and cytotoxicity and are sufficient for antiviral protection. *J Immunol* 2008; 181: 8568–8575.

[191] Moore TC, Vogel AJ, Petro TM, et al. IRF3 deficiency impacts granzyme B expression and maintenance of memory T cell function in response to viral infection. *Microbes Infect* 2015; 17: 426–439.

[192] Workman AM, Jacobs AK, Vogel AJ, et al. Inflammation enhances IL-2 driven differentiation of cytolytic CD4 T cells. *PLoS One* 2014; 9: e89010.

[193] Kischkel FC, Hellbardt S, Behrmann I, et al. Cytotoxicity-dependent APO-1 (Fas/CD95)-associated proteins form a death-inducing signaling complex (DISC) with the receptor. *EMBO J* 1995; 14: 5579–5588.

[194] Nagata S, Golstein P. The Fas death factor. *Science* 1995; 267: 1449–1456.

[195] Krammer PH. CD95's deadly mission in the immune system. *Nature* 2000; 407: 789–795.

[196] Kruidering M, Evan GI. Caspase-8 in apoptosis: the beginning of 'the end'? *IUBMB Life* 2000; 50: 85–90.

[197] Peters PJ, Borst J, Oorschot V, et al. Cytotoxic T lymphocyte granules are secretory lysosomes, containing both perforin and granzymes. *J Exp Med* 1991; 173: 1099–1109.

[198] Trapani JA, Smyth MJ. Functional significance of the perforin/granzyme cell death pathway. *Nat Rev Immunol* 2002; 2: 735–747.

[199] Podack ER, Young JD, Cohn ZA. Isolation and biochemical and functional characterization of perforin 1 from cytolytic T-cell granules. *Proc Natl Acad Sci U S A* 1985; 82: 8629–8633.

[200] Voskoboinik I, Whisstock JC, Trapani JA. Perforin and granzymes: function, dysfunction and human pathology. *Nat Rev Immunol* 2015; 15: 388–400.

[201] Cullen SP, Brunet M, Martin SJ. Granzymes in cancer and immunity. *Cell Death Differ* 2010; 17: 616–623.

[202] Anthony DA, Andrews DM, Watt SV, et al. Functional dissection of the granzyme family: cell death and inflammation. *Immunol Rev* 2010; 235: 73–92.

[203] Chowdhury D, Lieberman J. Death by a thousand cuts: granzyme pathways of programmed cell death. *Annu Rev Immunol* 2008; 26: 389–420.

[204] Van Damme P, Maurer-Stroh S, Hao H, et al. The substrate specificity profile of human granzyme A. *Biol Chem* 2010; 391: 983–997.

[205] Andrade F, Roy S, Nicholson D, et al. Granzyme B directly and efficiently cleaves several downstream caspase substrates: implications for CTL-induced apoptosis. *Immunity* 1998; 8: 451–460.

[206] Lunde E, Bogen B, Sandlie I. Immunoglobulin as a vehicle for foreign antigenic peptides immunogenic to T cells. *Mol Immunol* 1997; 34: 1167–1176.

[207] Lunde E, Munthe LA, Vabø A, et al. Antibodies engineered with IgD specificity efficiently deliver integrated T-cell epitopes for antigen presentation by B cells. *Nat Biotechnol* 1999; 17: 670–675.

[208] Lunde E, Lauvrak V, Rasmussen IB, et al. Troybodies and Pepbodies. *Biochemical Society Transactions* 2002; 30: 500–506.

[209] Rasmussen IB, Lunde E, Michaelsen TE, et al. The principle of delivery of T cell epitopes to antigen-presenting cells applied to peptides from influenza virus, ovalbumin, and hen egg lysozyme: implications for peptide vaccination. *Proc Natl Acad Sci USA* 2001; 98: 10296–10301.

[210] Gurer C, Strowig T, Brilot F, et al. Targeting the nuclear antigen 1 of Epstein-Barr virus to the human endocytic receptor DEC-205 stimulates protective T-cell responses. *Blood* 2008; 112: 1231–1239.

[211] Do Y, Koh H, Park CG, et al. Targeting of LcrV virulence protein from Yersinia pestis to dendritic cells protects mice against pneumonic plague. *Eur J Immunol* 2010; 40: 2791–2796.

[212] Idoyaga J, Lubkin A, Fiorese C, et al. Comparable T helper 1 (Th1) and CD8 T-cell immunity by targeting HIV gag p24 to CD8 dendritic cells within antibodies to Langerin, DEC205, and Clec9A. *Proc Natl Acad Sci U S A* 2011; 108: 2384–2389.

[213] Kreutz M, Giquel B, Hu Q, et al. Antibody-antigen-adjuvant conjugates enable co-delivery of antigen and adjuvant to dendritic cells in cis but only have partial targeting specificity. *PLoS One* 2012; 7: e40208.

[214] Leung CS, Maurer MA, Meixlsperger S, et al. Robust T-cell stimulation by Epstein-Barr virus–transformed B cells after antigen targeting to DEC-205. *Blood* 2013; 121: 1584–1594.

[215] Yu X, Ilecka M, Bartlett EJ, et al. Antigen-armed antibodies targeting B lymphoma cells effectively activate antigen-specific CD4+ T cells. *Blood* 2015; 125: 1601–1610.

[216] Schneidt V, Ilecka M, Dreger P, et al. Antibodies conjugated with viral antigens elicit a cytotoxic T cell response against primary CLL ex vivo. *Leukemia* 2019; 33: 88–98.

[217] Zhou S, Liu M, Ren F, et al. The landscape of bispecific T cell engager in cancer treatment. *Biomark Res* 2021; 9: 38.

[218] Jia B, Wang L, Claxton DF, et al. Bone marrow CD8 T cells express high frequency of PD-1 and exhibit reduced anti-leukemia response in newly diagnosed AML patients. *Blood Cancer Journal* 2018; 8: 1–5.

[219] Lamble AJ, Kosaka Y, Laderas T, et al. Reversible suppression of T cell function in the bone marrow microenvironment of acute myeloid leukemia. *Proceedings of the National Academy*

of Sciences 2020; 117: 14331–14341.

[220] Stein R, Gupta P, Chen X, et al. Therapy of B-cell malignancies by anti-HLA-DR humanized monoclonal antibody, IMMU-114, is mediated through hyperactivation of ERK and JNK MAP kinase signaling pathways. *Blood* 2010; 115: 5180–5190.

[221] Christopher MJ, Petti AA, Rettig MP, et al. Immune Escape of Relapsed AML Cells after Allogeneic Transplantation. *N Engl J Med* 2018; 379: 2330–2341.

[222] Balaian L, Zhong R, Ball ED. The inhibitory effect of anti-CD33 monoclonal antibodies on AML cell growth correlates with Syk and/or ZAP-70 expression. *Experimental Hematology* 2003; 31: 363–371.

[223] Andrews RG, Torok-Storb B, Bernstein ID. Myeloid-associated differentiation antigens on stem cells and their progeny identified by monoclonal antibodies. *Blood* 1983; 62: 124–132.

[224] Molica M, Perrone S, Mazzone C, et al. CD33 Expression and Gentuzumab Ozogamicin in Acute Myeloid Leukemia: Two Sides of the Same Coin. *Cancers (Basel)* 2021; 13: 3214.

[225] Jilani I, Estey E, Huh Y, et al. Differences in CD33 intensity between various myeloid neoplasms. *Am J Clin Pathol* 2002; 118: 560–566.

[226] Pollard JA, Alonzo TA, Loken M, et al. Correlation of CD33 expression level with disease characteristics and response to gemtuzumab ozogamicin containing chemotherapy in childhood AML. *Blood* 2012; 119: 3705–3711.

[227] Dinndorf PA, Buckley JD, Nesbit ME, et al. Expression of myeloid differentiation antigens in acute nonlymphocytic leukemia: increased concentration of CD33 antigen predicts poor outcome--a report from the Childrens Cancer Study Group. *Med Pediatr Oncol* 1992; 20: 192–200.

[228] Liu J, Tong J, Yang H. Targeting CD33 for acute myeloid leukemia therapy. *BMC Cancer* 2022; 22: 24.

[229] Feldman EJ, Brandwein J, Stone R, et al. Phase III randomized multicenter study of a humanized anti-CD33 monoclonal antibody, lintuzumab, in combination with chemotherapy, versus chemotherapy alone in patients with refractory or first-relapsed acute myeloid leukemia. *J Clin Oncol* 2005; 23: 4110–4116.

[230] Sekeres MA, Lancet JE, Wood BL, et al. Randomized phase IIb study of low-dose cytarabine and lintuzumab versus low-dose cytarabine and placebo in older adults with untreated acute myeloid leukemia. *Haematologica* 2013; 98: 119–128.

[231] Ravandi F, Walter RB, Subklewe M, et al. Updated results from phase I dose-escalation study of AMG 330, a bispecific T-cell engager molecule, in patients with relapsed/refractory acute myeloid leukemia (R/R AML). *Journal of Clinical Oncology* 2020; 38: 7508–7508.

[232] Westervelt P, Cortes JE, Altman JK, et al. Phase 1 First-in-Human Trial of AMV564, a Bivalent Bispecific (2:2) CD33/CD3 T-Cell Engager, in Patients with Relapsed/Refractory Acute Myeloid Leukemia (AML). *Blood* 2019; 134: 834.

[233] Wang Q, Wang Y, Lv H, et al. Treatment of CD33-directed chimeric antigen receptor-modified T cells in one patient with relapsed and refractory acute myeloid leukemia. *Mol Ther* 2015; 23: 184–191.

[234] Lane AA. Targeting CD123 in AML. *Clinical Lymphoma, Myeloma and Leukemia* 2020; 20: S67–S68.

[235] Guthridge MA, Stomski FC, Thomas D, et al. Mechanism of activation of the GM-CSF, IL-3, and IL-5 family of receptors. *Stem Cells* 1998; 16: 301–313.

[236] Taussig DC, Pearce DJ, Simpson C, et al. Hematopoietic stem cells express multiple myeloid markers: implications for the origin and targeted therapy of acute myeloid leukemia. *Blood* 2005; 106: 4086–4092.

[237] Korpelainen EI, Gamble JR, Vadas MA, et al. IL-3 receptor expression, regulation and

function in cells of the Vasculature. *Immunology & Cell Biology* 1996; 74: 1–7.

[238] Sugita M, Guzman ML. CD123 as a Therapeutic Target Against Malignant Stem Cells. *Hematol Oncol Clin North Am* 2020; 34: 553–564.

[239] Testa U, Pelosi E, Frankel A. CD 123 is a membrane biomarker and a therapeutic target in hematologic malignancies. *Biomarker Research* 2014; 2: 4.

[240] Ehninger A, Kramer M, Röllig C, et al. Distribution and levels of cell surface expression of CD33 and CD123 in acute myeloid leukemia. *Blood Cancer J* 2014; 4: e218.

[241] Testa U, Riccioni R, Militi S, et al. Elevated expression of IL-3Ralpha in acute myelogenous leukemia is associated with enhanced blast proliferation, increased cellularity, and poor prognosis. *Blood* 2002; 100: 2980–2988.

[242] Das N, Gupta R, Gupta SK, et al. A Real-world Perspective of CD123 Expression in Acute Leukemia as Promising Biomarker to Predict Treatment Outcome in B-ALL and AML. *Clin Lymphoma Myeloma Leuk* 2020; 20: e673–e684.

[243] Liu H. Emerging agents and regimens for AML. *Journal of Hematology & Oncology* 2021; 14: 49.

[244] Espinoza-Gutarra MR, Green SD, Zeidner JF, et al. CD123-targeted therapy in acute myeloid leukemia. *Expert Rev Hematol* 2021; 14: 561–576.

[245] Kubasch AS, Schulze F, Giagounidis A, et al. Single agent talacotuzumab demonstrates limited efficacy but considerable toxicity in elderly high-risk MDS or AML patients failing hypomethylating agents. *Leukemia* 2020; 34: 1182–1186.

[246] Montesinos P, Roboz GJ, Bulabois C-E, et al. Safety and efficacy of talacotuzumab plus decitabine or decitabine alone in patients with acute myeloid leukemia not eligible for chemotherapy: results from a multicenter, randomized, phase 2/3 study. *Leukemia* 2020; 1–13.

[247] Daver NG, Erba HP, Papadantonakis N, et al. A Phase 1b/2 Study of the CD123-Targeting Antibody-Drug Conjugate IMGN632 As Monotherapy or in Combination with Venetoclax and/or Azacitidine for Patients with CD123-Positive Acute Myeloid Leukemia. *Blood* 2019; 134: 2601.

[248] Ravandi F, Bashey A, Stock W, et al. Complete Responses in Relapsed/Refractory Acute Myeloid Leukemia (AML) Patients on a Weekly Dosing Schedule of Vibecotamab (XmAb14045), a CD123 x CD3 T Cell-Engaging Bispecific Antibody; Initial Results of a Phase 1 Study. *Blood* 2020; 136: 4–5.

[249] Aldoss I, Uy GL, Vey N, et al. Flotetuzumab As Salvage Therapy for Primary Induction Failure and Early Relapse Acute Myeloid Leukemia. *Blood* 2020; 136: 16–18.

[250] Budde LE, Song J, Real MD, et al. Abstract PR14: CD123CAR displays clinical activity in relapsed/refractory (r/r) acute myeloid leukemia (AML) and blastic plasmacytoid dendritic cell neoplasm (BPDCN): Safety and efficacy results from a phase 1 study. *Cancer Immunology Research* 2020; 8: PR14.

[251] Mai J, Virtue A, Shen J, et al. An evolving new paradigm: endothelial cells – conditional innate immune cells. *Journal of Hematology & Oncology* 2013; 6: 61.

[252] Turesson C. Endothelial Expression of MHC Class II Molecules in Autoimmune Disease. *Current Pharmaceutical Design* 1986; 10: 129–143.

[253] Marshall ASJ, Willment JA, Pyż E, et al. Human MICL (CLEC12A) is differentially glycosylated and is down-regulated following cellular activation. *European Journal of Immunology* 2006; 36: 2159–2169.

[254] Ma H, Padmanabhan IS, Parmar S, et al. Targeting CLL-1 for acute myeloid leukemia therapy. *Journal of Hematology & Oncology* 2019; 12: 41.

[255] Bakker ABH, van den Oudenrijn S, Bakker AQ, et al. C-type lectin-like molecule-1: a novel

myeloid cell surface marker associated with acute myeloid leukemia. *Cancer Res* 2004; 64: 8443–8450.

[256] Marshall ASJ, Willment JA, Lin H-H, et al. Identification and Characterization of a Novel Human Myeloid Inhibitory C-type Lectin-like Receptor (MICL) That Is Predominantly Expressed on Granulocytes and Monocytes *. *Journal of Biological Chemistry* 2004; 279: 14792–14802.

[257] Wang J, Chen S, Xiao W, et al. CAR-T cells targeting CLL-1 as an approach to treat acute myeloid leukemia. *Journal of Hematology & Oncology* 2018; 11: 7.

[258] Tashiro H, Sauer T, Shum T, et al. Treatment of Acute Myeloid Leukemia with T Cells Expressing Chimeric Antigen Receptors Directed to C-type Lectin-like Molecule 1. *Molecular Therapy* 2017; 25: 2202–2213.

[259] Larsen HØ, Roug AS, Just T, et al. Expression of the hMICL in acute myeloid leukemia—a highly reliable disease marker at diagnosis and during follow-up. *Cytometry Part B: Clinical Cytometry* 2012; 82B: 3–8.

[260] van Rhenen A, van Dongen GAMS, Kelder A, et al. The novel AML stem cell associated antigen CLL-1 aids in discrimination between normal and leukemic stem cells. *Blood* 2007; 110: 2659–2666.

[261] Li Q, Liang C, Xu X, et al. CLEC12A plays an important role in immunomodulatory function and prognostic significance of patients with acute myeloid leukemia. *Leukemia & Lymphoma* 2022; 0: 1–13.

[262] Willier S, Rothämel P, Hastreiter M, et al. CLEC12A and CD33 coexpression as a preferential target for pediatric AML combinatorial immunotherapy. *Blood* 2021; 137: 1037–1049.

[263] Zheng B, Yu S-F, Del Rosario G, et al. An Anti-CLL-1 Antibody-Drug Conjugate for the Treatment of Acute Myeloid Leukemia. *Clin Cancer Res* 2019; 25: 1358–1368.

[264] Leipold DD, Figueroa I, Masih S, et al. Preclinical pharmacokinetics and pharmacodynamics of DCLL9718A: An antibody-drug conjugate for the treatment of acute myeloid leukemia. *mAbs* 2018; 10: 1312–1321.

[265] Jiang Y-P, Liu BY, Zheng Q, et al. CLT030, a leukemic stem cell-targeting CLL1 antibody-drug conjugate for treatment of acute myeloid leukemia. *Blood Adv* 2018; 2: 1738–1749.

[266] Van Loo PF, Doornbos R, Dolstra H, et al. Preclinical Evaluation of MCLA117, a CLEC12AxCD3 Bispecific Antibody Efficiently Targeting a Novel Leukemic Stem Cell Associated Antigen in AML. *Blood* 2015; 126: 325.

[267] Liu F, Cao Y, Pinz K, et al. First-in-Human CLL1-CD33 Compound CAR T Cell Therapy Induces Complete Remission in Patients with Refractory Acute Myeloid Leukemia: Update on Phase 1 Clinical Trial. *Blood* 2018; 132: 901.

[268] Zhang H, Gan W-T, Hao W-G, et al. Successful Anti-CLL1 CAR T-Cell Therapy in Secondary Acute Myeloid Leukemia. *Front Oncol* 2020; 10: 685.

[269] Wibowo AS, Singh M, Reeder KM, et al. Structures of human folate receptors reveal biological trafficking states and diversity in folate and antifolate recognition. *Proc Natl Acad Sci U S A* 2013; 110: 15180–15188.

[270] Samaniego R, Domínguez-Soto Á, Ratnam M, et al. Folate Receptor β (FRβ) Expression in Tissue-Resident and Tumor-Associated Macrophages Associates with and Depends on the Expression of PU.1. *Cells* 2020; 9: 1445.

[271] Ross JF, Wang H, Behm FG, et al. Folate receptor type beta is a neutrophilic lineage marker and is differentially expressed in myeloid leukemia. *Cancer* 1999; 85: 348–357.

[272] Puig-Kröger A, Sierra-Filardi E, Domínguez-Soto A, et al. Folate receptor beta is expressed by tumor-associated macrophages and constitutes a marker for M2 anti-inflammatory/regulatory macrophages. *Cancer Res* 2009; 69: 9395–9403.

[273] Roy AG, Robinson JM, Sharma P, et al. Folate Receptor Beta as a Direct and Indirect Target for Antibody-Based Cancer Immunotherapy. *Int J Mol Sci* 2021; 22: 5572.

[274] Ratnam M, Hao H, Zheng X, et al. Receptor induction and targeted drug delivery: a new antileukaemia strategy. *Expert Opin Biol Ther* 2003; 3: 563–574.

[275] Y L, J W, J W, et al. Role of formulation composition in folate receptor-targeted liposomal doxorubicin delivery to acute myelogenous leukemia cells. *Molecular pharmaceutics*; 4. Epub ahead of print October 2007. DOI: 10.1021/mp070058l.

[276] Pan XQ, Zheng X, Shi G, et al. Strategy for the treatment of acute myelogenous leukemia based on folate receptor beta-targeted liposomal doxorubicin combined with receptor induction using all-trans retinoic acid. *Blood* 2002; 100: 594–602.

[277] Ghamari A, Pakzad P, Majd A, et al. Design and Production An Effective Bispecific Tandem Chimeric Antigen Receptor on T Cells against CD123 and Folate Receptor ß towards B-Acute Myeloid Leukaemia Blasts. *Cell J* 2021; 23: 650–657.

[278] Lynn RC, Feng Y, Schutsky K, et al. High-affinity FRβ-specific CAR T cells eradicate AML and normal myeloid lineage without HSC toxicity. *Leukemia* 2016; 30: 1355–1364.

[279] Lynn RC, Poussin M, Kalota A, et al. Targeting of folate receptor β on acute myeloid leukemia blasts with chimeric antigen receptor-expressing T cells. *Blood* 2015; 125: 3466–3476.

[280] Hislop AD, Taylor GS, Sauce D, et al. Cellular responses to viral infection in humans: lessons from Epstein-Barr virus. *Annu Rev Immunol* 2007; 25: 587–617.

[281] van Zyl DG, Tsai M-H, Shumilov A, et al. Immunogenic particles with a broad antigenic spectrum stimulate cytolytic T cells and offer increased protection against EBV infection ex vivo and in mice. *PLoS Pathog* 2018; 14: e1007464.

[282] Leen A, Meij P, Redchenko I, et al. Differential immunogenicity of Epstein-Barr virus latent-cycle proteins for human CD4(+) T-helper 1 responses. *J Virol* 2001; 75: 8649–8659.

[283] Walton SM, Wyrsch P, Munks MW, et al. The dynamics of mouse cytomegalovirus-specific CD4 T cell responses during acute and latent infection. *J Immunol* 2008; 181: 1128–1134.

[284] Zangger N, Oderbolz J, Oxenius A. CD4 T Cell-Mediated Immune Control of Cytomegalovirus Infection in Murine Salivary Glands. *Pathogens* 2021; 10: 1531.

[285] Arens R, Wang P, Sidney J, et al. Cutting Edge: Murine Cytomegalovirus Induces a Polyfunctional CD4 T Cell Response1. *The Journal of Immunology* 2008; 180: 6472–6476.

[286] Kovtun Y, Jones GE, Adams S, et al. A CD123-targeting antibody-drug conjugate, IMGN632, designed to eradicate AML while sparing normal bone marrow cells. *Blood Adv* 2018; 2: 848–858.

[287] Monteiro CAP, Oliveira ADPR, Silva RC, et al. Evaluating internalization and recycling of folate receptors in breast cancer cells using quantum dots. *J Photochem Photobiol B* 2020; 209: 111918.

[288] Wetzler M, McElwain BK, Stewart CC, et al. HLA-DR antigen-negative acute myeloid leukemia. *Leukemia* 2003; 17: 707–715.

[289] Scholtalbers J, Boegel S, Bukur T, et al. TCLP: an online cancer cell line catalogue integrating HLA type, predicted neo-epitopes, virus and gene expression. *Genome Med* 2015; 7: 118.

[290] Expasy - Cellosaurus, https://www.cellosaurus.org/ (accessed 27 September 2022).

[291] Bruhns P. Properties of mouse and human IgG receptors and their contribution to disease models. *Blood* 2012; 119: 5640–5649.

[292] Wilkinson I, Anderson S, Fry J, et al. Fc-engineered antibodies with immune effector functions completely abolished. *PLOS ONE* 2021; 16: e0260954.

[293] Jacob JB, Jacob MK, Parajuli P. Chapter Three - Review of immune checkpoint inhibitors in immuno-oncology. In: Copple BL, Rockwell CE (eds) *Advances in Pharmacology*. Academic

Press, pp. 111–139.

[294] Moran AE, Kovacsovics-Bankowski M, Weinberg AD. The TNFRs OX40, 4-1BB, and CD40 as targets for cancer immunotherapy. *Curr Opin Immunol* 2013; 25: 10.1016/j.coi.2013.01.004.

[295] Schuringa JJ, Bonifer C. Dissecting Clonal Heterogeneity in AML. *Cancer Cell* 2020; 38: 782–784.

[296] El-Sayes N, Vito A, Mossman K. Tumor Heterogeneity: A Great Barrier in the Age of Cancer Immunotherapy. *Cancers* 2021; 13: 806.

[297] Hashimoto H, Güngör D, Krickeberg N, et al. TH1 cytokines induce senescence in AML. *Leukemia Research* 2022; 117: 106842.

[298] Warner NL, Moore MAS, Metcalf D. A Transplantable Myelomonocytic Leukemia in BALB/c Mice: Cytology, Karyotype, and Muramidase Content23. *JNCI: Journal of the National Cancer Institute* 1969; 43: 963–982.

[299] Mopin A, Driss V, Brinster C. A Detailed Protocol for Characterizing the Murine C1498 Cell Line and its Associated Leukemia Mouse Model. *J Vis Exp* 2016; 54270.

[300] Salim LZA, Othman R, Abdulla MA, et al. Thymoquinone Inhibits Murine Leukemia WEHI-3 Cells In Vivo and In Vitro. *PLOS ONE* 2014; 9: e115340.

[301] Driss V, Leprêtre F, Briche I, et al. Sub-clonal analysis of the murine C1498 acute myeloid leukaemia cell line reveals genomic and immunogenic diversity. *Immunol Lett* 2017; 192: 27–34.

[302] Alves da Silva PH, Xing S, Kotini AG, et al. MICA/B antibody induces macrophage-mediated immunity against acute myeloid leukemia. *Blood* 2022; 139: 205–216.

[303] Saunders KO. Conceptual Approaches to Modulating Antibody Effector Functions and Circulation Half-Life. *Frontiers in Immunology*; 10, https://www.frontiersin.org/articles/10.3389/fimmu.2019.01296 (2019, accessed 25 October 2022).

[304] Ru Y, Zhu J, Song T, et al. Features of Epstein–Barr Virus and Cytomegalovirus Reactivation in Acute Leukemia Patients After Haplo-HCT With Myeloablative ATG-Containing Conditioning Regimen. *Frontiers in Cellular and Infection Microbiology*; 12, https://www.frontiersin.org/articles/10.3389/fcimb.2022.865170 (2022, accessed 19 December 2022).

[305] Axelrod ML, Cook RS, Johnson DB, et al. Biological Consequences of MHC-II Expression by Tumor Cells in Cancer. *Clinical Cancer Research* 2019; 25: 2392–2402.

[306] Shresta S, Pham CT, Thomas DA, et al. How do cytotoxic lymphocytes kill their targets? *Curr Opin Immunol* 1998; 10: 581–587.

[307] Pabst C, Krosl J, Fares I, et al. Identification of small molecules that support human leukemia stem cell activity ex vivo. *Nat Methods* 2014; 11: 436–442.

[308] Hino C, Pham B, Park D, et al. Targeting the Tumor Microenvironment in Acute Myeloid Leukemia: The Future of Immunotherapy and Natural Products. *Biomedicines* 2022; 10: 1410.

[309] Almosailleakh M, Schwaller J. Murine Models of Acute Myeloid Leukaemia. *Int J Mol Sci* 2019; 20: 453.

[310] DiLillo DJ, Ravetch JV. Differential Fc-Receptor Engagement Drives an Anti-tumor Vaccinal Effect. *Cell* 2015; 161: 1035–1045.

[311] Song HK, Hwang DY. Use of C57BL/6N mice on the variety of immunological researches. *Lab Anim Res* 2017; 33: 119–123.

[312] Chen A, Hu S, Wang Q-F. Tumor heterogeneity of acute myeloid leukemia: insights from single-cell sequencing. *Blood Science* 2019; 1: 73.

[313] Pankov D, Sjöström L, Kalidindi T, et al. In vivo immuno-targeting of an extracellular epitope of membrane bound preferentially expressed antigen in melanoma (PRAME). *Oncotarget* 2017; 8: 65917–65931.

[314] Wang H, Zhao D, Nguyen LX, et al. Targeting cell membrane HDM2: A novel therapeutic approach for acute myeloid leukemia. *Leukemia* 2020; 34: 75–86.

[315] Daver N, Alotaibi AS, Bücklein V, et al. T-cell-based immunotherapy of acute myeloid leukemia: current concepts and future developments. *Leukemia* 2021; 35: 1843–1863.

[316] Beers SA, Glennie MJ, White AL. Influence of immunoglobulin isotype on therapeutic antibody function. *Blood* 2016; 127: 1097–1101.

[317] Hedström AK, Huang J, Michel A, et al. High Levels of Epstein–Barr Virus Nuclear Antigen-1-Specific Antibodies and Infectious Mononucleosis Act Both Independently and Synergistically to Increase Multiple Sclerosis Risk. *Frontiers in Neurology*; 10, https://www.frontiersin.org/articles/10.3389/fneur.2019.01368 (2020, accessed 20 December 2022).

[318] Schottstedt V, Blümel J, Burger R, et al. Human Cytomegalovirus (HCMV) – Revised*. *Transfus Med Hemother* 2010; 37: 365–375.

[319] Ameres S, Liang X, Wiesner M, et al. A Diverse Repertoire of CD4 T Cells Targets the Immediate-Early 1 Protein of Human Cytomegalovirus. *Front Immunol* 2015; 6: 598.

[320] Blander JM. Regulation of the Cell Biology of Antigen Cross-Presentation. *Annual Review of Immunology* 2018; 36: 717–753.

[321] Jung K, Son M-J, Lee S-Y, et al. Antibody-mediated delivery of a viral MHC-I epitope into the cytosol of target tumor cells repurposes virus-specific CD8+ T cells for cancer immunotherapy. *Molecular Cancer* 2022; 21: 102.

[322] Heslop HE, Sharma S, Rooney CM. Adoptive T-Cell Therapy for Epstein-Barr Virus–Related Lymphomas. *J Clin Oncol* 2021; 39: 514–524.

[323] Hoegh-Petersen M, Sy S, Ugarte-Torres A, et al. High Epstein–Barr virus-specific T-cell counts are associated with near-zero likelihood of acute myeloid leukemia relapse after hematopoietic cell transplantation. *Leukemia* 2012; 26: 359–362.

[324] Quentmeier H, Pommerenke C, Dirks WG, et al. The LL-100 panel: 100 cell lines for blood cancer studies. *Sci Rep* 2019; 9: 8218.

[325] Ben-Bassat H, Korkesh A, Voss R, et al. Establishment and characterization of a new permanent cell line (GDM-1) from a patient with myelomonoblastic leukemia. *Leuk Res* 1982; 6: 743–752.

[326] Tiacci E, Spanhol-Rosseto A, Martelli MP, et al. The NPM1 wild-type OCI-AML2 and the NPM1-mutated OCI-AML3 cell lines carry DNMT3A mutations. *Leukemia* 2012; 26: 554–557.

[327] Quentmeier H, Reinhardt J, Zaborski M, et al. FLT3 mutations in acute myeloid leukemia cell lines. *Leukemia* 2003; 17: 120–124.

[328] Kato Y, Ogura M, Okumura M, et al. Establishment of peroxidase positive, human monocytic leukemia cell line (NOMO-1) and its characteristics. *Acta Haematologica Japan*; 49.

[329] Matsuo Y, MacLeod RA, Uphoff CC, et al. Two acute monocytic leukemia (AML-M5a) cell lines (MOLM-13 and MOLM-14) with interclonal phenotypic heterogeneity showing MLL-AF9 fusion resulting from an occult chromosome insertion, ins(11;9)(q23;p22p23). *Leukemia* 1997; 11: 1469–1477.

ACKNOWLEDGEMENT

First of all, I would like to express my deepest gratitude to Prof. Henri-Jacques Delecluse, the head of F100, for giving me the opportunity to conduct my doctoral work in his laboratory. I thank him for his careful supervision as well as for all the interesting discussions I was lucky to have with him, and that participated to enrich my knowledge of the research world.

I would also like to extend my sincere aknowlegments to Prof. Martin Müller (leader of the research group "Tumor virus-specific vaccination strategies", F035) and Prof. Josef Mautner (leader of the research group "Gene vectors", LMU Munich) for their valuable advice during my three Thesis Advisory Committee meetings. Our exchanges were of a prime importance for the achievement of my project. I additionally thank Prof. Mautner for providing me with $CD4^+$ T cell clones, LCLs and some chemicals for the *in vitro* part of my thesis, in parallel of precious advice.

Many thanks also go to Dr. Caroline Pabst (*Universitätsklinikum* Heidelberg), who kindly provided me with the samples from AML patients and very crucial recommendations.

Likewise, I thank all the persons who provided me with material (cell lines, hybridoma, …) which helped me to carry out this doctoral work.

Furthermore, I would like to thank Prof. Delecluse and Prof. Müller but also Prof. Walter-Emil Haefeli (*Universitätsklinikum* Heidelberg) and Dr. Tim Waterboer (head of F020) for accepting to be members of my PhD defense committee.

I am also very grateful to all the F100 members; it was a pleasure working with you for these past years. I very much appreciated the time shared with you all, both in and outside of the laboratory. Special thanks go to Dr. Marta Ilecka, Dr. Dwain van Zyl, Dr. Remy Poirey, Dr. Susanne Delecluse and Daniel Judt for their support during my doctoral work and for enriching discussions.

Last but not least, I would like to express my deepest appreciation to my beloved family for their continuous encouragment and support. A special recognition goes to my dear wife who stood on my side on a daily basis.